การสังเคราะห์และการศึกษาสมบัติทางกายภาพเชิงแสงของพอลิไทโอฟีนที่มีพอร์ไฟรินฝังตัว

นางสาวหทัยชนก ศีลาเจริญ

วิทยานิพนธ์นี้เป็นส่วนหนึ่งของการศึกษาตามหลักสูตรปริญญาวิทยาศาสตรมหาบัณฑิต
สาขาวิชาเคมี ภาควิชาเคมี
คณะวิทยาศาสตร์ จุฬาลงกรณ์มหาวิทยาลัย
ปีการศึกษา 2559

SYNTHESIS AND INVESTIGATION OF PHOTOPHYSICAL PROPERTIES OF PORPHYRIN-EMBEDDED POLYTHIOPHENE

Miss Hathaichanok Seelajaroen

A Thesis Submitted in Partial Fulfillment of the Requirements
for the Degree of Master of Science Program in Chemistry
Department of Chemistry
Faculty of Science
Chulalongkorn University
Academic Year 2016

Thesis Title	SYNTHESIS AND INVESTIGATION OF PHOTOPHYSICAL PROPERTIES OF PORPHYRIN-EMBEDDED POLYTHIOPHENE
By	Miss Hathaichanok Seelajaroen
Field of Study	Chemistry
Thesis Advisor	Assistant Professor Rojrit Rojanathanes, Ph.D.
Thesis Co-Advisor	Associate Professor Patchanita Thamyongkit, Dr.rer.nat.

Accepted by the Faculty of Science, Chulalongkorn University in Partial Fulfillment of the Requirements for the Master's Degree

.....Dean of the Faculty of Science
(Associate Professor Polkit Sangvanich, Ph.D.)

THESIS COMMITTEE

.....Chairman
(Associate Professor Vudhichai Parasuk, Ph.D.)

.....Thesis Advisor
(Assistant Professor Rojrit Rojanathanes, Ph.D.)

.....Thesis Co-Advisor
(Associate Professor Patchanita Thamyongkit, Dr.rer.nat.)

.....Examiner
(Assistant Professor Anawat Ajavakom, Ph.D.)

.....External Examiner
(Assistant Professor Vachiraporn Ajavakom, Ph.D.)

หทัยชนก ศีลาเจริญ : การสังเคราะห์และการศึกษาสมบัติทางกายภาพเชิงแสงของพอลิไทโอฟีนที่มีพอร์ไฟรินฝังตัว (SYNTHESIS AND INVESTIGATION OF PHOTOPHYSICAL PROPERTIES OF PORPHYRIN-EMBEDDED POLYTHIOPHENE) อ.ที่ปรึกษาวิทยานิพนธ์หลัก: ผศ. ดร.โรจน์ฤทธิ์ โรจนธเนศ, อ.ที่ปรึกษาวิทยานิพนธ์ร่วม: รศ. ดร.พัชณิตา ธรรมยงค์กิจ, 126 หน้า.

งานวิจัยนี้สังเคราะห์อนุพันธ์ทรานซ์-A_2B_2-พอร์ไฟรินและทรานซ์-A_2B_2-เบนโซพอร์ไฟรินที่มีหมู่แทนที่ที่ตำแหน่งมีโซเป็นฟีนิลและหมู่แทนที่ฐานไทโอฟีน และพิสูจน์เอกลักษณ์โดยเทคนิคนิวเคลียร์แมกเนติกเรโซแนนซ์สเปกโตรสโคปีและแมสสเปกโทรเมทรี สมบัติทางกายภาพเชิงแสงของสารประกอบเป้าหมายในรูปสารละลายและฟิล์มตรวจสอบด้วยเทคนิคยูวีวิสิเบิลและฟลูออเรสเซนต์สเปกโทรโฟโตเมทรี การศึกษาเปรียบเทียบพบว่าการแทนที่หมู่ฟีนิลด้วยหมู่ไทโอฟีนที่ตำแหน่งมีโซ การเพิ่มจำนวนวงไทโอฟีน และการขยายระบบไพคอนจูเกตส่งผลต่อสมบัติทางกายภาพเชิงแสงและเชิงเคมีไฟฟ้าของสารประกอบเหล่านี้อย่างมีนัยสำคัญ ค่าระดับพลังงานในออร์บิทัลของโมเลกุลชั้นสูงสุดที่มีอิเล็กตรอนบรรจุและระดับพลังงานในออร์บิทัลของโมเลกุลต่ำสุดที่ไม่มีอิเล็กตรอนบรรจุ และช่องว่างระหว่างแถบพลังงาน ได้รับการประเมินว่าอยู่ในช่วง –5.79 ถึง –5.55 –4.05 ถึง –3.87 และ 1.5 ถึง 1.9 อิเล็กตรอนโวลต์ ตามลำดับ ปฏิกิริยาพอลิเมอร์ไรเซชันเชิงไฟฟ้าผ่านหมู่ไบไทโอฟีนิลของสารประกอบเป้าหมายให้พอลิไทโอฟีนที่มีพอร์ไฟรินฝังตัวตามต้องการ โดยการเกิดขึ้นของพอลิเมอร์ยืนยันด้วยเทคนิคไซคลิกโวลแทมเมทรีและยูวีวิสิเบิลสเปกโทรโฟโตเมทรี ซึ่งสมบัติการดูดกลืนแสงของพอลิเมอร์ดังกล่าวสอดคล้องกับมอนอเมอร์และมีลักษณะกว้างขึ้นซึ่งเกิดขึ้นเป็นปกติสำหรับพอลิเมอร์ของพอร์ไฟริน

ภาควิชา เคมี	ลายมือชื่อนิสิต .....
สาขาวิชา เคมี	ลายมือชื่อ อ.ที่ปรึกษาหลัก .....
ปีการศึกษา 2559	ลายมือชื่อ อ.ที่ปรึกษาร่วม .....

5772198523 : MAJOR CHEMISTRY

KEYWORDS: PORPHYRINS / BENZOPORPHYRINS / POLYTHIOPHENE / ELECTROPOLYMERIZATION / REDUCTION OF CARBON DIOXIDE

HATHAICHANOK SEELAJAROEN: SYNTHESIS AND INVESTIGATION OF PHOTOPHYSICAL PROPERTIES OF PORPHYRIN- EMBEDDED POLYTHIOPHENE. ADVISOR: ASST. PROF. ROJRIT ROJANATHANES, Ph.D., CO-ADVISOR: ASSOC. PROF. PATCHANITA THAMYONGKIT, Dr.rer.nat., 126 pp.

In this research, *trans*- A_2B_2- porphyrins and *trans*- A_2B_2- benzoporphyrins bearing phenyl and thiophene- based *meso*- substituents were synthesized and characterized by nuclear magnetic resonance spectroscopy and mass spectrophotometry. The photophysical properties of both solutions and films of the target compounds were also investigated by UV- visible and fluorescence spectrophotometry. Comparative studies of these compounds revealed that the replacement of phenyl with thiophene *meso*- substituents, the introduction of the additional thiophene ring and the extension of the porphyrin **π**- conjugated system significantly affected their photophysical and electrochemical properties. Energy levels of their highest occupied molecular orbital and lowest unoccupied molecular orbital, and their energy gap were estimated and found to be in a range of –5.79 to –5.55, –4.05 to –3.87 and 1.5 to 1.9 eV, respectively. The electropolymerization through the bithiophenyl units of the target compounds gave desirable porphyrin- embedded polythiophenes, the formation of which was confirmed by cyclic voltammetry and UV-visible spectrophotometry. Their absorption properties of the resulting polymers were consistent with those of the monomers with broader typically occurred for the porphyrinic polymers.

Department:	Chemistry	Student's Signature	.....
Field of Study:	Chemistry	Advisor's Signature	.....
Academic Year:	2016	Co-Advisor's Signature	.....

ACKNOWLEDGEMENTS

Firstly, I would like to express my sincere gratitude to my thesis advisors Asst. Prof. Dr. Rojrit Rojanathanes and Assoc. Prof. Dr. Patchanita Thamyongkit for the continuous support of my study and research, for their patience, motivation and valuable advice. Their guidance helped me in all the time of studying, doing the research and writing the thesis. My thesis could not successful without suggestions of them.

Besides my advisors, I would like to thank the rest of my thesis committee: Assoc. Prof. Dr. Vudhichai Parasuk for serving as the chairman, Asst. Prof. Dr. Anawat Ajavakom and Asst. Prof. Dr. Vachiraporn Ajavakom for serving as examiner and external examiner, respectively, for their insightful suggestions in the research.

My sincere thanks also go to o.Univ. Prof. Mag. Dr. DDr. h.c. Niyazi Serdar Sariciftci who provided me an opportunity to access to his laboratory and research facilities for making electrochemical experiments and all of the Linz Institute for Organic Solar Cells members for helpful comments.

I thank to all of members in the research group for helpful discussions and all of the supports during these three years.

Finally, I must express my very gratitude to my parents for providing me with supports and continuous encouragement throughout my years of study. This accomplishment would not have been possible without them.

CONTENTS

Page

Page

Page

LIST OF FIGURES

LIST OF SCHEMES

LIST OF ABBREVIATIONS

Å	angstrom
°C	degree Celcius
calcd	calculated
$CDCl_3$	deuterated chloroform
CO_2	carbondioxide
^{13}C-NMR	carbpn nuclear magnetic resonance spsectroscopy
CV	cyclic voltammetry
d	doublet (NMR)
dd	doublet of doublet (NMR)
DMSO-d_6	deuterated dimethyl formamide
eV	electro volt(s)
E_g	energy bandgap
ESI-HR-MS	electrospray ionization-high resolution spectrometry
g	gram(s)
h	hour(s)
^{1}H-NMR	proton nuclear magnetic resonance spsectroscopy
HOMO	highest occupied molecular orbital
Hz	Hertz
J	coupling constant
LUMO	lowest unoccupied molecular orbital
m/z	mass to charge ratio
MALDI-TOF-MS	matrix-assisted laser desorption ionization-time of flight-mass spectrometry

MeOH	methanol
MHz	megahertz
min	minute(s)
ε	molar absorptivity
m	multiplet (NMR)
mmol	millimole(s)
mg	milligram(s)
mL	milliliter(s)
N_2	nitrogen
NHE	normal nitrogen electrode
nm	nanometer(s)
QRE	quasi-reference electrode
rt	room temperature
s	singlet (NMR)
t	triplet (NMR)
TEA	triethylamine
UV-Vis	ultraviolet and visible spectroscopy
λ	wavelength
λ_{abs}	absorption wavelength
λ_{em}	emission wavelength
λ_{ex}	excitation wavelength
μL	microliter(s)
δ	chemical shift
% yield	percentage yield

CHAPTER I
INTRODUCTION

The energy demanding tends to increase due to the growth of economy over the world. The energy resources of many industries mainly rely on fossil fuels such as coal, natural gas and petroleum.[1] Relating to large energy consuming, the conventional energy is starting to run out which will be problematic to many countries. Moreover, the burning of fossil fuels is known to be one of the causes of the rising global temperatures due to emission of green house gases, such as water vapor (H_2O), methane (CH_4) and carbon dioxide (CO_2). Consequently, the renewable, cleaner and more sustainable energies, for example, solar power, wind power and geothermal power, have gained attentions from both research and industry fields over the years.

One of the most attractive inexhaustible fuel sources is solar energy because the sun is the powerful energy resource which has unlimited lifetime and can be harnessed in almost areas of the world. The device that can directly convert solar energy to electricity is called photovoltaic cell or solar cell. This conversion was driven by the photovoltaic effect, which was firstly demonstrated by Becquerel in 1839.[2] The present dominant kind of the solar cells is based on inorganic materials, including Si-based materials (e.g. single-crystal Si and polycrystalline Si) and metal chalcogenides (e.g. CdTe and $CuIn_xGa_{1-x}Se_2$). The good points of inorganic-based solar cells are their high power conversion efficiency (20–40%) and long-term stability.[3] However, the production of this type of solar cells relies on expensive advanced fabrication technology and may require some rare metals such as tellurium.[4] To overcome these drawbacks, the organic solar cells are widely studied and developed with their key advantages which are light weight, semitransparent, flexible and low manufacturing cost.[5]

In the past decade, many research groups focused their topics on wide range of organic photoactive materials, including conjugated polymers and small molecules. Among these numerous conjugated polymers, polythiophene and its derivatives are promising materials owing to their good charge transfer properties and high

environmental stability.[6] The examples of popular thiophene-based polymers are poly(3-hexylthiophene-2,5-diyl) (P3HT) and poly(3,4-ethylenedioxythiophene) (PEDOT), whose structures are shown in **Figure 1–1**. They gained a lot of interest in several applications for example light-emitting diodes,[7] solar cells,[8] and chemical sensors.[9]

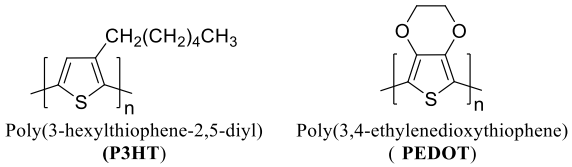

Figure 1–1: Examples of highlight polythiophene derivatives using in optoelectronic applications.

In addition, porphyrins are one of the most attractive molecules in the field of organic optoelectronic applications due to their characteristic photophysical properties,[10] photostability, as well as tunable electrochemical and photophysical properties resulting from variation of peripheral substituents[11] or a central metal.[12] Consequently, they have gained significant interest in diverse fields of applications, such as catalysis,[13] therapeutics,[14] and optoelectronics applications.[15] Recently, there is a spotlight report from Mitsubishi Chemical announcing an organic photovoltaic cell that reached power conversion efficiency up to 11.7% by using tetraphenyltetrabenzoporphyrin as a p-type material (**Figure 1–2**).[16]

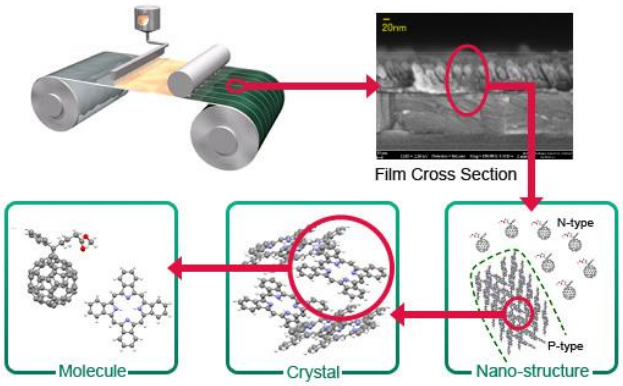

Figure 1–2: Photovoltaic cell from Mitsubishi Chemical containing tetrabenzoporphyrin as a p-type material.

However, the use of porphyrins as photoactive materials still has limitations due to their low charge mobility properties. One possible approach to enhance the charge mobility of the organic materials is to elongate **π** -conjugation system through conjugated polymer structure and/or to attach conductive unit(s).[17] In this research, we designed the novel porphyrinic compounds having two phenyl and two polymerizable oligothiophenyl *meso*-substituents at *trans*-positions to each other for being monomers in the electropolymerization (**Figure 1–3**). By this way, the porphyrins and oligothiophenyl units can be combined in the same polymeric network of porphyrin-embedded polythiophenes. The example of the structures of desirable polymeric form of the porphyrin derivative is shown in **Figure 1–3c**.

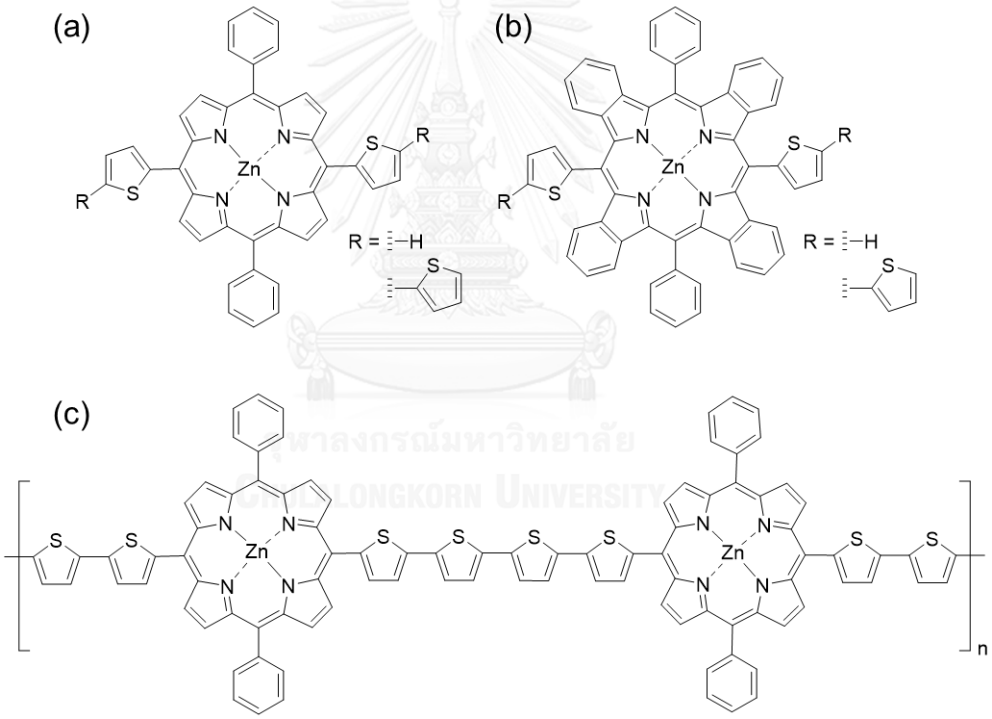

Figure 1–3: General structures of target a) porphyrins, b) benzoporphyrins and c) desired porphyrin-embedded polythiophene prepared from the porphyrin derivative.

1.1 Objective of this research

This research aims to synthesize porphyrin and benzoporphyrin derivatives bearing phenyl and thiophene-beased *meso*-substituents, and porphyrin-embedded

polythiophenes, as well as investigation of photophysical and electrochemical properties of these materials.

1.2 Scope of this research

The scope of this research covers the synthesis of novel *trans*-A_2B_2-porphyrin and benzoporphyrins bearing thiophene-based and phenyl *meso*-substituents at *trans*-positions to each other. All target compounds will be characterized by spectroscopic techniques, including mass spectrometry, as well as ^{1}H-NMR and ^{13}C-NMR spectroscopy. The electrochemical studies will be employed to determine the highest occupied molecular orbital and the lowest unoccupied molecular orbital (HOMO and LUMO, respectively) energy levels as well as energy bandgap (E_g) of the target compounds. In addition, polymerization of the target compounds will be electrochemically performed to obtain the desirable porphyrin-embedded polythiophene. Photophysical properties of both monomers and resulting polymers will be investigated by absorption and emission spectrometry.

CHAPTER II
THEORY AND LITERATURE REVIEWS

2.1 Optoelectronic device

Organic electronics is an interesting field of material science concerning about the design, synthesis, characterization and applications of small molecules or polymers that show desirable electronic properties such as conductivity and charge transfer properties.[18] Unlike conventional inorganic conductors and semiconductors, organic materials are constructed from organic small molecules and polymers. In addition, their synthetic methods are based on organic and polymer chemistry, which lead to the ease of structural modification of materials. Moreover, they have gained interests due to their low-cost fabrication process and great applications in flat and flexible panels.[19]

Organic optoelectronics is a branch of organic electronics that combines electronics and optics altogether.[20] Thus, organic optoelectronic devices are devices that interconvert between light and electricity in their operations using organic materials as photoactive compounds. These devices can be mainly divided into two types by their operation processes. The first one is a photoconductive device such as a photo resistor, a photodiode and a phototransistor. It can activate or deactivate electric circuits by detection of light intensities. The other one is a photovoltaic device which can convert light into electricity, for example a solar cell and an optical sensor.[21] The organic optoelectronic devices generally consist of two types of semiconductor materials, p-type and n-type materials that act as electron donors and electron acceptors, respectively.[22] The resulting junction, known as a p-n junction, is a major component in many optoelectronic devices such as organic light-emitting diodes (OLEDs), organic field-effect transistor (OFETs) and organic photovoltaics (OPVs) (**Figure 2–1**).

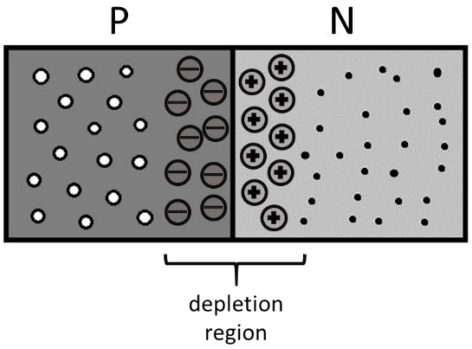

Figure 2–1: A schematic setup of a p-n junction.

The active materials that are used in organic optoelectronics are typically **π**-conjugated molecules containing aromatic hydrocarbons, heterocyclic compounds and unsaturated functional groups.[23] These active materials could be categorized into two main classes, conductive small molecules and conductive polymers. Most of the organic small molecules can be efficiently purified and form well-oriented films to give high charge carrier mobility.[24] For the conductive polymers, they have high electrical conductivity and high charge mobility in their doped state due to their large **π**-conjugation system through the whole polymer backbone.[25]

For optoelectronic applications, good organic material candidates should have long-term physical and chemical stability, well-oriented morphology in the solid state, good photophysical properties (such as wide absorption band and high absorption coefficient) and suitable electrochemical properties and charge mobility.[21] The examples of the popular organic materials are C_{60} derivatives, porphyrin derivatives, benzoporphyrin derivatives, poly(3-hexylthiophene-2,5-diyl) (P3HT), poly(*p*-phenylene vinylene) (PPV) and poly(3,4-ethylenedioxy-thiophene) (PEDOT) structures of which are shown in **Figure 2–2**.

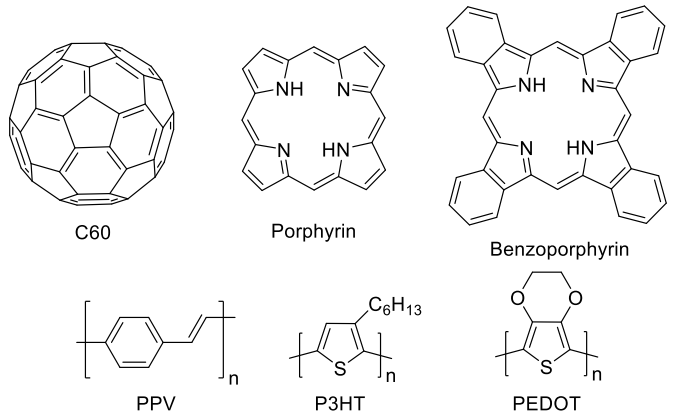

Figure 2–2: Molecular structures of some well-known photoactive materials used as organic semiconductors.

In the past decades, the development of BHJ-SCs gains a lot of interest due to their good power conversion efficiency and long lifetime, compared to other kinds of organic solar cells.[26] The high efficiency of the BHJ-SCs mainly results from the blending electron donor and acceptor materials which gives the large interfacial of the p-n junction. Additionally, in a field of catalysis, great interest has been focused on the catalyst development for the conversion of CO_2.[27] Within the electrochemical process, CO_2 can be converted to more valuable products, for example, CO, formic acid, formaldehyde, methanol, methane and ethane. This study therefore aims to the development of porphyrin-thiophene conjugated system for using in BHJ-SCs and (photo)electrocatalysis of the reduction of CO_2.

2.2 Polythiophene

Polythiophenes, polymers of thiophene repeating units (**Figure 2–3**), have been widely used as photoactive components in the organic electronic devices.[28] It is mainly because they can become conductive *via* doping processes. The study of polythiophenes and related polymers were recognized by awarding of Nobel Prize in Chemistry in the year of 2000 to Alan J. Heeger, Alan MacDiarmid, and Hideki Shirakawa for “the discovery and development of conductive polymers".[29] Electrical properties of their materials result from the delocalization of electrons through their conjugated backbone. Moreover, high environmental stability together with their well-established

structural modification have led to their great developments for electronic applications.[30]

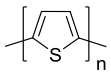

Figure 2–3: A structure of polythiophene.

Polythiophenes can be prepared by means of two routes, chemical and electrochemical synthesis.[31] In case of chemical synthetic routes, nickel- and palladium-based cross coupling chemistry are quickly adapted to the efficient synthesis of polythiophene and its derivatives. Two important features of these cross-coupling reactions are selective C-C bond formation and regioselectivity of the catalyst. **Scheme 2–1** shows published preparation procedures of polythiophenes using nickel- and palladium-based catalysts. The upper route involves in the formation of two intermediates by reacting 2,5-dibromothiophene with Rieke zinc (Zn*) under a Rieke's method.[32] The resulting Zn-complexes were accessed in the cross-coupling reaction using $Pd(PPh_3)_4$, affording polythiophenes. Another way is to synthesize intermediates through Grignard metathesis, followed by nickel-catalyzed coupling reaction to get the corresponding polymer.[33]

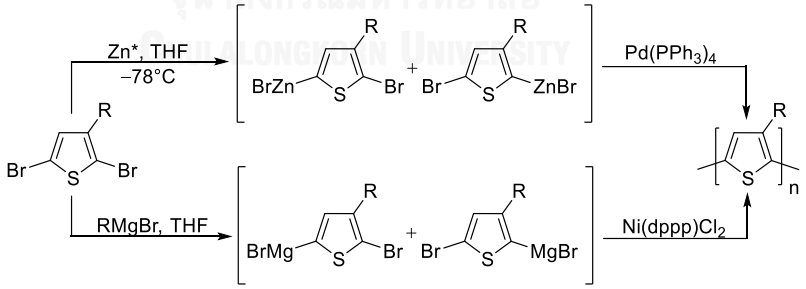

Scheme 2–1: Syntheses of polythiophene derivatives through Rieke's (upper)[32] and Grignard's (lower) routes.[33]

Another efficient synthetic method of the polythiophenes is electrochemical polymerization. Compared to the chemical method, anodic electropolymerization has several advantages, such as catalyst-free procedure, direct deposition of the doped polymer onto an electrode surface, easy control of film thickness and possibility for *in*

situ characterization of the polymerization by electrochemical and/or spectroscopic techniques.[6] The electrochemical formation processes start from the oxidation step generating cation radical species, followed by coupling and aromatization step to form dimer. After that, a sequence of subsequent dimerization steps proceeds to the formation of oligomers and polymers. The cyclic voltammograms and the proposed mechanism of the thiophene polymerization are shown in **Figure 2–4**. The graph reveals that current density increased as more polythiophene was formed on the electrode.[34]

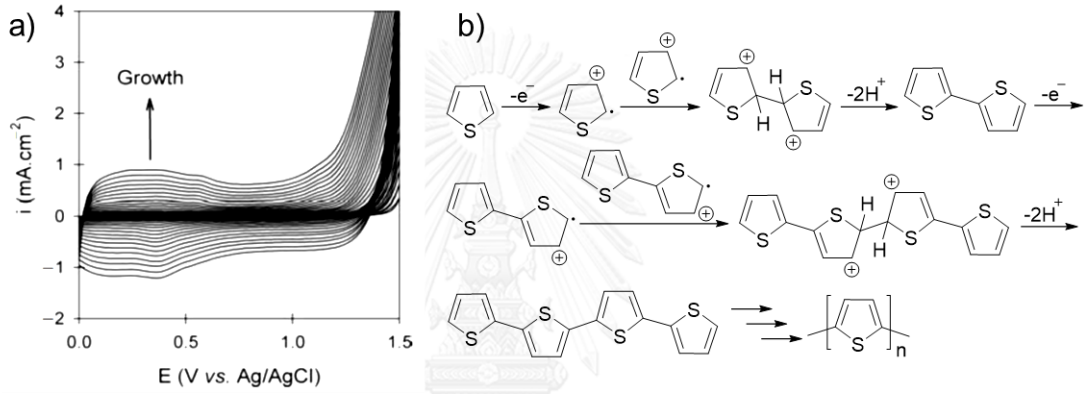

Figure 2–4: a) Cyclic voltammograms and b) the proposed mechanism of the electropolymerization of thiophene.

According to the useful functionalities of the polythiophene-based materials such as electronic conductivity and nonlinear optical effects,[35] polythiophene and its derivatives have attracted scientists' interest in diverse fields of research, for example, capacitors,[36] light-emitting diodes,[7] field-effect transistors,[37] solar cells[8] and electrochromic device.[38]

2.3 Porphyrin

As a word, porphyrin is originated from Greek: *porphura* that means violet and all of the porphyrin compounds are intensely colored.[12] They are an important class of natural macrocyclic molecules found in biological systems. The natural porphyrinic compounds were also called "the color of life" due to their important roles in

metabolism of living organisms.[39] Without porphyrins, life cycles of human and animals are interrupted. That is because of the ability of an iron-containing porphyrin or heme (**Figure 2–5**) in hemoglobin in delivering oxygen to the target tissues.[40] Moreover, the chlorophyll derivatives are naturally found in green plants, algae and cyanobacteria of which their function is to absorb light and transfer it to other parts of photosystem which is an initial step of photosynthesis.[41]

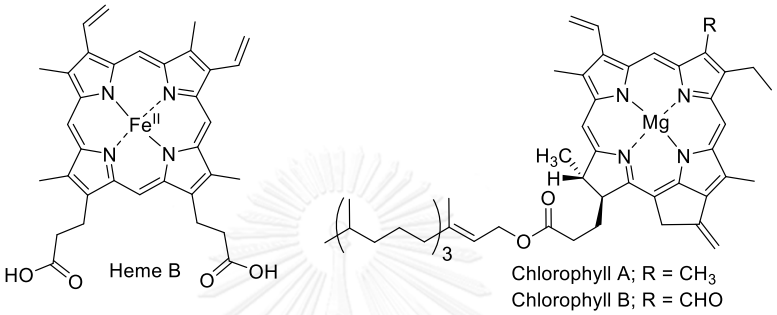

Figure 2–5: Structures of heme B and chlorophyll derivatives.

The systematic IUPAC nomenclature of porphyrins was introduced with the numbering system for all atoms on the macrocycle as shown in **Figure 2–6**.[42] Moreover, in case of substituents, their positions are classified into three groups, i.e. *meso*-, α and β-positions. The *meso*-positions are 5, 10, 15 and 20, while the α-position are 1, 4, 6, 9, 11, 14 and 16 positions on the macrocycle. In a similar way, the 2, 3, 7, 8, 12, 13, 17 and 18 positions are referred as β-positions.

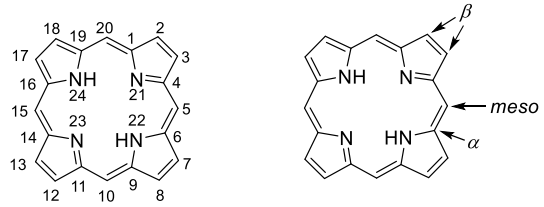

Figure 2–6: General structure of the porphyrin core and positions of all atoms.

The porphyrin macrocycle is an aromatic system that is made up of four pyrrole rings joined by four methine (meso) carbons.[43] Even though the porphyrin core has 22 π-electrons, only 18 of them are actually anticipated in any one of the several

delocalization pathways as shown in **Figure 2–7**. The aromaticity of porphyrin is allowed due to the Huckle's rule (**π** -electrons = 4n+2, where n = 4).

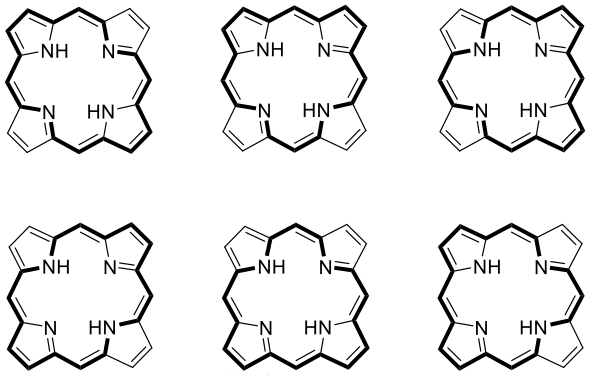

Figure 2–7: Possible **π** -electrons delocalization pathways.

The strong **π** -conjugation gives the porphyrins stability toward thermal and chemical conditions.[12] Moreover, it also leads to characteristic photophysical properties of the porphyrins. In their absorption spectra, the porphyrins usually show an intense Soret band at around 400 nm and several weaker absorption bands between 450 and 800 nm as known as Q-bands. The Soret absorption band results from the strong transition of the ground state (S_0) to the second excited state (S_2), while the Q-bands are from the weak transition from S_0 to the first excited state (S_1). Both of the Soret and Q-bands are raised from **π** -**π** * transitions. As shown in **Figure 2–8**, four frontier molecular orbitals consist of two **π** orbitals (a_{1u} and a_{2u}) and a degenerate pair of **π** * orbitals (e_{gx} and e_{gy}). These orbitals mix together by the configuration interactions which are constructive and destructive combinations, resulting in different intensity bands (Soret and Q-bands). In case of fluorescence, emission of the porphyrins is only detected from the transition of S_1 to S_0 because the conversion of S_2 to S_1 is rapid.

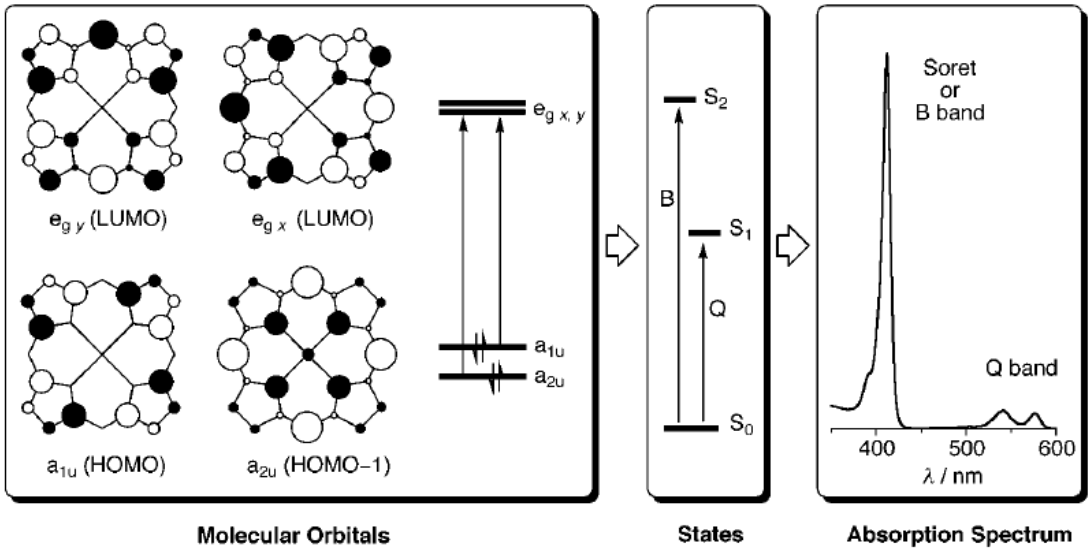

Figure 2–8: Four molecular orbitals and illustration of electronic transition states of the porphyrins.[12]

According to their interesting properties, the porphyrin derivatives have been studied in various fields of research. In medical and biological field, porphyrins are used in several applications, for example, molecular sensors,[44] molecular recognition,[45] photodynamic therapy (PDT),[46] boron neutron capture therapy (BNCT)[47] and cell imaging.[48] In the optoelectronic field, the potential of the porphyrinic compounds for organic solar cells,[49] light emitting diodes[50] and photo(electro)catalysts[51] have been widely studied.

However, utilization of the porphyrins in diverse fields of studies requires the ability to tailor physical, photophysical and electrochemical properties. The physical properties include solubility and stability of compounds, while their photophysical properties cover absorption, emission and molecular absorption coefficient. The electrochemical properties normally refer to electrochemical behavior, redox potentials, and electrochemical HOMO/LUMO energy levels and energy gap. The structural modification of the porphyrins through changing substituents at *meso*- and *β*-positions of the macrocyclic core enables tuning of these properties. The *meso*-substituents can be varied into several kinds of groups such as alkyl, aryl, heterocyclic, organometallic or even other macrocyclic groups.[11] This type of modification gains a

lot of interest due to the ease of the synthesis method through condensation of pyrrole with an appropriate aldehyde. On the other hand, variation of the substituents at the β-positions is more difficult because the synthesis of modified pyrrole precursor is required. Another popular way to tune up properties of the porphyrins is coordination with several kinds of central metal of the porphyrin core to obtain complexes called as metalloporphyrins.[12]

2.3.1 Synthesis of porphyrin

The synthetic methods of the porphyrinic compounds have been well-developed over decades. In 1930, the structure of haemin, a porphyrinic compound found in blood, and its synthetic route were first highlighted in the Nobel prize lecture given by Fischer.[52] After that, in 1935, the synthetic method of tetramethylporphyrin was reported by Rothemund by mixing pyrrole and acetaldehyde together.[53] After that, the modified conditions were developed for reacting pyrrole with other aldehydes in the presence of pyridine in a seal tube at up to 140–150 ºC for 24 hours, and was named as Rothemund's method.[54] Route A in **Scheme 2–2** shows an example of the formation of tetraphenylporphyrin (**TPP**) by a reaction between pyrrole and benzaldehyde under the Rothemund's condition.[55]

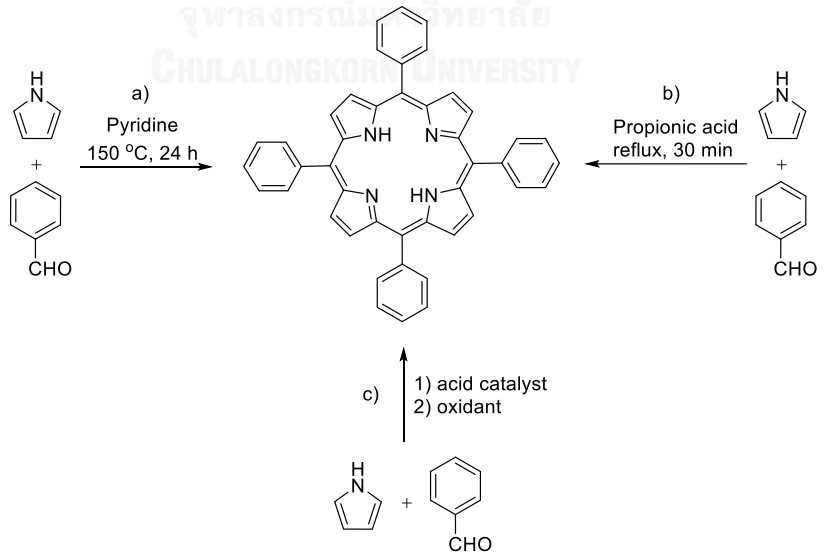

Scheme 2–2: Formation of **TPP** under conditions described by a) Rothemund,[55] b) Adler and Longo[56] and c) Lindsey.[57]

Due to a harsh reaction condition of the Rothemund's method, Adler and Longo developed more practical synthetic method by refluxing pyrrole and aldehyde in propionic acid for 30 min as shown in **Scheme 2–2** (route b).[56] By this condition, the product yield was improved by up to 20%, compared with that of Rothemund's method.

However, these two procedures still have a limitation to synthesize the *meso*-substituted porphyrin compounds bearing sensitive functional groups due to the relatively harsh acid condition. To overcome this limitation, Lindsey and co-workers suggested a new one-pot two-step procedure using a milder condition, leading to the porphyrins in high yield without encountering complicated purification.[57] The synthesis relies on the formation of porphyrinogen through acid-catalyzed condensation between pyrrole and aldehyde, followed by an oxidation reaction (**Scheme 2–2**, route c). Additionally, towards various Lewis acids and Brønsted acids, acids commonly used in the porphyrin formation are $BF_3{\cdot}OEt_2$ and trifluoroacetic acid,[58] while oxidants typically used in the oxidation step are DDQ or *p*-chloranil.[59]

However, these classical methods are suitable generally for synthesis of A_4-porphyrin derivatives.[60] In case of the porphyrins bearing distinct *meso*-substituents, rational synthetic routes were developed instead of classical one-pot condensation of pyrrole and mixture of aldehydes that can provide a statistical mixture of several possible porphyrin. In order to obtain the *meso*-substituted porphyrins bearing two different substituents in a *trans*-configuration or *trans*-A_2B_2-porphyrins, the synthesis relies on a reaction between 5-substituted dipyrromethane bearing an 'A' substituent and an appropriate aldehyde bearing a 'B' substituent in the presence of an acid catalyst, followed by DDQ- or *p*-chloranil- oxidation.[13f] As an example, a condensation between 5-phenyldipyrromethane and *p*-tolualdehyde was performed in the presence of $BF_3{\cdot}OEt_2$, followed by oxidation with DDQ, affording 5,15-bis-(4-methylphenyl)-10,20-diphenylporphyrin (**Scheme 2–3**).[61]

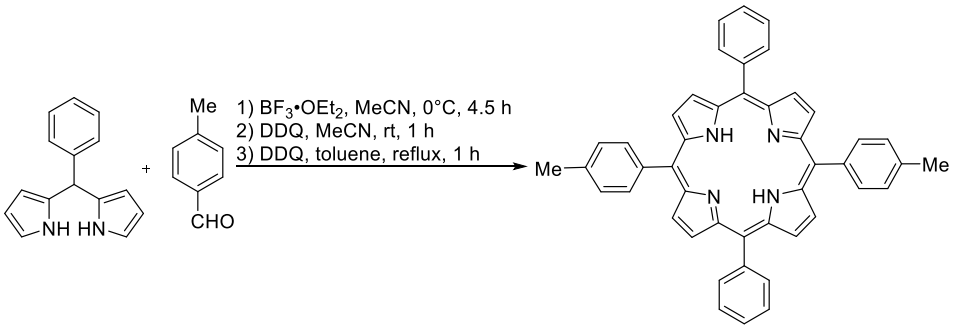

Scheme 2–3: A synthetic route of 5,15-bis-(4-methylphenyl)-10,20-diphenyl porphyrin reported by Lindsey *et al*.[61]

Other than the *trans*-A_2B_2-porphyrins, this work also focuses on the synthesis of *trans*-A_2B_2-benzoporphyrins, of which synthetic approaches have been reported. Cheprakov *et al*. described the synthesis of *trans*-diaryloctahydrotetrabenzoporphyrin derivatives using tetrahydroisoindole derivatives as precursors.[62] **Scheme 2–4** shows a synthetic route of *meso*-5,15-diphenyloctahydrotetrabenzoporphyrin starting with tetrahydroisoindole ester. The indole precursor was reacted with dimethoxymethane in the presence of *p*-TsOH, affording *meso*-unsubstituted dipyrromethene derivative. The resulting dipyrrolemethane was decarboxylated and then subjected to the condensation with benzaldehyde under the Lindsey's condition. After the oxidation with DDQ, the target compound was obtained. However, the further oxidization of this precursor into tetrabenzoporphyrin could not be obtained through several attempts of oxidation and the reason of these observation have been unclear.

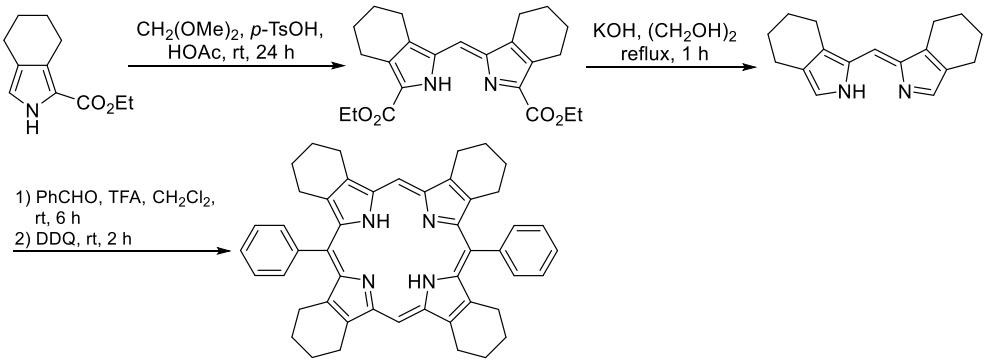

Scheme 2–4: A synthesis route of *meso*-5,15-diphenyloctahydrotetrabenzoporphyrin reported by Cheprakov *et al*.[62]

2.4 Photophysical properties

In general, the photophysical properties of matter are thought as characteristic properties related to light or photon, for example absorption and emission properties.[63] These features involve in the electronic transitions of ground and excited states energy levels as illustrated in a Jablonski diagram (**Figure 2–9**).

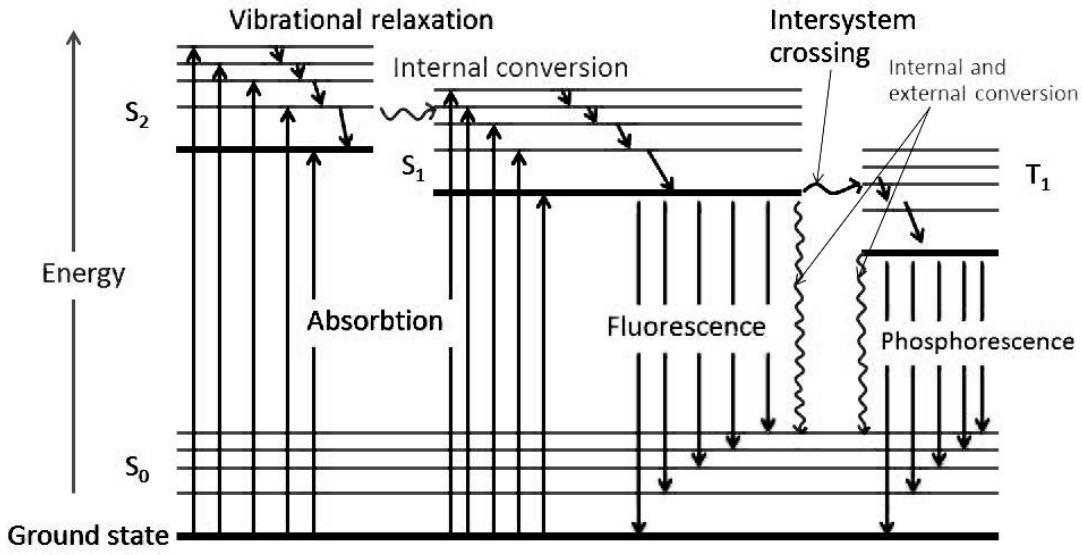

Figure 2–9: Jablonski diagram.[63]

The Jablonski diagram is basically an energy diagram, arranged with the energy on a vertical axis. The rest of the diagram is represented as columns of sets of specific spin multiplicity energy levels. The diagram illustrates a singlet ground state (S_0) and several excited singlet states (S_2, S_3, ...) together with triplet states (T_1, T_2, ...) in horizontal lines. Bold horizontal lines are representations of electronic energy levels, while the thinner ones denote several vibrational states (rotational energy states are ignored). Straight arrows show the electronic transitions associated with the absorption or emission of photon. The other transitions of electrons without any interactions with light, namely internal conversion and intersystem crossing, are displayed as wavy lines. Within the Jablonski diagram, several pathways show how matters may accept energy from photon and then release the energy through various possible process.[63]

To excite the molecule from the ground state to the excited state, the energy of absorbed light has to higher than the energy difference between those two states. The energies involved these transitions can be converted from the frequency of the electromagnetic wave or the wavelength of photon, described by the following equation:

$$E = h\nu = h\frac{c}{\lambda}$$

where E is the energy of the photon, *h* is a Planck's constant, ν is frequency, *c* is speed of light and λ is the wavelength of the photon. If absorbed photon contains more energy than the minimum energy required for an electronic transition, the excessive energy can be converted into vibrational and rotational energy.

After the absorption of the photon, the molecule will first relax from higher vibrational levels to the lowest vibrational energy level *via* a process called vibrational relaxation. This non-radiative process occurs through two types of relaxation, thermal (loss of heat) and collisional (collision with other molecules) relaxations. If the vibrational energy levels strongly overlap with other electronic energy levels bearing the same spin multiplicity, the transition of the excited electron can take place from a vibration level in one electronic state to another vibration level in a lower electronic state. This process is called internal conversion. Another pathway that can happen is photon emission called fluorescence. Fluorescence is a slow transition process which enables to the transition between the electron staying in the same multiplicity manifold. The most frequently observed fluorescence comes from the transition between the first excited state (S_1) and the ground state (S_0) energy levels because at the higher energies, it is more likely that energy will be dissipated through the internal conversion and the vibrational relaxation. Another path to dissipate energy is called intersystem crossing. This process involves the change of spin multiplicity from an excited singlet state to an excited triplet state. The intersystem crossing leads to several interesting pathways back to the ground electronic state. One direct transition is phosphorescence, where a radiative transition from the excited triplet state to the singlet ground state occurs.

In addition, there are non-emitting transitions from the excited state to the ground state that account for prohibiting fluorescence or phosphorescence behavior of the molecule. This quenching phenomenon can result from several processes, such as excited state reaction, complex formation and molecular collisions. These non-emitting processes generally compete with fluorescence as the molecular relaxes back down to the ground electronic state.

Literature review for porphyrin-thiophene conjugates

In 1992, Shimidzu *et al*. successfully synthesized novel phosphorus(V) tetraphenylporphyrin derivatives containing oligothiophenylalkoxy groups (n = 1–3) at axial positions of the central phosphorus atom *via* a reaction of dichloro phosphorus(V) tetraphenylporphyrin and the corresponding oligothiophenyl alcohols (**Figure 2–10**).[64] The resulting porphyrin derivatives **BT1** and **TT1** were then electrochemically polymerized in 0.1 M tetrabutylammonium tetrafluoroborate ($TBABF_4$) in acetonitrile using an ITO-coated glass, a Pt and a saturated calomel electrode (SCE) as a working electrode, a counter electrode and a reference electrode, respectively, to afford corresponding one-dimensional polymers, whereas porphyrins **T1** was scarcely polymerized. Moreover, their photoconductivity studies revealed that the conductivity of the resulting polymers were strongly enhanced by the photoirradiation.

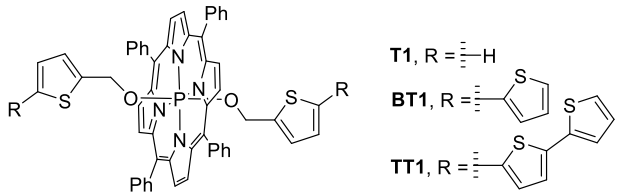

Figure 2–10: General structures of phosphorus(V) porphyrins **T1**, **BT1** and **TT1** studied by Shimidzu *et al*.[64]

Later on, Shimidzu *et al*. studied the polymerization of zinc- and palladium-porphyrin derivatives bearing bithiophenyl or terthiophenyl *meso*-substituents (**Figure 2–11a**).[65] The oxidative electropolymerization of the porphyrin derivatives was performed in 0.1 M $TBABF_4$ in CH_2Cl using an ITO-coated glass, a Pt and a saturated

calomel electrode (SCE) as a working electrode, a counter electrode and a reference electrode, respectively. The cyclic voltammograms of the electropolymerization of a zinc-porphyrin of interest, **ZnTBTP**, is shown in **Figure 2–11b**.

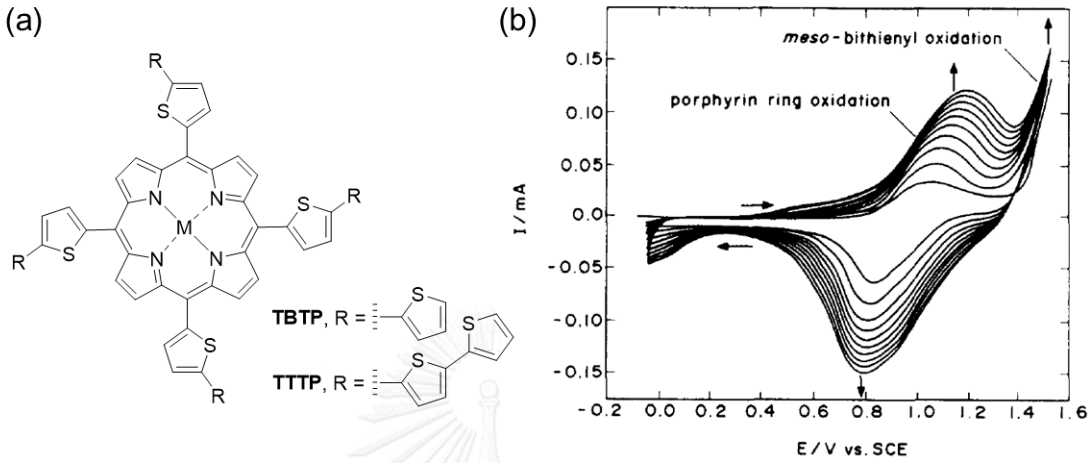

Figure 2–11: a) General structures of **TBTP** and **TTTP** and b) the cyclic voltammograms of the electropolymerization of **ZnTBTP**.

Joo *et al*. described the use of novel zinc porphyrins linked with oligothiophenyl groups by phenyl (**TTP1**, **TTP2** and **TTP3**) or ethynyl (**BTP1** and **BTP2**) linkers as electron donors in the BHJ-SCs (**Figure 2–12**).[66] The absorption properties of these compounds revealed that the red shift of their absorption maxima was observed as the number of thiophene rings was increased. Moreover, the enhancement of Q-band intensity at 700 nm was clearly observed for **BTPs**, compared to those of **TTPs** as a result of more efficient conjugation *via* the ethynyl linkers.

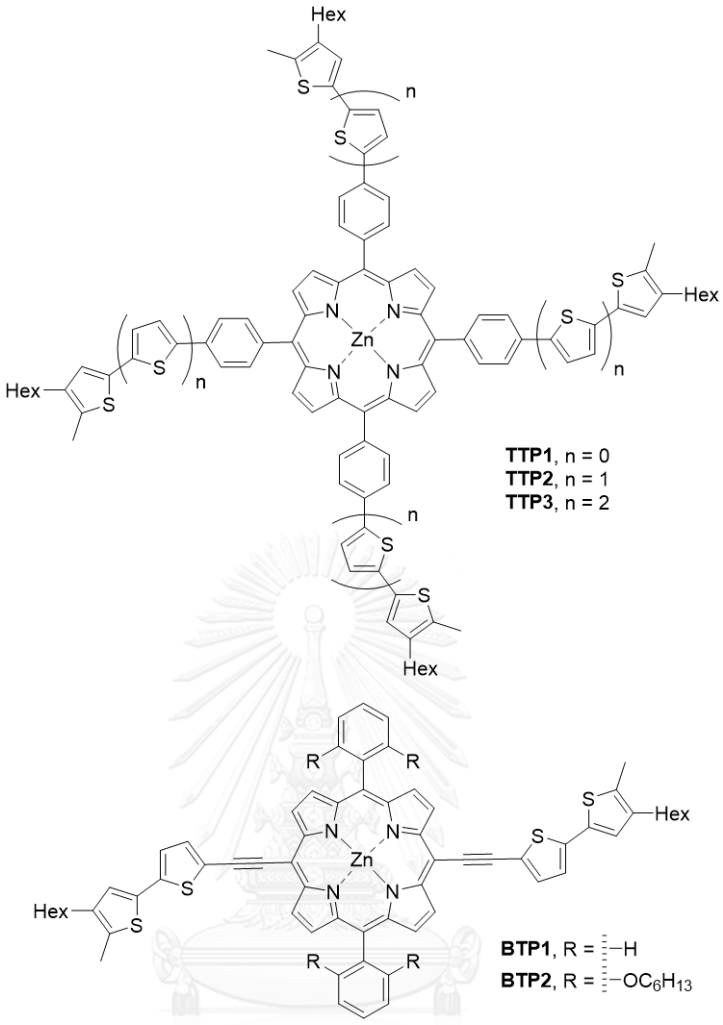

Figure 2–12: General structures of **TTPs** and **BTPs**.

Later, Keawsongsaeng *et al.* successfully synthesized a series of zinc porphyrin and zinc benzoporphyrin derivatives bearing phenyl, thienyl and bithiophenyl *meso*-substituents (**Figure 2–13**a).[67] According to the results, the optimum ternary BHJ-SCs (**Figure 2–13**b) having these compounds as additives in an active layer of P3HT and PCBM exhibited a maximum energy conversion efficiency of 4.3%, corresponding to 19% enhancement of the efficiency, compared with the standard BHJ-SC.

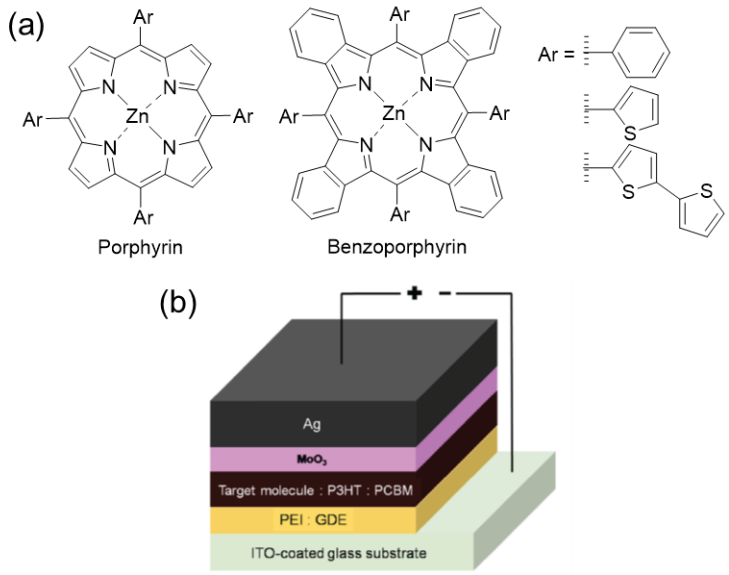

Figure 2–13: a) General structures of porphyrin and benzoporphyrin derivatives and b) the schematic setup of the inverted ternary BHJ-SCs reported by Keawsongsaeng *et al.* [67]

CHAPTER III
EXPERIMENTS

3.1 Synthesis

3.1.1 Materials and methods

All chemicals were analytical grade, purchased from commercial sources and used as received, unless noted otherwise.

^{1}H-NMR (400 MHz) and ^{13}C-NMR (100 MHz) spectra were recorded in $CDCl_3$ or $(CD_3)_2SO$. Chemical shifts (δ) are reported in parts per million (ppm) relative to the residual $CHCl_3$ signal (7.26 ppm for ^{1}H-NMR and 77.0 ppm for ^{13}C-NMR spectroscopy) and $(CH_3)_2SO$ signal (2.50 ppm for ^{1}H-NMR and 39.5 ppm for ^{13}C-NMR spectroscopy). Coupling constants (*J*) are reported in Hertz (Hz).

Mass spectra were obtained using high resolution electrospray ionization (HR-ESI) and matrix-assisted laser desorption ionization (MALDI) mass spectrometry using dithranol as a matrix.

Absorption spectra of solutions were measured in toluene at room temperature by UV-Vis spectrophotometer and molar extinction coefficient (ε) were reported in $L \cdot mol^{-1} \cdot cm^{-1}$. In addition, absorption spectra of films were investigated at room temperature by UV-Vis spectrophotometer. The monomer films were prepared by drop-casting tetrahydrofuran (THF) solutions of the compounds at the concentration of 10 $mg \cdot mL^{-1}$ on indium tin oxide (ITO)-coated glass substrates. Emission spectra of the solutions were recorded in toluene at room temperature using a luminescence spectrophotometer.

Noncommercial compounds: 5,10,15,20-tetraphenylporphyrinato zinc(II) (**ZnP-Ph**), 5,10,15,20-tetra(2,2′-bithiophen-5-yl)porphyrinatozinc(II) (**ZnP-2Th**), 5,10,15,20-tetraphenyltetrabenzoporphyrinatozinc(II) (**ZnBP-Ph**) were previously synthesized in our research group by following the reported procedure.[67]

3.1.2 5-Phenyldipyrromethane (1)

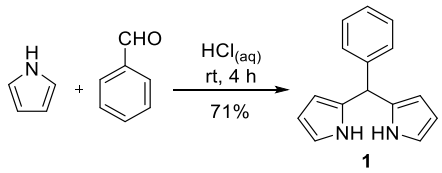

Following a reported procedure,[68] a 0.18 M aqueous HCl solution (100 mL) was placed in a round-bottomed flask. Then, pyrrole (1.0 mL, 15 mmol, 3 equivalents) was added at room temperature, followed by the addition of benzaldehyde (0.50 mL, 5.0 mmol, 1 equivalent). The resulting mixture was stirred at room temperature for 4 h. The solid was then filtered off and dissolved with CH_2Cl_2 (50 mL). After that, the resulting solution was washed out with deionized (DI) water (50 mL) and dried over anhydrous Na_2SO_4. After the solvent was removed under reduced pressure, the resulting crude was purified by a silica column (hexanes/CH_2Cl_2 = 1:1) to afford a yellow oil. After precipitation with hexanes, compound **1** was obtained as an off-white solid (0.781 g, 71%). ^{1}H-NMR ($CDCl_3$) δ 5.48 (s, 1H), 5.86–5.97 (m, 2H), 6.16 (dd, *J* = 3.2, 2.8 Hz, 2H), 6.65–6.74 (m, 2H), 7.19–7.37 (m, 5H), 7.93 (br s, 2H) (**Figure A–1**). Other spectroscopic data are consistent with those described in the literatures.[68-69]

3.1.3 5,15-Bis(phenyl)-10,20-bis(thiophen-2-yl)porphyrin (*t*-H_2P-Th)

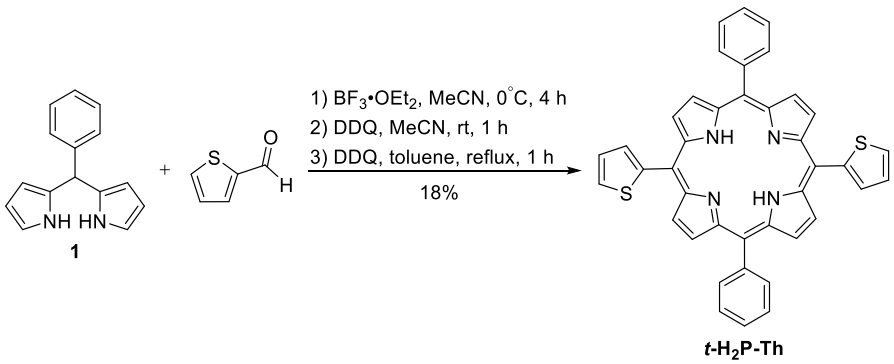

According to a previous method,[61] a solution of compound **1** (0.672 g, 3.00 mmol, 1 equivalent), 2-thiophene carboxadehyde (0.280 mL, 3.00 mmol, 1 equivalent) and NH_4Cl (1.6 g, 30 mmol, 10 equivalents) in acetonitrile (300 mL) was reacted with

$BF_3{\cdot}OEt_2$ (24 μL, 0.30 mmol, 0.1 equivalent) under N_2 atmosphere at 0 °C for 4 h. After that, 2,3-dichloro-5,6-dicyano-1,4-benzoquinone (DDQ) (0.681 g, 3.00 mmol, 1 equivalent) was added and stirred at room temperature for an additional hour. To quench the reaction, triethylamine (0.5 mL) was added and the solution was filtrated through a pad of silica eluted by CH_2Cl_2. After removal of the solvents, the resulting crude was redissolved with toluene (120 mL) and treated with DDQ (0.681 g, 3.00 mmol, 1 equivalent). After refluxing for an hour, the resulting mixture was passed through a pad of silica using CH_2Cl_2 as eluent. After removal of the solvents, the crude was purified by a silica column (hexanes/CH_2Cl_2 = 1:1), followed by washing with hexanes and methanol under ultrasonic agitation to afford 5,15-bis(phenyl)-10,20-bis(2-thienyl)porphyrin (***t*-H_2P-Th**) as a purple solid (0.168 g, 18%). ^{1}H-NMR ($CDCl_3$) δ –2.72 (s, 2H), 7.48–7.54 (m, 2H), 7.73–7.83 (m, 6H), 7.84–7.89 (m, 2H), 7.91–7.95 (m, 2H), 8.18–8.25 (m, 4H), 8.84 (d, *J* = 4.4 Hz, 4H), 9.05 (d, *J* = 4.4 Hz, 4H) (**Figure A–2**). Due to low solubility of ***t*-H_2P-Th**, a well-resolved ^{13}C-spectrum could not be obtained. HR-ESI-MS *m/z*: $[M+H]^+$ calcd for $C_{40}H_{26}N_4S_2$, 627.1672; found, 627.1677 (**Figure A–3**); λ_{abs} 422, 518, 553, 595, 650 nm (**Figure A-4**); λ_{em} (λ_{ex} = 422 nm) 660, 723 nm (**Figure A–5**).

3.1.4 5,15-Bis(phenyl)-10,20-bis(thiophen-2-yl)porphyrinatozinc(II) (*t*-ZnP-Th)

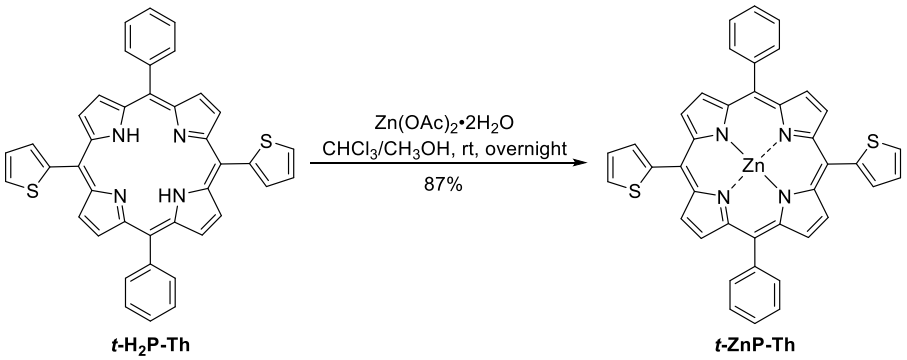

Following a standard method,[70] a solution of ***t*-H_2P-Th** (31 mg, 0.050 mmol, 1 equivalent) in $CHCl_3$ (20 mL) was reacted with a solution of $Zn(OAc)_2{\cdot}2H_2O$ (55 mg, 0.25 mmol, 5 equivalents) in methanol (3 mL) at room temperature for 12 h. The resulting

solution was washed with a 10% aqueous $NaHCO_3$ solution (20 mL) and DI water (20 mL), and dried over anhydrous $MgSO_4$. Then, the crude product was purified by a silica column using CH_2Cl_2 as eluent, followed by washing with hexanes and methanol under ultrasonic agitation to yield 5,15-bis(phenyl)-10,20-bis(thiophen-2-yl)porphyrinatozinc(II) (***t*-ZnP-Th**) as a purple solid (30 mg, 87%). ^{1}H-NMR ($CDCl_3$) δ 7.50 (dd, *J* = 5.2, 3.6 Hz, 2H), 7.72–7.80 (m, 6H), 7.84 (dd, *J* = 5.2, 1.2 Hz, 2H), 7.92 (dd, *J* = 3.6, 1.2 Hz, 2H), 8.19–8.23 (m, 4H), 8.94 (d, *J* = 4.8 Hz, 4H), 9.16 (d, *J* = 4.8 Hz, 4H) (**Figure A-6**); ^{13}C-NMR ($CDCl_3$) δ 112.7, 122.0, 126.0, 126.7, 127.5, 127.8, 132.1, 132.4, 133.6, 134.5, 142.8, 143.8, 150.7, 151.2 (**Figure A–7**); HR-ESI-MS *m/z*: $[M+H]^+$ calcd for $C_{40}H_{24}N_4S_2Zn$, 689.0807; found, 689.0802 (**Figure A–8**); λ_{abs} (ε) 426 (4.7×10^5), 554, 594 nm (**Figures A–9** and **A–10**); λ_{em} (λ_{ex} = 426 nm) 607, 653 nm (**Figure A–11**).

3.1.5 5,15-Bis(phenyl)-10,20-bis(2,2'-bithiophen-5-yl)porphyrin (*t*-H_2P-2Th)

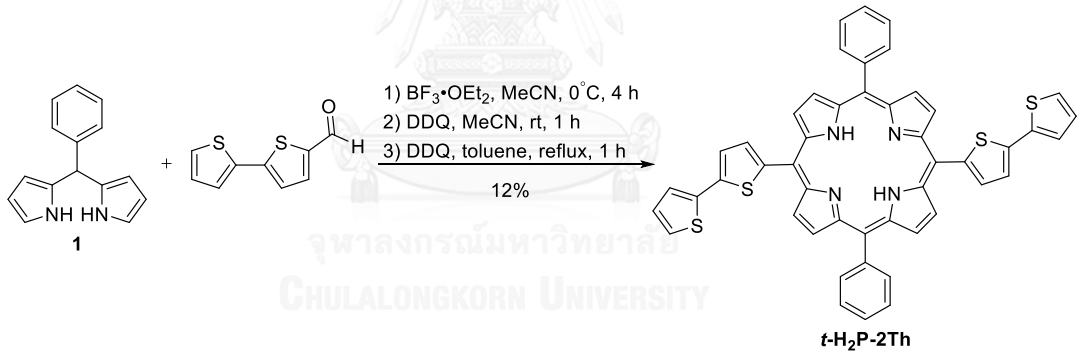

Following to a reported procedure,[61] a solution of compound **1** (0.667 g, 3.00 mmol, 1 equivalent), 2,2'-bithiophene-5-carboxaldehyde (0.583 g, 3.00 mmol, 1 equivalent) and NH_4Cl (1.6 g, 30 mmol, 10 equivalents) in acetonitrile (300 mL) was reacted with $BF_3{\cdot}OEt_2$ (24 μL, 0.30 mmol, 0.1 equivalent) at 0 °C under N_2 atmosphere for 4 h. After that, the solution mixture was treated with DDQ (0.681 g, 3.00 mmol, 1 equivalent) at room temperature for an additional hour. After quenching the reaction by treating with triethylamine (0.5 mL), the solution was passed through a pad of silica eluted with 2% THF in CH_2Cl_2. Then, the crude product was re-oxidized by refluxing with DDQ (0.681 g, 3.00 mmol, 1 equivalent) in toluene (120 mL) for an hour. The

resulting solution was passed through a pad of silica eluted with a solution of 2% THF in CH_2Cl_2. After that, the crude product was purified by column chromatography (silica, hexanes/CH_2Cl_2 = 1:1), followed by washing with hexanes and methanol under ultrasonic agitation to obtain 5,15-bis(phenyl)-10,20-bis(2,2'-bithiophen-5-yl)porphyrin (***t*-H$_2$P-2Th**) as a purple solid (0.148 g, 12%). ^{1}H-NMR ($CDCl_3$) δ –2.67 (s, 2H), 7.14 (dd, *J* = 5.2, 3.6 Hz, 2H), 7.35 (dd, *J* = 5.2, 1.2 Hz, 2H), 7.43 (dd, *J* = 3.6, 1.2 Hz, 2H), 7.59 (d, *J* = 3.6 Hz, 2H), 7.73–7.85 (m, 8H), 8.18–8.26 (m, 4H), 8.86 (d, *J* = 4.8 Hz, 4H), 9.19 (d, *J* = 4.8 Hz, 4H) (**Figure A–12**). Due to low solubility of ***t*-H$_2$P-2Th**, a well-resolved ^{13}C-spectrum could not be obtained. HR-ESI-MS *m/z*: $[M+H]^+$ calcd for $C_{48}H_{30}N_4S_4$, 791.1426; found, 791.1424 (**Figure A–13**); λ_{abs} 429, 520, 561, 594, 656 nm (**Figure A–14**); λ_{em} (λ_{ex} = 429 nm) 671, 730 nm (**Figure A–15**).

3.1.6 5,15-Bis(phenyl)-10,20-bis(2,2'-bithiophen-5-yl)porphyrinatozinc(II) (*t*-ZnP-2Th)

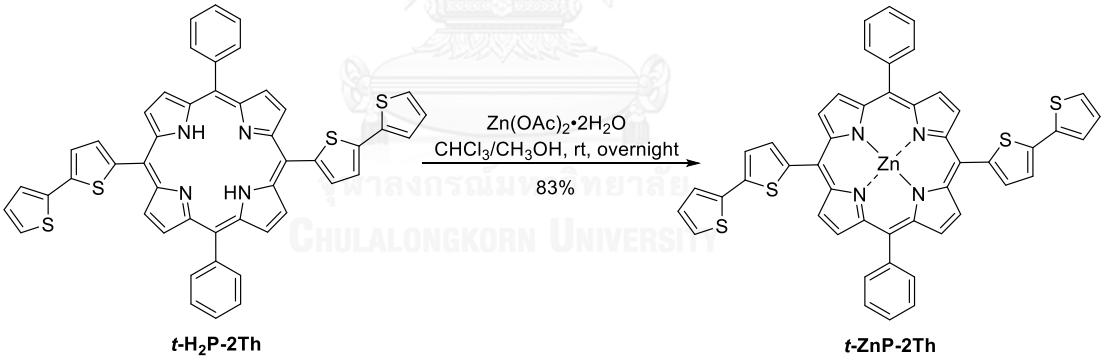

Following a standard metalation method,[70] a solution of ***t*-H$_2$P-2Th** (79 mg, 0.10 mmol, 1 equivalent) in $CHCl_3$ (40 mL) was reacted with a solution of $Zn(OAc)_2{\cdot}2H_2O$ (0.110 g, 0.500 mmol, 5 equivalents) in methanol (5 mL) at room temperature for 12 h. After that, the reaction solution was washed with a 10% aqueous $NaHCO_3$ solution (40 mL), DI water (40 mL) and brine (40 mL), and was dried over anhydrous $MgSO_4$. After removal of the solvents, the crude was purified by a silica column using 1% THF in CH_2Cl_2 as an eluent, followed by washing with hexanes and methanol to afford 5,15-bis(phenyl)-10,20-bis(2,2'-bithiophen-5-yl)porphyrinatozinc(II) (***t*-ZnP-2Th**) as a purple

solid (71 mg, 83%). ^{1}H-NMR (DMSO-d_6) δ 7.22 (dd, J = 5.2, 3.6 Hz, 2H), 7.58 (dd, J = 3.6, 1.2 Hz, 2H), 7.65 (dd, J = 5.2, 1.2 Hz, 2H), 7.76 (d, J = 3.6 Hz, 2H), 7.78–7.88 (m, 6H), 7.90 (d, J = 3.6 Hz, 2H), 8.16–8.24 (m, 4H), 8.81 (d, J = 4.8 Hz, 4H), 9.16 (d, J = 4.8 Hz, 4H) (**Figure A–16**); ^{13}C-NMR (DMSO-d_6) δ 110.9, 121.3, 123.2, 124.3, 125.7, 126.6, 127.6, 128.5, 131.5, 132.0, 134.1, 134.3, 136.3, 138.8, 142.2, 142.4, 149.7, 150.0 (**Figure A–17**); HR-ESI-MS *m/z*: $[M+2H]^+$ calcd for $C_{48}H_{28}N_4S_4Zn$, 854.0645; found, 854.0637 (**Figure A–18**); λ_{abs} (ε) 432 (3.2×10^5), 550, 600 nm (**Figures A–19** and **A–20**); λ_{em} (λ_{ex} = 432 nm) 625 nm (**Figure A–21**).

3.1.7 Ethyl-4,5,6,7-tetrahydroisoindole ester (2)

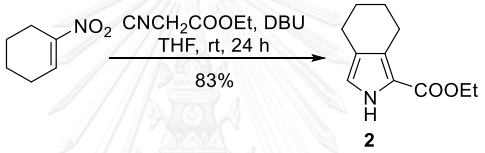

2

Following a previously published procedure,[71] a solution of 1-nitrocyclohexene (1.15 mL, 10.0 mmol, 1 equivalent) and ethyl isocyanoacetate (1.10 mL, 10.0 mmol, 1 equivalent) in THF (40 mL) was treated with 1,8-diazabicyclo[5.4.0]undec-7-ene (DBU) (1.50 mL, 10.0 mmol, 1 equivalent) under N_2 atmosphere at room temperature for 24 h. After the solvent was removed under reduced pressure, the resulting light brown solid was dissolved with CH_2Cl_2 (50 mL). The solution was washed with DI water (50 mL) and brine (50 mL), and dried over anhydrous $MgSO_4$. After removal of the solvents, the crude product was purified by column chromatography (silica, CH_2Cl_2/hexanes = 3:1). The product was recrystallized in hexanes, yielding compound **2** as a colorless crystal (1.126 g, 83%). ^{1}H-NMR ($CDCl_3$) δ 1.34 (t, J = 7.2 Hz, 3H), 1.64–1.82 (m, 4H), 2.54 (t, J = 5.6 Hz, 2H), 2.81 (t, J = 5.6 Hz, 2H), 4.29 (q, J = 7.2 Hz, 2H), 6.64 (s, 1H), 8.75 (br s, 1H) (**Figure A–22**). Other spectroscopic data are consistent with those described in the literatures.[71-72]

3.1.8 8-Phenyl-bis(3-ethoxycarbonyl-4,5,6,7-tetrahydro-*2H*-isoindolyl)methane (3)

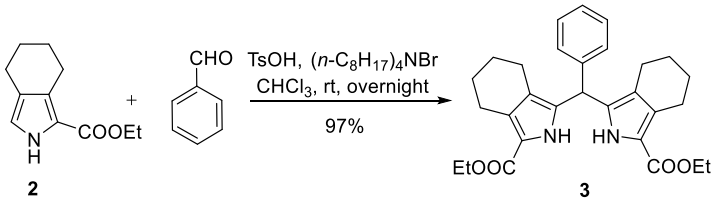

2 3

Following a published method, [73] a solution of isoindole **2** (1.372 g, 7.100 mmol, 2 equivalents) and benzaldehyde (0.36 mL, 3.6 mmol, 1 equivalent) in $CHCl_3$ (70 mL) was treated with *p*-TsOH·H_2O (68 mg, 0.35 mmol, 0.1 equivalent) and then *n*-tetraoctylammonium bromide (78 mg, 0.14 mmol, 0.04 equivalent) at room temperature for 12 h. The resulting light pink solution was washed with a saturated aqueous solution of $NaHCO_3$ (70 mL), DI water (70 mL) and brine (70 mL), and then dried over anhydrous Na_2SO_4. The crude product that was obtained after removal of the solvent was purified by column chromatography (silica, CH_2Cl_2/hexanes = 3:1), leading to compound **3** as an orange crystal (1.629 g, 97%). ^{1}H-NMR ($CDCl_3$) δ 1.31 (t, *J* = 7.2 Hz, 6H), 1.59–1.78 (m, 8H), 2.11–2.22 (m, 4H), 2.79 (t, *J* = 6.0 Hz, 4H), 4.24 (q, *J* = 7.2 Hz, 4H), 5.39 (s, 1H), 7.11 (d, *J* = 7.6 Hz, 2H), 7.26–7.39 (m, 3H), 8.34 (br s, 2H) (**Figure A–23**). Other spectroscopic data are consistent with those described in the literature.[73]

3.1.9 Compound *t*-CuBP-Th

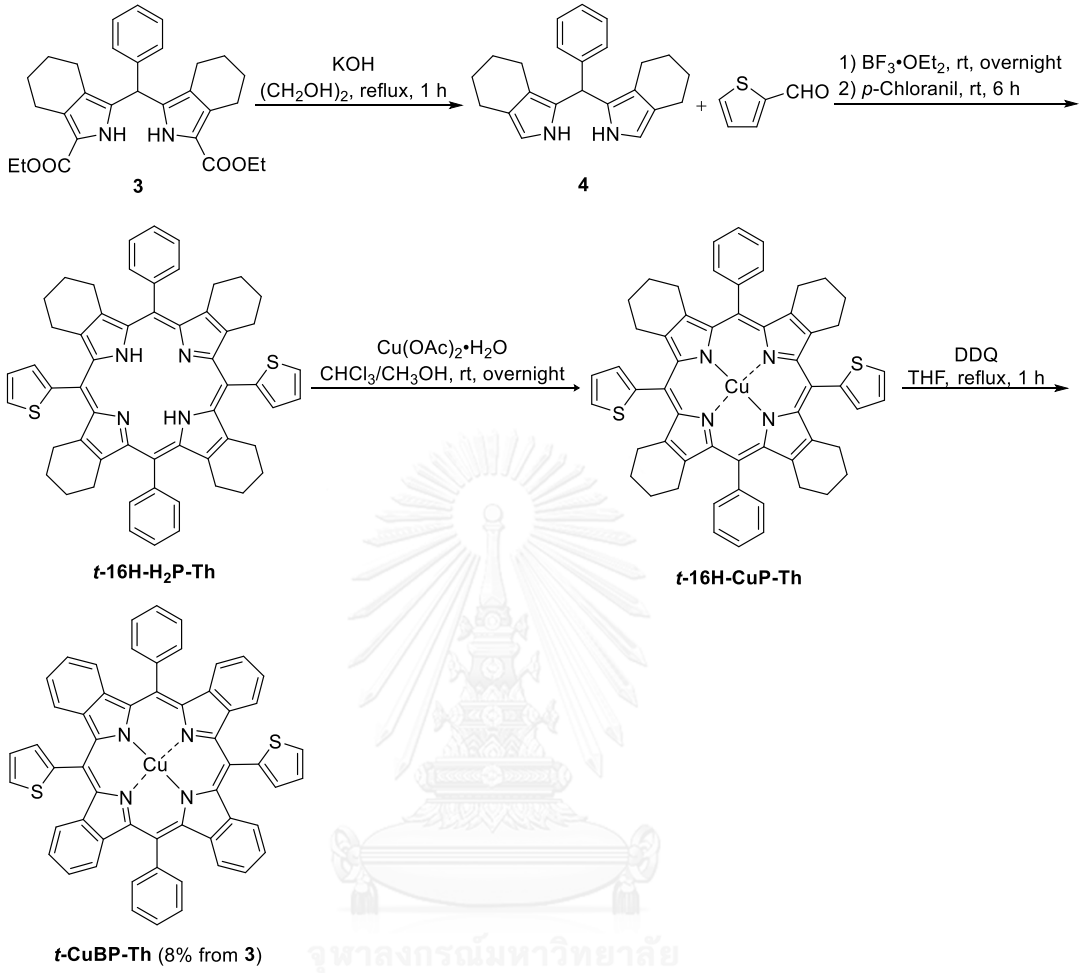

Following a reported procedure,[62] a mixture of dipyrromethane **3** (0.627 g, 1.32 mmol, 1 equivalent) and KOH (0.741 g, 13.2 mmol, 10 equivalents) in ethylene glycol (13 mL) was refluxed for 1 h. After that, the reaction mixture was cooled down to room temperature and diluted with CH_2Cl_2 (25 mL). The resulting solution was washed with DI water (2 × 25 mL) and brine (25 mL), and dried over anhydrous Na_2SO_4. The solution mixture was concentrated under reduced pressure. The crude was redissolved with CH_2Cl_2 (10 mL) and then the solution was passed through a flash silica column using CH_2Cl_2 as an eluent. The pale brown fraction was collected and concentrated to dryness, to afford brown oil containing dipyrromethene **4** (0.417 g) which was immediately used in the next step without further purification.

With a slight modification from a previous procedure,[74] a solution of the resulting oil containing dipyrromethane **4** (0.417 g) in CH_2Cl_2 (50 mL) was treated with 2-thiophene carboxaldehyde (0.130 mL, 1.39 mmol) and $BF_3{\cdot}OEt_2$ (0.016 mL, 0.126 mmol) under N_2 atmosphere at 0 ºC and then the reaction was continued at room temperature for 12 h. After that, *p*-chloranil (0.310 g, 1.26 mmol) was added to the reaction mixture and then the stirring was continued at room temperature for additional 6 h. Subsequently, the reaction mixture was filtered through a pad of silica eluted with EtOAc. After removal of the solvents, the crude product was further purified by column chromatography (silica, CH_2Cl_2 to CH_2Cl_2/EtOAc = 1:1). The purple fraction was concentrated to give a purplish black solid containing ***t*-16H-H_2P-Th** (0.191 g). This solid was treated in the next step without further purification.

According to the standard method,[70] the above-mentioned solid (0.191 g) was dissolved in $CHCl_3$ (60 mL) and treated with a solution of $Cu(OAc)_2{\cdot}H_2O$ (0.300 mg, 1.15 mmol) in methanol (7 mL) at room temperature for 12 h. After that, the solution was washed with a 10% aqueous $NaHCO_3$ solution (60 mL), DI water (60 mL) and brine (60 mL), and dried over anhydrous $MgSO_4$. After removal of the solvent, the resulting crude product was purified by column chromatography (silica, hexanes/CH_2Cl_2 = 1:1), followed by washing with hexanes and methanol under ultrasonic agitation, affording as a dark purple solid containing ***t*-16H-CuP-Th** (0.162 g). MALDI-TOF-MS *m/z* (%): found, 902.841 (100) [M^+]; calcd, 904.694 (M^+; M =$C_{56}H_{48}CuN_4S_2$) (**Figure A–24**). Due to low solubility of this compound, other spectroscopic data could not be obtained properly. This solid was used in the further step immediately.

Following a published procedure,[72] a solution of the resulting solid containing ***t*-16H-CuP-Th** (0.162 g) and DDQ (0.650 g, 2.86 mmol) in THF (100 mL) was refluxed for 90 min. After that, the reaction mixture was cooled down to room temperature and the solvent was removed under reduced pressure. The reaction crude was redissolved with CH_2Cl_2 (100 mL), and the solution was washed with a 10% aqueous solution of Na_2SO_3 (100 mL) and brine (100 mL). The resulting organic layer was dried over $MgSO_4$ and concentrated to dryness. The crude product was purified by a silica column using CH_2Cl_2 as an eluent, followed by washing with hexanes and methanol

under ultrasonic agitation to afford ***t*-CuBP-Th** as a dark green solid (62 mg, 8% from compound **3**). MALDI-TOF-MS *m/z* (%): found, 887.495 [M^+]; calcd, 888.566 (M^+, M = $C_{56}H_{32}CuN_4S_2$) (**Figure A–25**); λ_{abs} 465, 605, 656 nm (**Figure A–26**); Upon excitation at 465 nm, no emission peak was observed (**Figure A–27**).

3.1.10 Compound *t*-H_2BP-Th

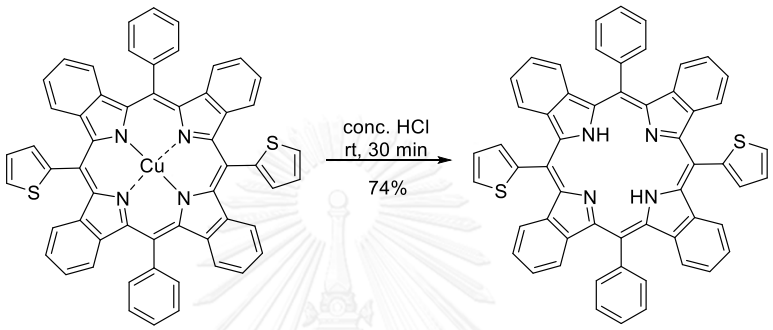

A solution of ***t*-CuBP-Th** (62 mg, 0.070 mmol) in CH_2Cl_2 (120 mL) was treated with conc. HCl (6.50 mL) dropwise at 0 °C. The reaction mixture was then stirred at room temperature for 30 min and the solution was poured into DI water (120 mL). After that, the organic layer was collected, washed with a saturated $NaHCO_3$ solution (2 × 120 mL) and brine (120 mL), dried over anhydrous $MgSO_4$ and concentrated to dryness. The crude was purified by column chromatography (silica, hexanes/CH_2Cl_2 = 1:1), followed by washing with hexanes and methanol under ultrasonic agitation to obtain ***t*-H_2BP-Th** as a green solid (43 mg, 74%). ^{1}H-NMR ($CDCl_3$) δ –1.12 (s, 2H), 6.91–7.35 (m, 16H), 7.59–7.65 (m, 2H), 7.87 (t, *J* = 7.2 Hz, 4H), 7.90–7.98 (m, 4H), 7.99 (m, 2H), 8.36 (br s, 4H) (**Figure A–28**). Due to low solubility of ***t*-H_2BP-Th**, a well-resolved ^{13}C-spectrum could not be obtained. MALDI-TOF-MS *m/z* (%): found, 826.379 (100) [M^+]; calcd, 827.036 (M^+; M = $C_{56}H_{34}N_4S_2$) (**Figure A–29**), λ_{abs} 468, 592, 631, 640, 703 nm (**Figure A–30**); λ_{em} (λ_{ex} = 468 nm) 710, 792 nm (**Figure A–31**).

3.1.11 Compound *t*-ZnBP-Th

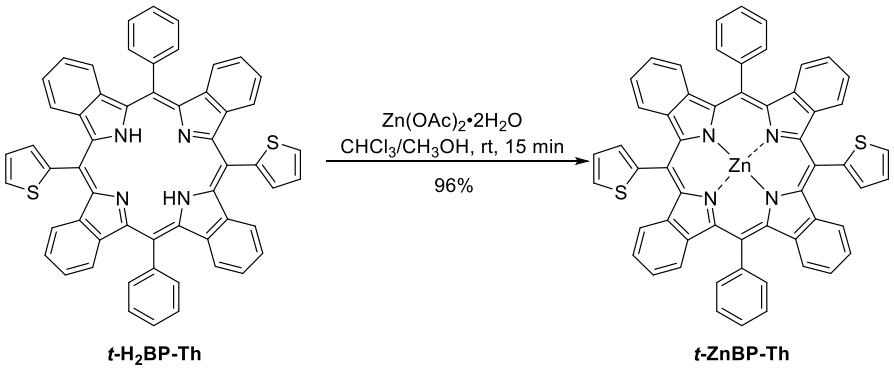

***t*-H_2BP-Th** ***t*-ZnBP-Th**

Following a standard procedure,[70] a solution of ***t*-H_2BP-Th** (43 mg, 0.052 mmol, 1 equivalent) in $CHCl_3$ (52 mL) was reacted with a solution of $Zn(OAc)_2{\cdot}2H_2O$ (57 mg, 0.26 mmol, 5 equivalents) in methanol (6 mL) at room temperature for 15 min. After that, the reaction solution was washed with a 10% aqueous $NaHCO_3$ solution (50 mL), water (50 mL) and brine (50 mL), and dried over anhydrous $MgSO_4$. The solvent was removed under the reduced pressure and the crude product was purified by a silica column using CH_2Cl_2 as an eluent, followed by washing with hexanes and methanol under ultrasonic agitation to obtain ***t*-ZnBP-Th** as a purple solid (44 mg, 96%). ^{1}H-NMR ($CDCl_3$) δ 7.15 (d, *J* = 8.4 Hz, 4H), 7.27–7.34 (m, 4H), 7.34–7.45 (m, 8H), 7.64 (dd, *J* = 5.2, 3.6 Hz, 2H), 7.87 (t, *J* = 7.6 Hz, 4H), 7.90–7.98 (m, 4H), 8.00 (dd, *J* = 5.2, 0.8 Hz, 2H), 8.29 (d, *J* = 7.2 Hz, 4H) (**Figure A–32**); ^{13}C-NMR ($CDCl_3$) δ 108.0, 118.0, 124.2, 124.6, 125.8, 125.9, 128.1, 128.7, 129.1, 129.2, 132.5, 134.3, 138.6, 138.7, 143.1, 143.8, 144.6, 146.0 (**Figure A–33**); HR-ESI-MS *m/z*: $[M]^+$ calcd for $C_{56}H_{32}N_4S_2Zn$, 888.1360; found, 888.1382 (**Figure A–34**); λ_{abs} (ε) 463 (3.0×10^5), 608, 660 (8.1×10^4) nm (**Figures A–35**, **A–36** and **A–37**); λ_{em} (λ_{ex} = 463 nm) 670, 732 nm (**Figure A-38**).

3.1.12 Compound *t*-CuBP-2Th

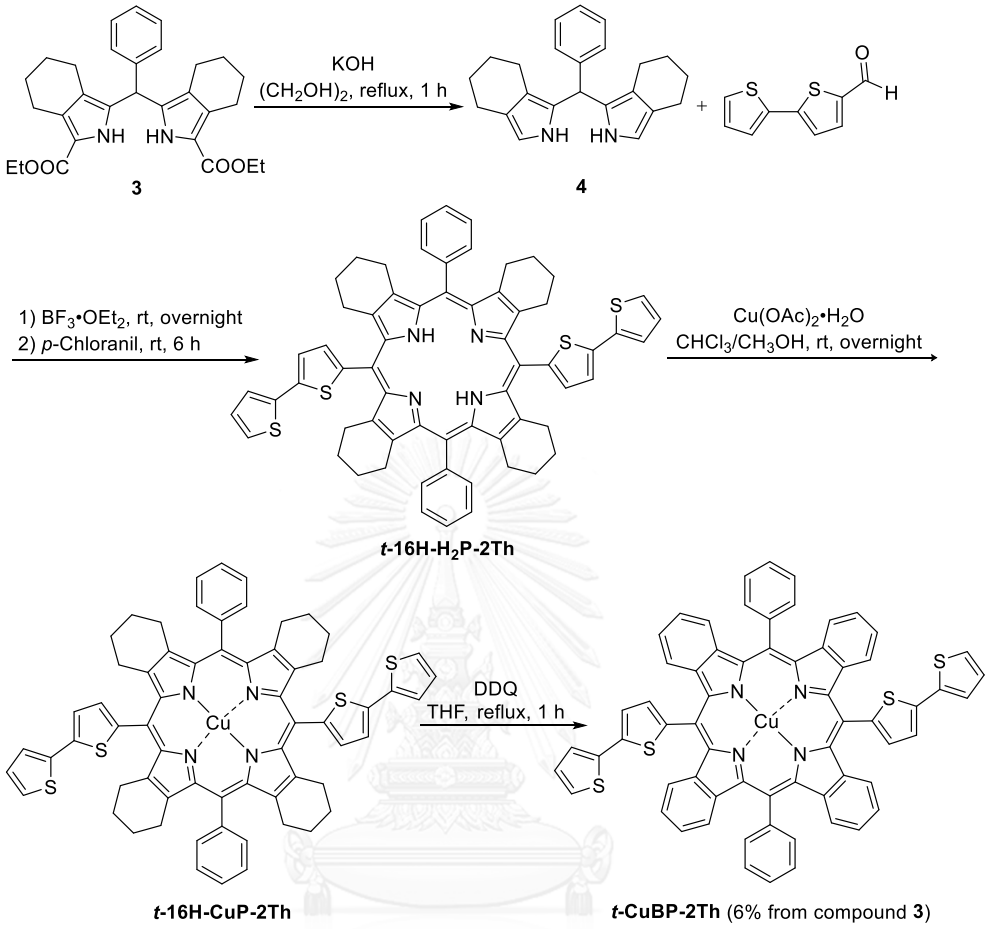

Following a reported procedure[62] and the one described for ***t*-CuBP-Th**, dipyrromethane **3** (1.436 g, 3.02 mmol, 1 equivalent) was reacted with KOH (1.694 g, 30.2 mmol, 10 equivalents) in ethylene glycol (30 mL) under reflux for 1 h. Brown oil containing dipyrromethene **4** (0.970 g) was obtained and immediately used in next step without purification.

Following a previously reported procedure with a slight modification[74] and the method described for ***t*-CuBP-Th**, a solution of dipyrromethane **4** (0.970 g) in CH_2Cl_2 (120 mL) was treated with 2,2'-bithiophene-5-carboxaldehyde (0.626 g, 3.22 mmol) and $BF_3{\cdot}OEt_2$ (37 μL, 0.29 mmol). After the further treatment with *p*-chloranil (1.081 g, 4.395 mmol), the resulting mixture was passed through a pad of silica eluted with a solution of 10% THF in CH_2Cl_2 and subjected to column chromatography (silica,

CH_2Cl_2/EtOAc = 1:1) to obtain a purplish black solid containing ***t*-16H-H_2P-2Th** (0.481 g). The crude solid was used in the next step without further purification.

According to the standard metalation procedure[70] and that described for ***t*-CuBP-Th**, the solid containing ***t*-16H-H_2P-2Th** (0.481 g) was dissolved in $CHCl_3$ (120 mL) and reacted with a solution of $Cu(OAc)_2 \cdot H_2O$ (0.479 g, 2.40 mmol) in methanol (15 mL) at room temperature for 12 h. After a work-up process, the resulting crude product was purified by a silica column (hexanes/CH_2Cl_2 = 1:3) and washed with hexanes and methanol under ultrasonic agitation, affording a dark purple solid containing ***t*-16H-CuP-2Th** (0.311 g). MALDI-TOF-MS *m/z* (%): found, 1067.380 [M^+]; calcd, 1068.934 (M^+, M = $C_{64}H_{52}CuN_4S_4$) (**Figure A–39**). Due to low solubility of this compound, the other spectroscopic data could not be obtained properly. This solid was used in the demetallation step immediately.

Following a reported procedure[72] and the one described for ***t*-CuBP-Th**, the solid containing ***t*-16H-CuP-2Th** (0.311 g) was reacted with DDQ (1.051 g, 4.63 mmol) in THF (200 mL) under reflux for 1 hour. After a work-up process, purification by column chromatography (silica, CH_2Cl_2) and washing with hexanes and methanol under ultrasonic agitation, ***t*-CuBP-2Th** was obtained as a dark green solid (90 mg, 6% from compound **3**). MALDI-TOF-MS *m/z* (%): found, 1051.584 [M^+]; calcd, 1052.806 (M^+, M = $C_{64}H_{36}CuN_4S_4$) (**Figure A–40**); λ_{abs} 461, 655 nm (**Figure A–41**). Upon excitation at 461 nm, no significant emission peak was observed (**Figure A–42**).

3.1.13 Compound *t*-H_2BP-2Th

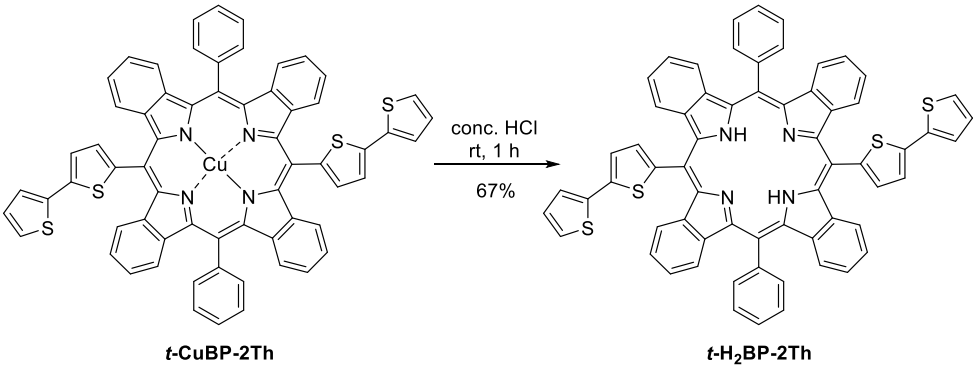

Following a demetalation procedure described for ***t*-H_2BP-Th**, a solution of ***t*-CuBP-2Th** (99 mg, 0.094 mmol) in CH_2Cl_2 (150 mL) was reacted with conc. HCl (10 mL) at 0 °C and the reaction mixture was stirred at room temperature for 1 hour. After a work-up process, purification by a silica column (hexanes/CH_2Cl_2 = 1:1) and washing with methanol under ultrasonic agitation, ***t*-H_2BP-2Th** was yielded as a green solid (62 mg, 67%). ^{1}H-NMR ($CDCl_3$) –1.09 (s, 2H), 6.98–7.19 (m, 4H), 7.14–7.19 (m, 2H), 7.28–7.83 (m, 12H), 7.38 (d, *J* = 4.8 Hz, 2H), 7.48 (d, *J* = 3.2 Hz, 2H), 7.71 (d, *J* = 3.2 Hz, 2H), 7.83–7.91 (m, 6H), 7.91–7.98 (m, 2H), 8.37 (br s, 4H) (**Figure A–43**). Due to low solubility of ***t*-H_2BP-2Th**, a well-resolved ^{13}C-spectrum could not be obtained. MALDI-TOF-MS *m/z* (%): found, 990.903 [M^+]; calcd, 991.276 (M^+, M = $C_{60}H_{38}N_4S_4$) (**Figure A–44**), λ_{abs} 476, 594, 633, 644, 705 nm (**Figure A–45**); λ_{em} (λ_{ex} = 476 nm) 713, 795 nm (**Figure A–46**).

3.1.14 Compound *t*-ZnBP-2Th

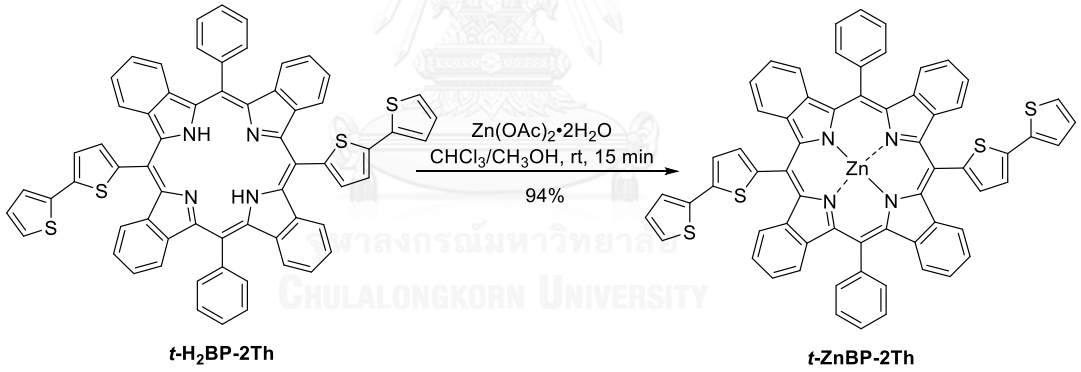

Following a standard metalation procedure[70] and that described for ***t*-ZnBP-Th**, a solution of ***t*-H_2BP-2Th** (24 mg, 0.024 mmol, 1 equivalent) in $CHCl_3$ (25 mL) was treated with a solution of $Zn(OAc)_2{\cdot}2H_2O$ (26 mg, 0.12 mmol, 5 equivalent) in methanol (3 mL) at room temperature for 15 min. After a work-up step and purification by a silica column (CH_2Cl_2) followed by washing with hexanes and methanol under ultrasonic agitation, ***t*-ZnBP-2Th** was obtained as a bluish green solid (24 mg, 94%). ^{1}H-NMR ($CDCl_3$) δ 7.12–7.20 (m, 6H), 7.28–7.34 (m, 4H), 7.36–7.39 (m, 2H), 7.39–7.45 (m, 4H), 7.45–7.49 (m, 2H), 7.73 (d, *J* = 3.6 Hz, 2H), 7.78 (d, *J* = 8.0 Hz, 4H), 7.83 (d, *J* = 3.6 Hz, 2H), 7.84–7.91 (m, 4H), 7.92–7.98 (m, 2H), 8.30 (br s, 4H) (**Figure A–47**); ^{13}C-NMR

($CDCl_3$) δ 107.6, 118.1, 124.4, 124.4, 124.6, 124.8, 126.0, 126.1, 128.2, 129.1, 129.2, 133.4, 134.3, 137.9, 138.4, 138.7, 140.8, 143.0, 143.9, 144.6, 144.7 (**Figure A–48**); HR-ESI-MS *m/z*: $[M]^+$ calcd for $C_{64}H_{36}N_4S_4Zn$, 1054.1100; found, 1054.1124 (**Figure A–49**); λ_{abs} (ε) 470 (2.3×10^5), 615, 663 (6.3×10^4) nm (**Figures A–50**, **A–51** and **A–52**); λ_{em} (λ_{ex} = 470 nm) 674, 739 nm (**Figure A–53**).

3.2 Electrochemical studies

3.2.1 Electrochemical properties study

Electrochemical properties of ***t*-ZnP-Th**, ***t*-ZnP-2Th**, ***t*-ZnBP-Th** and ***t*-ZnBP-2Th** were determined by cyclic voltammetry in acetonitrile containing 0.1 M tetrabutylammonium hexafluorophosphate ($TBAPF_6$) by using a ITO-coated glass working electrode, a Pt wire counter electrode and a silver chloride coated on a silver wire (Ag/AgCl) quasi-reference electrode (QRE) with scan rate of 10 $mV{\cdot}s^{-1}$. The resulting redox potentials were externally calibrated with a ferrocene/ferrocenium couple of which the potential value of 0.69 V vs. normal hydrogen electrode (NHE) was used.[75] The value of the NHE vs. vacuum level used in this work is –4.75 eV.[76]

3.2.2 Electropolymerization studies

Followed a previous study,[65] electropolymerization of **ZnP-2Th**, ***t*-ZnP-2Th** and ***t*-ZnBP-2Th** were performed by cyclic voltammetry in CH_2Cl_2 solution containing 0.1 M $TBAPF_6$ as a supporting electrolyte solution with a three-electrode system. An ITO-coated glass was used as a working electrode and a substrate for the polymer film. A Pt plate and silver chloride coated on a silver wire (Ag/AgCl) were used as a counter electrode and a QRE, respectively. Polymerization was electrochemically carried out under N_2 atmosphere by cyclic potential between 0 mV to 1600 mV vs. Ag/AgCl QRE with the scan rate of 50 $mV{\cdot}s^{-1}$ and the number of scanning cycles of 10.

CHAPTER IV
RESULTS AND DISCUSSION

This research mainly focuses on synthesis, characterization and investigation of photophysical and electrochemical properties of novel *trans*-A_2B_2-porphyrins and benzoporphyrins bearing phenyl and thienyl or bithiophenyl *meso*-substituents. The target compounds bearing the thiophene-based *meso*-groups were subjected to electropolymerize. The photophysical and electrochemical properties of the target monomers (***t*-ZnP-Th**, ***t*-ZnP-2Th**, ***t*-ZnBP-Th** and ***t*-ZnP-Th**) and the resulting polymer films (poly(**ZnP-2Th**) and poly(***t*-ZnP-2Th**)) were then investigated. Thus, in this chapter, the contents were divided into three sections, including synthesis and characterization of the target monomers, the photophysical properties of the target monomers and the electrochemical polymerization and the investigation of electrochemical and photophysical properties of the resulting films.

4.1 Synthesis and characterization of the *trans*-A_2B_2-porphyrin and the *trans*-A_2B_2-benzoporphyrin derivatives

4.1.1 Synthesis of the *trans*-A_2B_2-porphyrin derivatives

The synthesis of target *trans*-A_2B_2-porphyrins started with the synthesis of dipyrromethene **1** as a starting material through condensation between benzaldehyde and an excess amount of pyrrole with a catalytic amount of trifluoroacetic acid as reported by Lindsey *et al*. (**Scheme 4–1**).[69] However, based on thin-layer chromatography (TLC) analysis, the resulting crude product could not be completely purified due to the production of oligo- and polypyrrole byproducts as a result of the use of the high concentration of pyrrole. Thus, the reaction was alternatively carried out in a HCl aqueous medium containing 1 equivalent of benzaldehyde and 3 equivalents of pyrrole, according to another reported procedure.[68] After column chromatography and recrystallization, dipyrromethane **1** was obtained in good purity with a yield of 71%. From its ^{1}H-NMR spectrum, 2 protons at pyrrolic N-H sites gave a broad singlet at 7.93 ppm, while two multiplet and a doublet of doublet signals were

observed for other 6 pyrrolic protons at around 5.86–6.84 ppm. Moreover, a multiplet signal at 7.19–7.37 ppm and a broad singlet signal at 5.48 ppm were observed, indicating five phenylic protons and a proton at the *meso*-position, respectively.

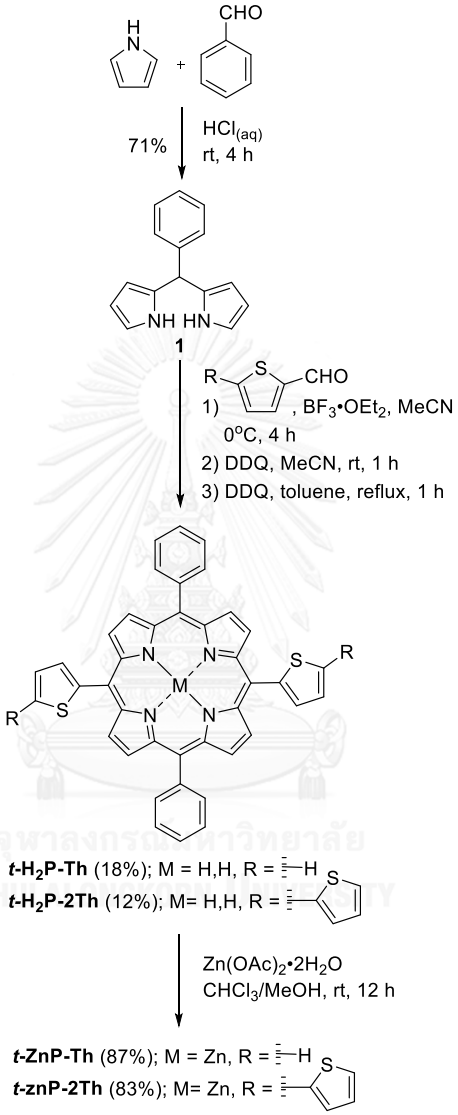

Scheme 4–1: Synthesis of *trans*-A_2B_2-porphyrins ***t*-ZnP-Th** and ***t*-ZnP-2Th**.

The first attempt of the synthesis of ***t*-H_2P-Th** and ***t*-H_2P-2Th** was made through the standard Lindsey's condition under catalysis of trifluoroacetic acid or $BF_3{\cdot}OEt_2$ in a common organic solvent, like CH_2Cl_2, at room temperature.[58] However, based on a MALDI-TOF mass spectrum of the resulting crude product, the reaction gave a mixture of porphyrin derivatives which were difficult to separate from each other by column

chromatography. It is likely that undesired products were produced from a substituent scrambling reaction which is known to be problematic when a dipyrromethane bearing a non-steric *meso*-substituent, for example 5-phenyldipyrromethane, is used.[61] **Scheme 4–2** illustrates mechanism of the scrambling process in a porphyrinogen formation. The mechanism consists of two steps, which are acidolysis and fragment recombination.[77]

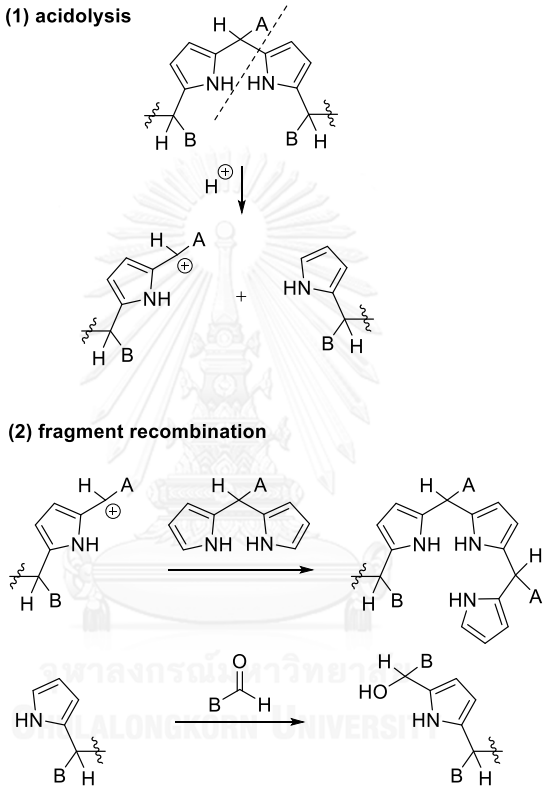

Scheme 4–2: Mechanism of substituent scrambling of porphyrin in an acidic condition.

To suppress the production of the undesired porphyrinic product, a milder condition was required, i.e. in case of non-steric dipyrromethane, lower reaction temperature together with addition of an inorganic salt, i.e. NH_4Cl.[61] This mild condition can slow down the rate of the condensation leading to low scrambling products, although the yield of desired product could be lower. As expected, ***t*-H_2P-Th** and ***t*-H_2P-2Th** were successfully synthesized through acid-catalyzed condensation reaction between dipyrromethane **1** and a corresponding aldehyde in acetonitrile solution

containing $BF_3{\cdot}OEt_2$ and NH_4Cl at 0 ºC for 4 h, followed by oxidation by DDQ. After purification by column chromatography, ***t*-H_2P-Th** and ***t*-H_2P-2Th** were afforded in 18% and 12%, respectively. Nevertheless, the yields of product were moderate as a result of the production of the pyrrolic oligomers as evidenced by the presence of dark brown spot at baseline on a TLC plate.

Based on a ^{1}H-NMR spectrum of ***t*-H_2P-Th**, a characteristic singlet signal of its inner protons was observed at –2.72 ppm. This low chemical shift was caused by shielding effect from circulated **π**-electrons of the porphyrin core. Two β protons on each pyrrole ring gave two doublet signals at 8.84 and 9.05 ppm, while aromatic protons of the thienyl and phenyl units were found at around 7.51–8.25 ppm. In case of ***t*-H_2P-2Th**, its 8 pyrrolic protons and 10 phenylic protons gave the similar signal as those of ***t*-H_2P-Th**, while 10 protons of the bithiophenyl groups were observed at around 7.14–7.85 ppm. Additionally, the inner protons of ***t*-H_2P-2Th** were found at –2.67 ppm which was slightly deshielded, compared with those of ***t*-H_2P-Th**. The observation is attributed to the decreas in ring current over the porphyrin ring from electron delocalization to the bithiophenyl substituents. Besides, HR-ESI mass spectra also confirmed the formation of ***t*-H_2P-Th** and ***t*-H_2P-2Th** by showing their molecular ion peaks at *m/z* 627.1677 and 791.1424, respectively.

To obtain desired ***t*-ZnP-Th** and ***t*-ZnP-2Th**, subsequent zinc-metallation of the corresponding freebase porphyrins were performed by the reaction with $Zn(OAc)_2{\cdot}2H_2O$ in $CHCl_3$/MeOH at room temperature overnight. ***t*-ZnP-Th** and ***t*-ZnP-2Th** were obtained in 87% and 83% yield, respectively. The formation of ***t*-ZnP-Th** and ***t*-ZnP-2Th** was also confirmed by their HR-ESI mass spectra exhibiting the molecular ion peaks at *m/z* 689.0802 and 854.0645, respectively. In addition, the complete metallation of the freebase precursors was proven by disappearance of the peaks of the inner protons in their ^{1}H-NMR spectra, together with the absence of an emission peak at 723 nm for ***t*-ZnP-Th** and the one at 730 nm for ***t*-ZnP-2Th**.

4.1.2 Synthesis of the *trans*-A_2B_2-benzoporphyrin derivatives

trans-A_2B_2-Benzoporphyrin derivatives can be achieved through a series of reaction shown in **Schemes 4–3** and **4–4**.

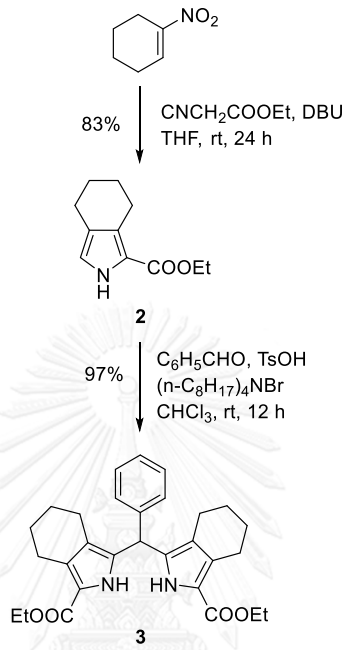

Scheme 4–3: Synthesis of compound **3**.

As a starting material of the entire synthetic route, tetrahydroisoindole ester **2** was prepared from Barton-Zard reaction between readily available 1-nitrocyclohexene and ethyl isocyanoactate in the presence of DBU as a base.[71] The formation of compound **2** was confirmed by a characteristic broad singlet peak of an N-H proton of the pyrrole ring at 8.75 ppm, and a triplet peak at 1.34 ppm and a quartet peak at 4.29 ppm indicating an ethyl ester group. After that, condensation between the resulting tetrahydroisoindole ester **2** and benzaldehyde was performed in the presence of *p*-TsOH as an acid catalyst and anhydrous (n–C_8H_{17})$_4$NBr as a water scavenger.[73] The successful synthesis of dipyrromethane **3** was confirmed by its ^{1}H-NMR spectra showing a broad singlet peak of the N-H proton of the pyrrole ring at 8.34 ppm, a broad singlet peak at 5.39 ppm of its *meso*-proton, together with a quartet and a triplet signals of five protons of the ethyl ester group at 4.24 and 1.31 ppm, respectively. Moreover, the aromatic protons of the phenyl group were found at around 7.11–7.39 ppm.

Compound **3** was further converted to 1,9-unsubstituted dipyrromethane **4** by decarboxylation with KOH in refluxing ethylene glycol for an hour, followed by passing a pad of silica.[62] The resulting dipyrromethane **4** was immediately used in the next step to avoid self-oligomerization at its 1- and 9-positions. Compound **4** was reacted with thiophene carboxaldehyde or 2,2'-bithiophene carboxaldehyde in the presence of $BF_3{\cdot}OEt_2$, followed by oxidation with *p*-chloranil to form **16H-H_2P-Th** or ***t*-16H-H_2P-2Th**, respectively.[74] The crude mixture was passed through a pad of silica with gradient elution to greenish brown fractions containing the desired freebase porphyrin. According to a previous study,[72] freebase tetracyclohexanoporphyrin could not be easily aromatized by normal oxidants i.e. *p*-chloranil and DDQ, even after several hours under reflux, possibly due to rapid formation of dication species upon addition of oxidants. Unlike the freebase porphyrins that have high proton affinity, bivalent metal complexes of the porphyrins, such as of Cu-, Ni- and Pd-porphyrins can be readily oxidized into corresponding tetrabenzoporphyrins by the conventional oxidants. Thus, these bivalent metals are suitable to use as a template for the synthesis of benzoporphyrin. There are two criteria for choosing an effective metal template: (1) the metal has to give stable complex with tetracyclohexanoporphyrin during aromatization reaction, and (2) the resulting complex is required to be labile enough to perform demetallation reaction later on. Among several metals, copper is one of the most effective metals, according to its complexes which were stable enough in aromatization step and also copper can be removed from tetrabenzoporphyrins without destroying macrocycles.[72]

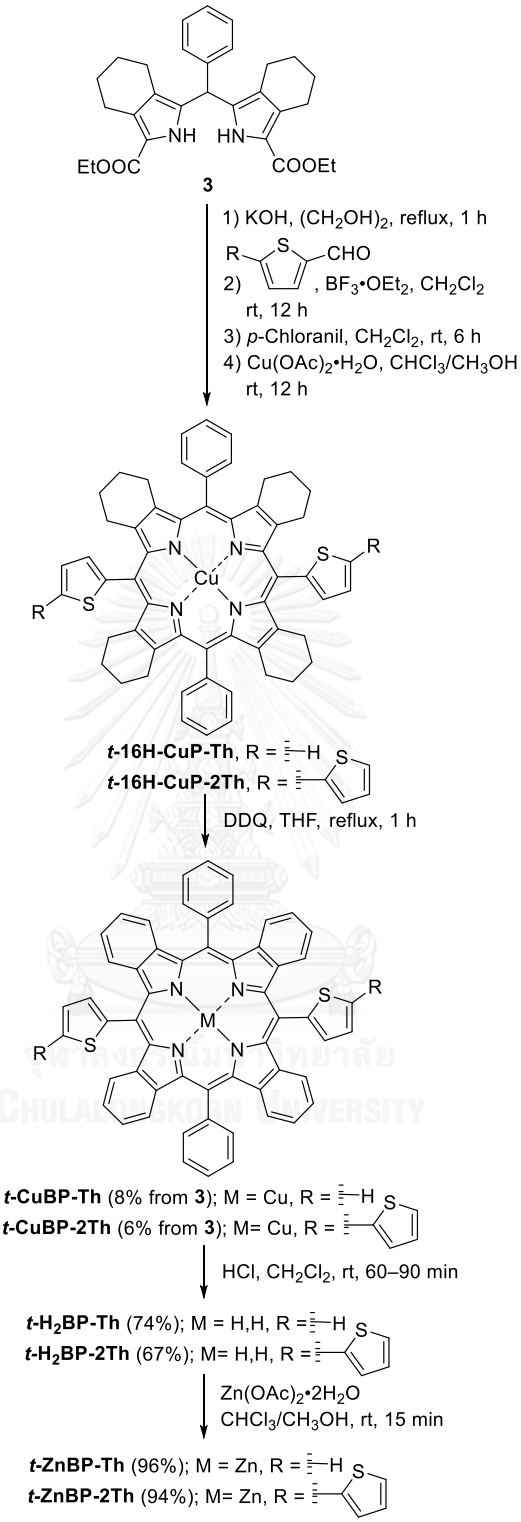

Scheme 4–4: Synthesis of *trans*-A_2B_2-benzoporphyrins ***t*-ZnBP-Th** and ***t*-ZnBP-2Th**.

As above discussion, the subsequent copper-metallation of the crude of the freebase tetracyclohexanoporphyrins by reacting with $Cu(OAc)_2{\cdot}H_2O$ was carried out at

room temperature overnight, affording copper metalloporphyrins ***t*-16H-CuP-Th** and ***t*-16H-CuP-2Th**. The MALDI-TOF mass spectra confirmed the formation of ***t*-16H-CuP-Th** and ***t*-16H-CuP-2Th** by showing their molecular ion peaks at *m/z* 902.841 and 1068.934, respectively. These complexes were subsequently aromatized by refluxing with DDQ in THF for an hour, affording ***t*-CuBP-Th** and ***t*-CuBP-2Th** in 8% and 6% overall yield from compound **3**, respectively. The low yields were resulted from oligomerization of dipyrromethane and formation of other *N*-fused compounds in the porphyrin formation step, together with the breaking of the macrocycles during the DDQ-oxidation step. The MALDI-TOF mass spectra showed the molecular ion peaks at *m/z* 887.495 for ***t*-CuBP-Th** and 1051.112 for ***t*-CuBP-2Th**.

Demetallation of copper-benzoporphyrins ***t*-CuBP-Th** and ***t*-CuBP-2Th** was performed by treating with conc. HCl in CH_2Cl_2 at room temperature for 60–90 min. Instead of using H_2SO_4 as reported in a previous procedure,[72] conc. HCl was chosen in order to prevent undesired side reactions, e.g. sulfonation of thiophene units.[78] The desirable freebase benzoporphyrins ***t*-H_2BP-Th** and ***t*-H_2BP-2Th** were obtained in 74% and 67%, respectively. The formation of ***t*-H_2BP-Th** and ***t*-H_2BP-2Th** were confirmed by their molecular ion peaks in the MALDI-TOF mass spectra at *m/z* 826.379 and 990.903, respectively. In a ^{1}H-NMR spectrum of ***t*-H_2BP-Th**, a broad singlet signal of 2 inner protons was observed at –1.12 ppm and its 16 aromatic protons on the β-fused phenyl rings exhibited a multiplet signal at 6.91–7.35 ppm. Its spectrum also showed a multiplet signal of 2 3-thiophene protons at 7.90–7.99 ppm, a multiplet signal of 2 4-thiophene protons at 7.59–7.65 ppm and a doublet signal of 2 5-thiophene protons at 7.99 ppm. Moreover, a signal of *p*-phenylic protons was found at 7.90–7.99 ppm while *o*- and *m*-phenylic protons gave a broad singlet at 8.36 ppm and a triplet at 7.87 ppm, respectively. These results indicated that the anisotropic effect of the benzoporphyrin core was more influenced to *o*-phenylic protons, compared with other phenylic protons, likely to be because the phenyl ring was reportedly almost perpendicular to a plane of the benzoporphyrin core,[72] causing the *o*-phenylic protons to protrude into the benzoporphyrin plane. In a similar manner, a ^{1}H-NMR spectrum of ***t*-H_2BP-2Th** exhibited a broad singlet of 2 inner N-H protons at –1.13 ppm, a

multiplet peak of 16 protons of *β*-fused phenyl rings at 6.98–7.83 ppm. Moreover, bithiophenyl protons gave 3 doublet and 2 multiplet signals in the range of 7.14–7.91 ppm, while phenylic protons gave a broad singlet and 2 multiplet signals at 7.83–8.37 ppm.

To obtain the target compounds, the freebase benzoporphyrins ***t*-H_2BP-Th** and ***t*-H_2BP-2Th** were zinc-metallated with $Zn(OAc)_2 \cdot 2H_2O$ in $CHCl_3$/MeOH at room temperature for 15 min, affording ***t*-ZnBP-Th** and ***t*-ZnBP-2Th** in 96% and 94%, respectively. The complete metallation reaction was confirmed by the disappearance of emission peak of the freebase benzoporphyrins at 792 nm, in case of ***t*-H_2BP-Th**, and 795 nm, in case of ***t*-H_2BP-2Th**, as well as absence of their inner protons in their ^{1}H-NMR spectra. Additionally, the HR-ESI mass spectra showed the molecular ion peaks at *m/z* 888.1382 and 1054.1124 for ***t*-ZnBP-Th** and ***t*-ZnBP-2Th**, respectively.

4.2 Investigation of photophysical properties

The absorption and emission spectra of the target *trans*-A_2B_2-porphyrins and *trans*-A_2B_2-benzoporphyrins were recorded in toluene at room temperature and shown in **Figure 4–1** and **Figure 4–3**.

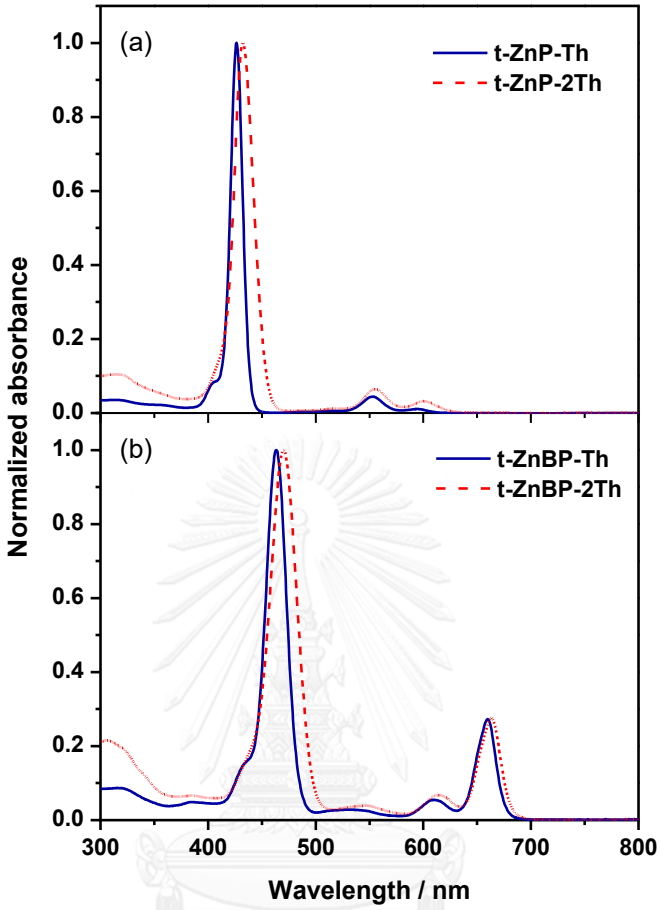

Figure 4–1: Normalized absorption spectra of the target a) *trans*-A_2B_2-porphyrins and b) *trans*-A_2B_2-benzoporphyrins.

The absorption spectra of all target porphyrins and benzoporphyrins exhibited characteristic peaks including an intense Soret band in the range of 400–500 nm and Q-bands at 500–700 nm. The absorption data of all target compounds are summarized in **Table 4–1**.

Table 4–1. Photophysical properties of the target porphyrins and benzoporphyrins

Compound	λ_{abs} / nm (ε / L·mol^{-1}·cm^{-1})		λ_{em} / nm
	Soret-band	Q-bands	
ZnP-Ph[a]	422 (2.55×10^5)	548[b], 588[b]	596, 647
***t*-ZnP-Th**	426 (4.7×10^5)	554[b], 594[b]	607, 653
***t*-ZnP-2Th**	432 (3.2×10^5)	550[b], 600[b]	625
ZnBP-Ph[c]	461 (2.8×10^5)	607[b], 652[b]	658, 724
***t*-ZnBP-Th**	463 (3.0×10^5)	608[b], 660 (8.1×10^4)	670, 732
***t*-ZnBP-2Th**	470 (2.3×10^5)	615[b], 663 (6.3×10^4)	674, 739

[a]Data was reported for a toluene solution in a previous study.[79]

[b]Due to low absorption, the ε value could not be determined.

[c]Data was reported for a toluene solution in a previous study.[80]

The results show that the absorption maxima ($\lambda_{abs,max}$) of the benzoporphyrin derivatives were shifted to the higher wavelength by 37–39 nm, compared with those of the porphyrin analog bearing the same *meso*-substituents. This observation directly resulted from extended π-conjugation system at the β-positions of the porphyrin core. Upon the replacement of the phenyl *meso*-groups with the thienyl ones on the macrocycles, $\lambda_{abs,max}$ was red shifted by 2–4 nm, as seen from a comparison of $\lambda_{abs,max}$ of **ZnP-Ph** with that of ***t*-ZnP-Th** and $\lambda_{abs,max}$ of ***t*-ZnBP-Ph** with that of ***t*-ZnBP-Th**. The replacement of the phenyl *meso*-substituents with the thienyl ones led to more efficient electronic communication between the porphyrin macrocycle and the thienyl ring, compared with the porphyrin core where the phenyl *meso*-groups are attached.[79] This is because the steric interaction between *o*-phenylic hydrogens and β-pyrrolic hydrogens of the porphyrins or hydrogens on exocyclic phenyl rings of benzoporphyrins prevents the co-planarity and suppresses the π-conjugation between the macrocycles and the *meso*-substituents as shown in **Figure 4–2**.[81] Moreover, the reduction of steric hindrance caused by smaller ring size of the thienyl

ring should lead to possible co-planarity between the macrocycle and the thiophene ring and therefore, should facilitate the delocalization of the π-electrons between two systems.

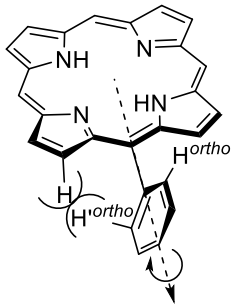

Figure 4–2: Illustration of the steric interaction between *o*-phenylic hydrogens and β-pyrrolic hydrogens.

The effect of the introduction of the additional thiophene rings on the α-positions of the thienyl groups of ***t*-ZnP-Th** and ***t*-ZnBP-Th** can be determined by comparing $\lambda_{abs,max}$ of ***t*-ZnP-2Th** with that of ***t*-ZnP-Th** and $\lambda_{abs,max}$ of ***t*-ZnBP-2Th** with that of ***t*-ZnBP-Th**. The results reveal that the addition of another thienyl ring resulted in the bathochromic shift of $\lambda_{abs,max}$ by 6–7 nm. These observations were consistent with those described in the literature reporting that the extended π-conjugation at the β-positions of the macrocycle, the replacement of the phenyl *meso*-groups with the thienyl units and the introduction of the additional thiophene ring at the α-position of the thienyl *meso*-groups led to the red shift of $\lambda_{abs,max}$.[67]

To confirm this explanation, a crystal structure of bis(methanol)[5,15-Bis(phenyl)-10,20-bis(thiophen-2-yl)porphyrinato]zinc(II) (***t*-ZnP-Th(MeOH)$_2$**) obtained from recrystallization of ***t*-ZnP-Th** $CHCl_3$/methanol was investigated (**Figure 4–3**). Zinc atom of ***t*-ZnP-Th** was found to be weakly bound to methanol molecules (Zn-O = 2.412 Å). To compare the orientation of the phenyl and the thienyl *meso*-substituents in the crystal, dihedral angles between their planes and that of the porphyrin core were determined. In case of the phenyl group, the dihedral angles were obtained from considering C6-C5-C21-C26 and C4-C5-C21-C22 bonds and found to be 70.9° and 71.45°, respectively. These results are consistent with the reported dihedral angles of

a toluene solvate of tetraphenylporphinatozinc(II) (68.0° and 71.7°).[82] The dihedral angles between the thienyl and the porphyrin planes were determined from C1-C10-C27-C30 bond and found to be 60.99°. The results reveal that the thienyl ring is more co-planar with the macrocycle than the phenyl one.

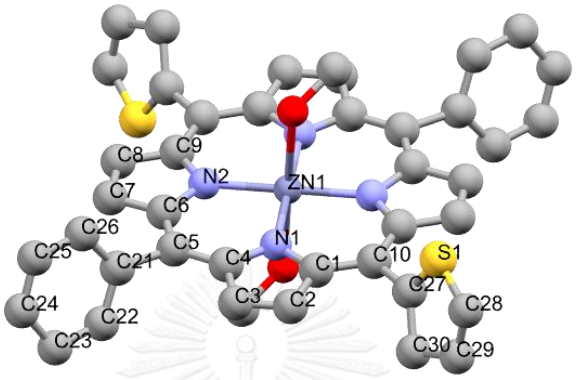

Figure 4–3: The structure of ***t*-ZnP-Th(MeOH)$_2$**, showing the 50% probability displacement ellipsoids and the atom-numbering scheme of the asymmetric unit. Hydrogen atoms have been omitted for clarity.

The effect of the thiophene-based *meso*-substituents on the emission properties of the target compounds was also studied. Upon the excitation at absorption maxima, all emission spectra recorded in toluene at room temperature are shown in **Figure 4–4** and the emission data are summarized in **Table 4–1**. The emission maxima ($\lambda_{em,max}$) of the benzoporphyrins were redshifted by 49–63 nm, compared to those of porphyrins bearing the similar *meso*-groups. This observation resulted from the extended π-conjugation system at the β-positions of the porphyrin core. Moreover, the effect of the replacement of the phenyl *meso*-substituents with the thienyl ones was determined by comparing $\lambda_{em,max}$ of ***t*-ZnP-Th** with that of **ZnP-Ph** and $\lambda_{em,max}$ of ***t*-ZnBP-Th** with that of **ZnBP-Ph**. The thienyl-substituted derivatives gave the red shift of $\lambda_{em,max}$ by 11–12 nm, compared with the phenyl-substituents ones. Additionally, the introduction of the additional thiophene ring on the α-positions of the thienyl *meso*-groups gave the red shift of $\lambda_{em,max}$ by 4–18 nm as seen from a comparison of $\lambda_{em,max}$ of ***t*-ZnP-2Th** with that of ***t*-ZnP-Th** and $\lambda_{em,max}$ of ***t*-**

ZnBP-2Th with that of ***t*-ZnBP-Th**. These results were also consistent with the previous report. [67]

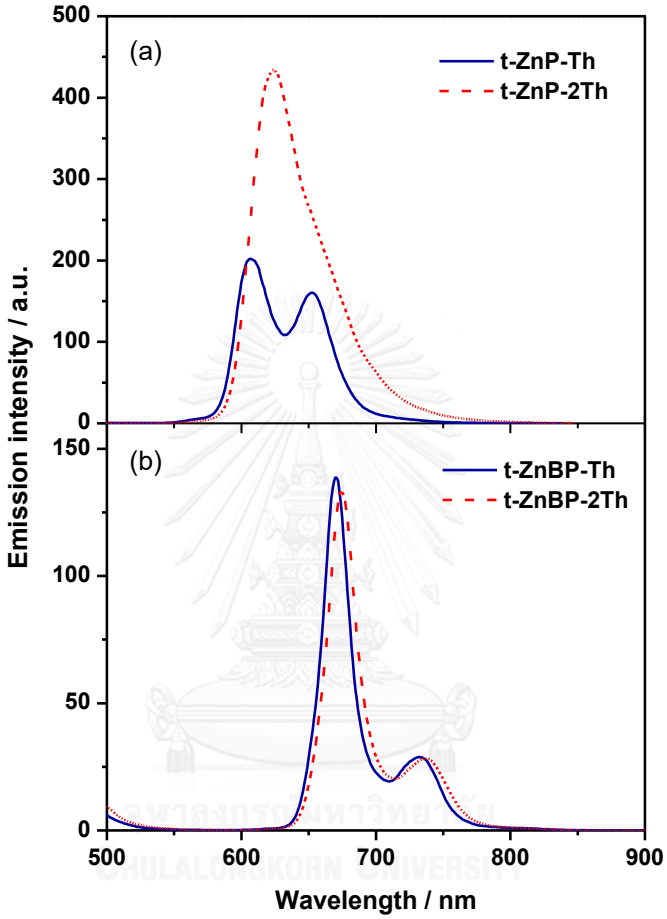

Figure 4–4: Emission spectra of the target a) *trans*-A_2B_2-porphyrins and b) *trans*-A_2B_2-benzoporphyrins.

4.3 Electrochemical studies

4.3.1 Investigation of electrochemical properties of the target monomers

Since a goal of this research is to use the target porphyrins and benzoporphyrins as photoactive materials in organic optoelectronics systems, the electrochemical characteristics of these compounds in a solid form was investigated by cyclic voltammetry (CV).

The experiments were performed in acetonitrile containing 0.1 M $TBAPF_6$ as supporting electrolyte. A three-electrode setup consisted of the ITO-coated glass as a working electrode, the Pt plate as a counter electrode and the Ag/AgCl QRE. The films of the target monomers on the ITO-coated glass were prepared by drop-casting their THF solutions. The CV scans were performed under N_2 atmosphere with a scan rate of 10 $mV \cdot s^{-1}$ and the number of scan of 3. However, after the first full CV scan, the films on the ITO-coated glass was dissolved into the electrolyte solution. Therefore, complete first oxidation and reduction peaks of the films could not be obtained by the routine CV measurement, and onset potentials of the first oxidation and reduction peaks ($E_{ox,onset}$ and $E_{red,onset}$, respectively) were used to estimate HOMO and LUMO energy level (E_{HOMO} and E_{LUMO}) of each material instead. In order to obtain the onset potentials and avoid degradation of the films by unexpected redox process, the CV was sequentially performed with the increment of the potential range of 50 mV per step. **Table 4–2** shows the $E_{ox,onset}$ and $E_{red,onset}$ of each compound, which were calibrated with a ferrocene/ferrocenium couple using the potential of 0.69 V vs. NHE as a reference value.[75] Consequently, the resulting potentials were used to approximate E_{HOMO} and E_{LUMO}, as well as energy gap (E_g) of the target monomers with an estimated energy value for NHE vs. Vacuum –4.75 eV by using the following equations (1)–(3).[76] The estimated values are summarized in **Table 4–3**.

$$E_g = E_{HOMO} - E_{LUMO} \quad (1)$$

$$E_{HOMO} = -(E_{ox,onset} + 4.75) \quad (2)$$

$$E_{LUMO} = -(E_{red,onset} + 4.75) \quad (3)$$

Table 4–3. Electrochemical properties of the target porphyrin and benzoporphyrin derivatives.

Compound	Potential / V (vs. NHE)		Energy / eV (vs. vacuum)		
	$E_{ox,onset}$	$E_{red,onset}$	E_{HOMO}	E_{LUMO}	E_g
***t*-ZnP-Th**	+0.675	–0.876	–5.79	–3.87	1.9
***t*-ZnP-2Th**	+0.613	–0.839	–5.73	–3.91	1.8
***t*-ZnBP-Th**	+0.496	–0.719	–5.61	–3.92	1.7
***t*-ZnBP-2Th**	+0.468	–0.699	–5.55	–4.05	1.5

According to these results, the effect of the introduction of the additional thiophene ring on the α-position of the thienyl *meso*-substituents on the electrochemical properties was determined by a comparison E_{HOMO}, E_{LUMO} and E_g of ***t*-ZnP-2Th** with those of ***t*-ZnP-Th** and E_{HOMO}, E_{LUMO} and E_g of ***t*-ZnBP-2Th** with those of ***t*-ZnBP-Th**. In case of porphyrins, the results reveal that the introduction of the additional thienyl groups resulted in the higher E_{HOMO} and lower E_{LUMO} by 0.06 and 0.04 eV, respectively. Similarly, benzoporphyrin ***t*-ZnBP-2Th** gave higher E_{HOMO} and lower E_{LUMO} by 0.06 and 0.07 eV, respectively. Comparing between the target benzoporphyrins and porphyrins bearing the same *meso*-substituents, the benzoporphyrins exhibited higher E_{HOMO} by 0.12–0.24 eV and lower E_{LUMO} by 0.05–0.14 eV. The increasing of E_{HOMO} and the lowering of E_{LUMO} led to smaller energy band gaps of the substances which were attributed to larger overlap of π-π orbitals together with π^*-π^* orbitals as increasing π-conjugation system of the target compounds.[19] The effect of structural modification of the porphyrins through the introduction of the additional thiophene ring and the β-fused rings on the electrochemical properties of the target molecules observed in this study are consistent to those described in the previous report.[67]

To determine the possibility of the use of these target compounds in BHJ-SCs, the calculated E_{HOMO} and E_{LUMO} of the target monomers were plotted together with

work functions (WFs) of ITO, poly(3,4-ethylenedioxythiophene):poly(styrenesulfonate) (PEDOT:PSS) and Al, and E_{HOMO} and E_{LUMO} of poly(3-hexylthiophene-2,5-diyl) (P3HT) and phenyl-C_{61}-butyric acid methyl ester (PCBM),[83] as illustrated in **Figure 4–5**.

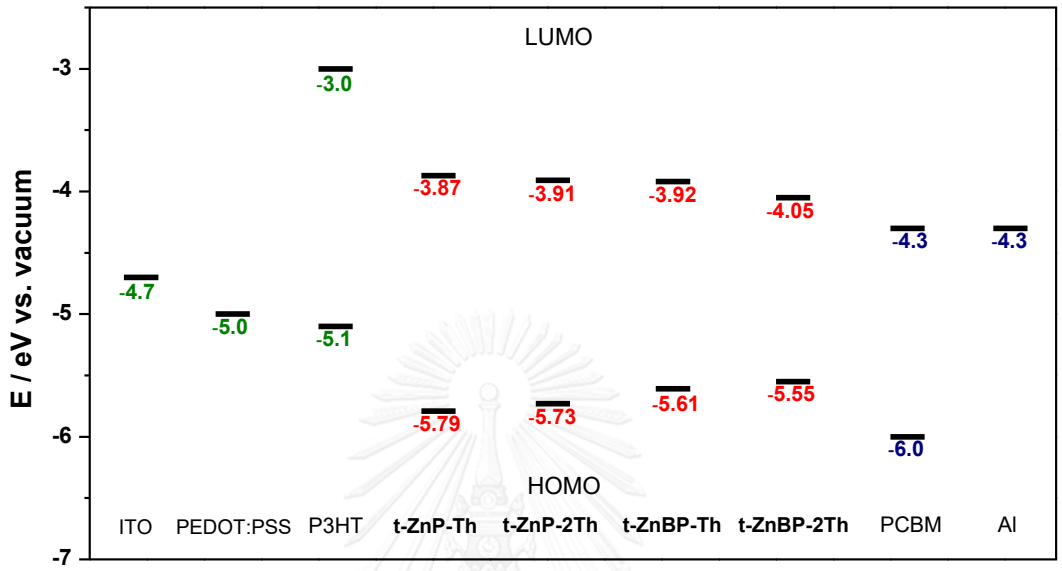

Figure 4–5: Comparative energy diagram of the E_{HOMO} and E_{LUMO} of the target porphyrins and benzoporphyrins, P3HT and PCBM, and WFs of ITO, PEDOT:PSS and Al.

The plot reveals that the LUMOs of all compounds are located below that of P3HT. Thus, the electron transfer from the excited P3HT to the target compounds and then to Al should be thermodynamically allowed, and the target compounds should then be able to act as an electron donor for P3HT. In addition, this plot also suggests their LUMOs are higher than that of that of PCBM. Thus, the electron from the excited target compounds should be able to transfer to PCBM, and then Al. At the same time, and their HOMOs are positioned at the higher energy level than WF of PEDOT:PSS, enabling charge compensation from PEDOT:PSS to the target compounds. The further photoluminescence and device studies to confirm the use of these target compounds in the BHJ-SCs will be performed and reported elsewhere.

4.3.2 Electrochemical polymerization of ZnP-2Th and *t*-ZnP-2Th and *t*-ZnBP-2Th.

According to a previous study,[64] porphyrin containing the thienyl groups was barely polymerized under oxidative polymerization condition due to their high oxidation potential, while the bithiophenyl units have lower oxidation potential due to larger **π** -conjugation system for stabilizing radical cation species.[34] Thus, the first attempts to polymerize the target compounds were made on [5,10,15,20-tetra(2,2′-bithiophen-5-yl)porphyrinato]zinc (**ZnP-2Th**) which was known to be polymerizable, according to a previous study.[65] After that, the target compounds bearing the bithiophenyl, ***t*-ZnP-2Th** and ***t*-ZnBP-2Th** were investigated.

First of all, **ZnP-2Th** was electropolymerized on the ITO-coated glass as a substrate in the one-compartment electrochemical cell consisting of the ITO-coated glass working electrode, a Pt counter electrode and a Ag/AgCl QRE. The experiment was performed in a THF solution containing 0.1 M $TBAPF_6$ as the supporting electrolyte. The oxidative electropolymerization of **ZnP-2Th** was carried out under N_2 atmosphere at the potential between –200 mV and 1600 mV vs. Ag/AgCl QRE at the concentration of **ZnP-2Th** of 2.5 mM at the scan rate of 50 $mV{\cdot}s^{-1}$ and the number of scanning cycles of 10. The resulting ITO-coated glass was found to be covered with light brown thin film. The electropolymerization of ***t*-ZnP-2Th** was performed in the similar manner with the potential between –200mV and 1750 mV. The number of scanning cycles was increased 100 due to slow polymerization which is attributed to fewer bithiophenyl units of ***t*-ZnP-2Th**, compared to those of **ZnP-2Th**. After washing remaining monomer with acetone, the resulting polymer film was found to be light yellow and looked relatively thin. Cyclic voltammograms of both compounds are shown in **Figure 4–6**. The cyclic voltammogram of **ZnP-2Th** showed an oxidation peak at 1250 mV vs. Ag/AgCl in the first scanning cycle and the current density increased as the number of scanning cycles increased. In case of ***t*-ZnP-2Th**, the cyclic voltammogram gave two oxidation peaks at 1151 and 1600 mV vs. Ag/AgCl and the decrease in the current density was observed as the number of scanning cycles incresed. However, when polymerizations of these two compounds were repeated, it

was found that the cyclic voltammograms from each experiment were inconsistent with each other. It could be resulted from the narrow potential window of THF.

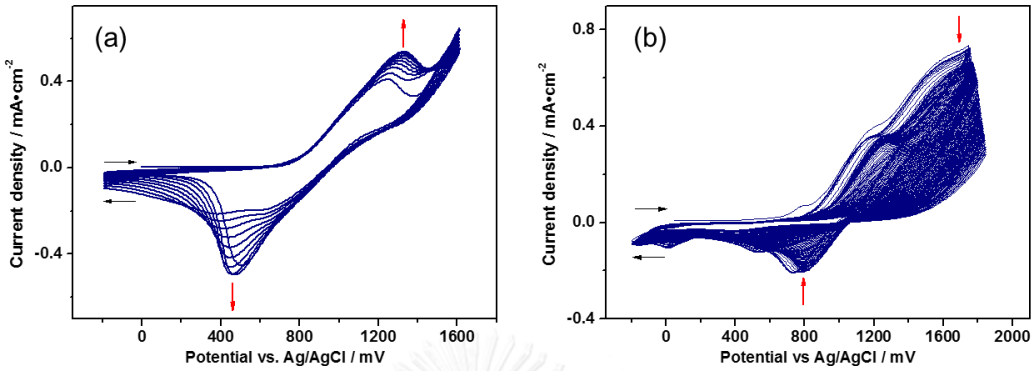

Figure 4–6: Cyclic voltammograms upon electropolymerization in THF solutions of a) **ZnP-2Th** and b) ***t*-ZnP-2Th**.

One possible approach to overcome this reproducibility problem is to change the solvent to another solvent that has higher oxidation electrochemical window. In this study, CH_2Cl_2 was chosen because it has wider potential window, compare with that of THF (**Figure 4–7**). Moreover, CH_2Cl_2 is inert to electrochemical process, and can dissolve the target compounds, although at a slightly lower concentration, compared with THF. Therefore, the concentration of the target compounds in the supporting electrolyte solution was decreased to 0.20 mM.

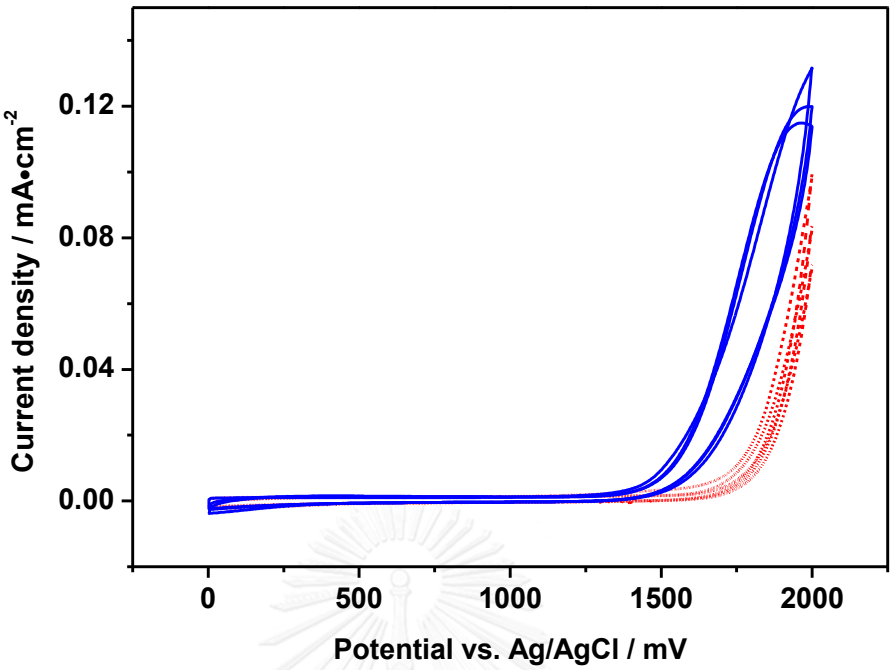

Figure 4–7: Cyclic voltammograms of blank experiments in a) THF solution (solid line) and b) CH_2Cl_2 solution (dashed line).

The polymerization of **ZnP-2Th** in CH_2Cl_2 was electrochemically performed under N_2 atmosphere at the potential between 0 mV and 1600 mV vs. Ag/AgCl QRE with the scan rate and the number of scanning cycles of 50 $mV{\cdot}s^{-1}$ and 10 cycles, respectively. As shown in **Figure 4–8a**, in the first scan, two oxidation peaks at 890 mV and 1372 mV vs. Ag/AgCl QRE, corresponding to the oxidation of porphyrin core and the bithiophenyl units, respectively,[65] were observed. Upon the polymerization, the current density of the peak at around 900 mV vs. Ag/AgCl QRE increased and shifted to more positive oxidation potential as more polymer was formed on the electrode. A small broad peak at around 500 mV vs. Ag/AgCl QRE indicated the thiophene-based unit and/or newly formed oligothiophene. After the polymerization and the washing of the excessive monomer with acetone, the resulting ITO-coated glass was found to be coated with pale brown smooth film of poly(**ZnP-2Th**) as shown in **Figure 4–8b**.

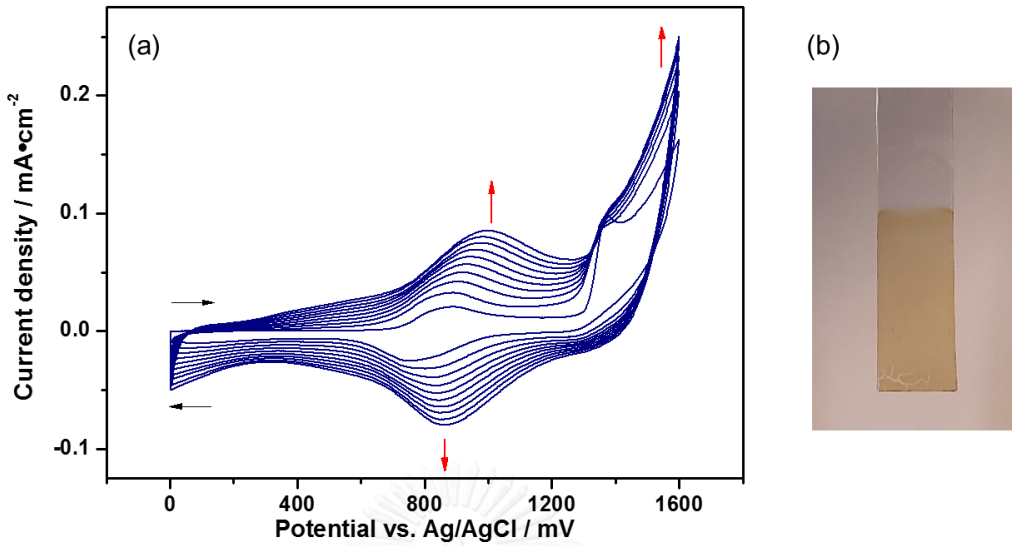

Figure 4–8: Cyclic voltammograms of the electropolymerization of **ZnP-2Th** in the CH_2Cl_2 solution and b) the resulting polymeric **ZnP-2Th** film on the ITO-coated glass.

In a similar manner, the electropolymerization of ***t*-ZnP-2Th** and ***t*-ZnBP-2Th** were studied. The electropolymerization of ***t*-ZnP-2Th** was performed under N_2 atmosphere at the potential between 0 mV and 1600 mV vs. Ag/AgCl QRE at the scan rate of 50 $mV \cdot s^{-1}$ with the scanning cycles of 10. In the first scan of the polymerization as shown in **Figure 4–9a**, three oxidation peaks were observed. The peaks at 855 mV and 1004 mV vs. Ag/AgCl QRE correspond to the oxidation of the phenyl units and the porphyrin core, respectively. The first oxidation peak position at 855 mV of the oxidation of the phenyl units was consistent with that of the previous report for **ZnP-Ph**.[84] The peak at around 1510 mV vs. Ag/AgCl resulted from the oxidation of the bithiophenyl units. Upon the polymerization, the current density of the peak at around 850 and 1000 mV vs. Ag/AgCl increased and shifted to more positive oxidation potential as more polymer was formed on the electrode. A small broad peak at around 500 mV vs. Ag/AgCl indicating the thiophene-based unit and/or newly formed oligothiophene was found and its current density increased as the number of scanning cycle increased. After polymerization, the ITO-coated glass was coated with light brown film of ***t*-ZnP-2Th** (poly(***t*-ZnP-2Th**)), as shown in **Figure 4–9b**. However, the

film was found to be cracked after washing with acetone. The effect of the replacement two phenyl *meso*-groups with the thienyl ones on the electrochemical behavior of the compounds was determined by a comparison of the peak positions in the first scanning cycle of ***t*-ZnP-2Th** with those of **ZnP-2Th.** The results reveal that ***t*-ZnP-2Th** exhibited another oxidation peaks indicating to the oxidation of the phenyl groups and the oxidation peak of the bithiophenyl groups was shifted to higher oxidation potential by 138 mV which was implied that the electropolymerization of ***t*-ZnP-2Th** required higher applied potential to occur.

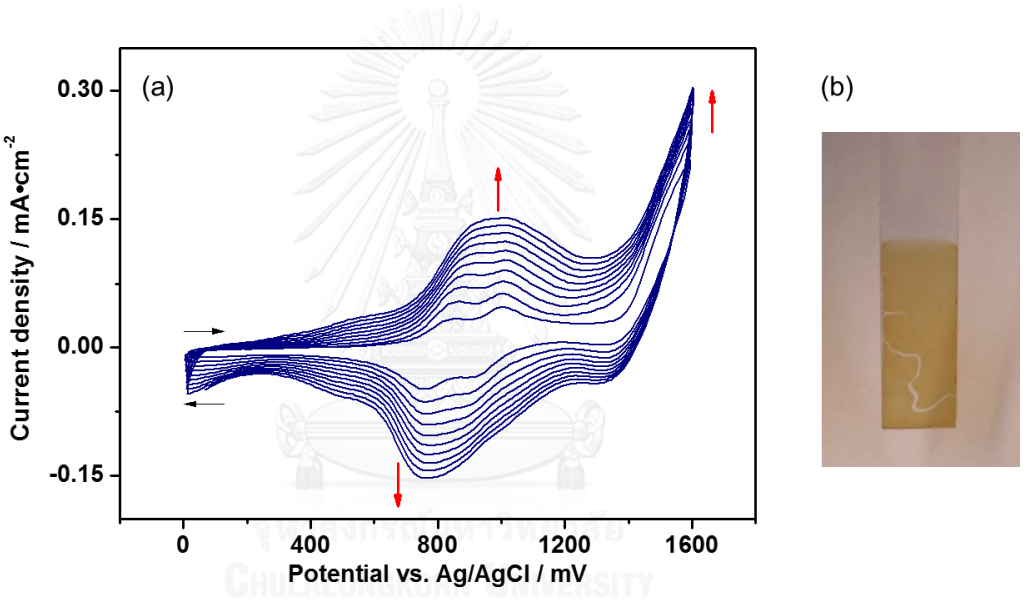

Figure 4–9: a) Cyclic voltammograms of electropolymerization of ***t*-ZnP-2Th** in the CH_2Cl_2 solution and b) the resulting polymeric ***t*-ZnP-2Th** film on the ITO-coated glass.

The electropolymerization of ***t*-ZnBP-2Th** was performed at the al between 0 mV and 1750 mV vs. Ag/AgCl QRE. As shown in **Figure 4–10**, there are three oxidation peaks at 442 mV, 679 mV and 1384 mV vs. Ag/AgCl in the first scanning cycle, corresponding to the oxidation of the β-benzo fused rings on the porphyrin core,[85] the porphyrin core and the bithiophenyl units, respectively. When the scanning cycles were increased, the current density of each peaks was not increased as expected. After the electropolymerization and the washing process, no polymer film on the ITO-coated

glass was observed. It is likely that electrochemical polymerization of ***t*-ZnBP-2Th** may give small oligomers which can be easily washed off of the substrate by acetone. The effect of the extended **π**-conjugation system at the **β**-positions of the macrocycle on the electrochemical behavior can be determined by comparing the peak positions in the first scanning cycle of ***t*-ZnBP-2Th** with those of ***t*-ZnP-2Th.** The results reveal that ***t*-ZnBP-2Th** gave lower first oxidation potential than the porphyrin one according to the stronger stabilization of positive species occurred in the reaction.

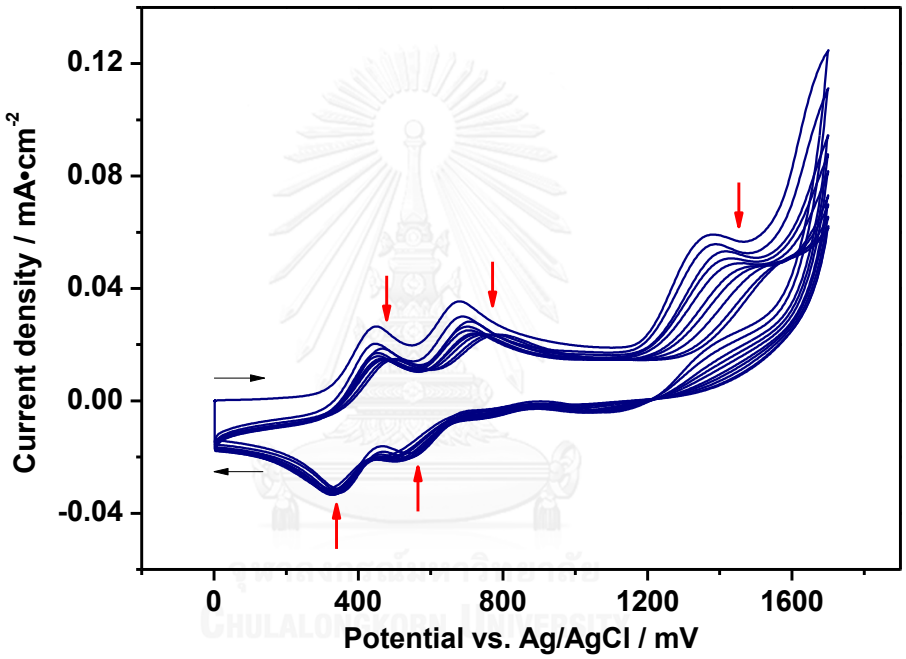

Figure 4–10: Cyclic voltammograms of electropolymerization of ***t*-ZnBP-2Th** in the CH_2Cl_2 solution.

4.3.3 Investigation of the photophysical properties of the polymer films

The photophysical properties of the resulting poly(**ZnP-2Th**) and poly(***t*-ZnP-2Th**) was investigated by UV-visible spectrophotometry. **Figure 4–11** shows that the absorption spectra of poly(**ZnP-2Th**) and poly(***t*-ZnP-2Th**) film were consistent with those of their monomer films with broader features, which is attributed to higher aggregation of the porphyrin macromolecules in the polymeric layers. As for the ITO-coated glass obtained from the electropolymerization experiment of ***t*-ZnBP-2Th**, its

absorption spectrum showed no characteristic absorption peak of the porphyrin indicating no polymerization of ***t*-ZnBP-2Th**.

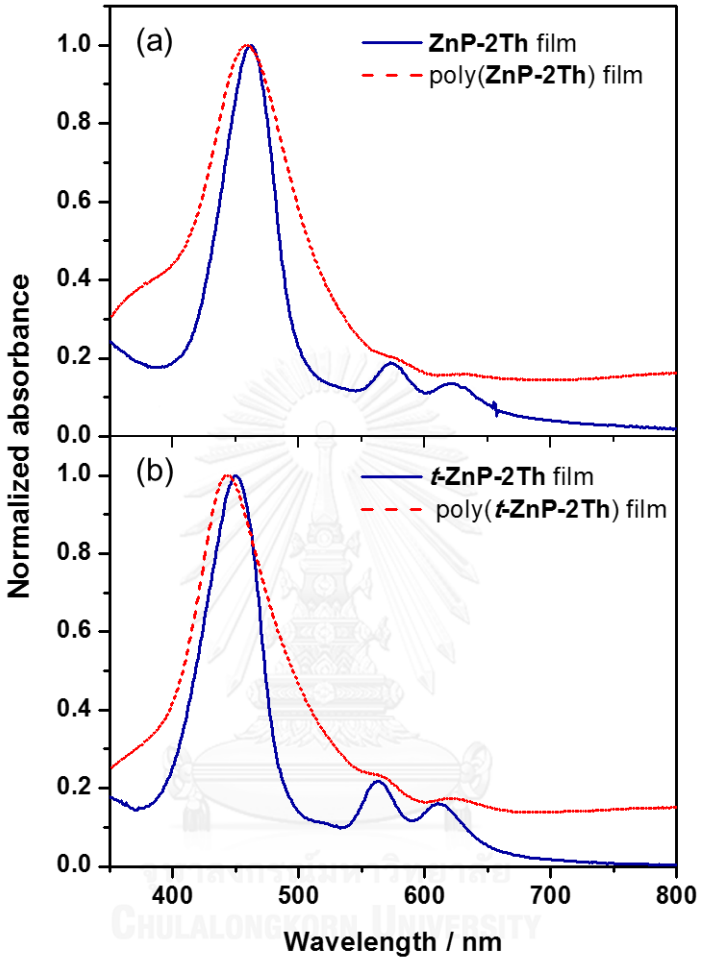

Figure 4–11: Normalized absorption spectra of the monomer (solid line) and polymeric films (dashed line) of a) **ZnP-2Th** and b) ***t*-ZnP-2Th**.

CHAPTER V
CONCLUSION

Novel zinc complexes of *trans*-A_2B_2-porphyrin and *trans*-A_2B_2-benzoporphyrin derivatives having two phenyl and two thiophene-based, i.e. thienyl or bithiophenyl, *meso*-substituents were successfully synthesized. The characterization of the target compounds was investigated by ^{1}H-NMR and ^{13}C-NMR spectroscopy, mass spectrometry, UV-Vis spectrophotometry and fluorescence spectrophotometry. The absorption maxima of the compounds were found to be red shifted due to the introduction of the β-fused phenyl rings, the replacement of the phenyl with the thienyl *meso*-groups and the introduction of the additional thiophene ring. Moreover, the HOMO and LUMO energy level of the target porphyrins and benzoporphyrins could be tuned by the introduction of thienyl and bithiophenyl *meso*-substituents and the extended π-conjugation system at β-positions of the pyrrole rings. The estimated HOMO and LUMO energy levels of all derivatives were estimated to be in the proper range, allowing efficient charge transport BHJ-SCs. The target *trans*-A_2B_2-porphyrin having the phenyl and bithiophenyl *meso*-substituents was successfully polymerized to obtain the polymeric film, absorption characteristic of which was consistent with that of its monomer. However, in case of *trans*-A_2B_2-benzoporphyrin, no polymer film on the electrode was observed. Thus, the optimization of the electropolymerizable conditions of this compound, as well as the determination of the potential use of their polymer films in optoelectronics will be further studied and described elsewhere.

REFERENCES

1. Global Economic Symposium Proposal - The Energy Crisis and Climate Change. http://www.global-economic-symposium.org/knowledgebase/the-global-environment/the-energy-crisis-and-climate-change/proposals/the-energy-crisis-and-climate-change (accessed 8 Jan 2017).

2. (a) Wei, D., "Dye Sensitized Solar Cells" *Int. J. Mol. Sci.* **2010**, *11*(*3*), 1103–1113; (b) Becquerel, A. E., "Recherches sur les effets de la radiation chimique de la lumiere solaire au moyen des courants electriques" *Comptes Rendus de L´Academie des Sciences* **1839**, *9*, 145–149.

3. Tao, M., "Inorganic Photovoltaic Solar Cells" *Electrochem. Soc. Interface* **2008**, *17*(*4*), 30–35.

4. Wright, M.; Uddin, A., "Organic—Inorganic Hybrid Solar Cells: A Comparative Review" *Sol. Energy Mater. Sol. Cells* **2012**, *107*, 87–111.

5. Mohammad Bagher, A., "Comparison of Organic Solar Cells and Inorganic Solar Cells" *Int. J. Renewable Sustainable Energy* **2014**, *3*(*3*), 53–58.

6. Roncali, J., "Conjugated Poly(thiophenes): Synthesis, Functionalization, and Applications" *Chem. Rev.* **1992**, *92*(*4*), 711-738.

7. Selected publications: (a) Aizawa, M.; Shinohara, H.; Yamada, T.; Akagi, K.; Shirakawa, H., "Electrochemical Fabrication of a Polypyrrole/Polythiophene P-N Junction Diode" *Synth. Met.* **1987**, *18*(*1*), 711–714; (b) Dyreklev, P.; Berggren, M.; Inganäs, O.; Andersson, M. R.; Wennerström, O.; Hjertberg, T., "Polarized Electroluminescence from an Oriented Substituted Polythiophene in a Light Emitting Diode" *Adv. Mater.* **1995**, *7*(*1*), 43–45; (c) Kaminorz, Y.; Smela, E.; Inganäs, O.; Brehmer, L., "Sensitivity of Polythiophene Planar Light-Emitting Diodes to Oxygen" *Adv. Mater.* **1998**, *10*(*10*), 765–769; (d) Ng, S.-C.; Xu, J.-M.; S. O. Chan, H.; Fujii, A.; Yoshino, K., "Regioregular Poly[3-butyl-2,5-thienylene-alt-1,4-phenylene]: Synthesis, Preliminary Characterization Aspects and Application in the Fabrication of Light-Emitting Diodes" *J. Mater. Chem.* **1999**, *9*(*2*), 381–385; (e) R. Andersson, M.; Thomas, O.; Mammo, W.; Svensson, M.; Theander, M.; Inganas, O., "Substituted Polythiophenes Designed for Optoelectronic

Devices and Conductors" *J. Mater. Chem.* **1999**, *9*(*9*), 1933–1940; (f) Lere-Porte, J.-P.; Moreau, J. J. E.; Serein-Spirau, F.; Torreilles, C.; Righi, A.; Sauvajol, J.-L.; Brunet, M., "Synthesis, Orientation and Optical Properties of Thiophene-Dialkoxyphenylene Copolymers" *J. Mater. Chem.* **2000**, *10*(*4*), 927–932; (g) Ding, A.-L.; Pei, J.; Lai, Y.-H.; Huang, W., "Phenylene-Functionalized Polythiophene Derivatives for Light-Emitting Diodes: Their Synthesis, Characterization and Properties" *J. Mater. Chem.* **2001**, *11*(*12*), 3082–3086; (h) Wang, X. J.; Andersson, M. R.; Thompson, M. E.; Inganäs, O., "Electrophosphorescence from Polythiophene Blends Light-Emitting Diodes" *Synth. Met.* **2003**, *137*(*1–3*), 1019–1020; (i) Xia, Y.; Luo, J.; Deng, X.; Li, X.; Li, D.; Zhu, X.; Yang, W.; Cao, Y., "Novel Random Low-Band-Gap Fluorene-Based Copolymers for Deep Red/Near Infrared Light-Emitting Diodes and Bulk Heterojunction Photovoltaic Cells" *Macromol. Chem. Phys.* **2006**, *207*(*5*), 511–520; (j) Fehse, K.; Walzer, K.; Leo, K.; Lövenich, W.; Elschner, A., "Highly Conductive Polymer Anodes as Replacements for Inorganic Materials in High-Efficiency Organic Light-Emitting Diodes" *Adv. Mater.* **2007**, *19*(*3*), 441–444.

8. Selected publications: (a) Yoshino, K.; Kaneto, K., "Application of Insulator-Metal Transition of Conducting Polymers" *Mol. Cryst. Liq. Cryst.* **1985**, *121*, 247–254; (b) Garnier, F.; Horowitz, G., "Organic Semiconducting Polymers as Molecular Material for Electronic Devices" *Synth. Met.* **1987**, *18*(*1*), 693–698; (c) Smestad, G. P.; Spiekermann, S.; Kowalik, J.; Grant, C. D.; Schwartzberg, A. M.; Zhang, J.; Tolbert, L. M.; Moons, E., "A Technique to Compare Polythiophene Solid-State Dye Sensitized TiO_2 Solar Cells to Liquid Junction Devices" *Sol. Energy Mater. Sol. Cells* **2003**, *76*(*1*), 85–105; (d) Colladet, K.; Fourier, S.; Cleij, T. J.; Lutsen, L.; Gelan, J.; Vanderzande, D.; Huong Nguyen, L.; Neugebauer, H.; Sariciftci, S.; Aguirre, A.; Janssen, G.; Goovaerts, E., "Low Band Gap Donor–Acceptor Conjugated Polymers toward Organic Solar Cells Applications" *Macromolecules* **2007**, *40*(*1*), 65–72; (e) Tan, Z. a.; Hou, J.; He, Y.; Zhou, E.; Yang, C.; Li, Y., "Synthesis and Photovoltaic Properties of a Donor–Acceptor Double-Cable Polythiophene with High Content of C_{60} Pendant" *Macromolecules* **2007**, *40*(*6*), 1868–1873; (f) Woo, C. H.; Holcombe, T. W.; Unruh, D. A.; Sellinger, A.; Fréchet, J. M. J., "Phenyl vs Alkyl Polythiophene: A Solar Cell Comparison Using a Vinazene Derivative as Acceptor" *Chem. Mater.* **2010**, *22*(*5*), 1673–1679; (g) Oosterhout, S. D.; Koster, L. J. A.;

van Bavel, S. S.; Loos, J.; Stenzel, O.; Thiedmann, R.; Schmidt, V.; Campo, B.; Cleij, T. J.; Lutzen, L.; Vanderzande, D.; Wienk, M. M.; Janssen, R. A. J., "Controlling the Morphology and Efficiency of Hybrid ZnO:Polythiophene Solar Cells Via Side Chain Functionalization" *Adv. Energy Mater.* **2011**, *1*(*1*), 90–96; (h) Hu, H.; Jiang, K.; Yang, G.; Liu, J.; Li, Z.; Lin, H.; Liu, Y.; Zhao, J.; Zhang, J.; Huang, F.; Qu, Y.; Ma, W.; Yan, H., "Terthiophene-Based D–A Polymer with an Asymmetric Arrangement of Alkyl Chains That Enables Efficient Polymer Solar Cells" *J. Am. Chem. Soc.* **2015**, *137*(*44*), 14149–14157.

9. Selected publications: (a) Ho, H.-A.; Boissinot, M.; Bergeron, M. G.; Corbeil, G.; Doré, K.; Boudreau, D.; Leclerc, M., "Colorimetric and Fluorometric Detection of Nucleic Acids Using Cationic Polythiophene Derivatives" *Angew. Chem. Int. Ed.* **2002**, *41*(*9*), 1548–1551; (b) Ho, H. A.; Leclerc, M., "New Colorimetric and Fluorometric Chemosensor Based on a Cationic Polythiophene Derivative for Iodide-Specific Detection" *J. Am. Chem. Soc.* **2003**, *125*(*15*), 4412–4413; (c) Janata, J.; Josowicz, M., "Conducting Polymers in Electronic Chemical Sensors" *Nat. Mater.* **2003**, *2*(*1*), 19–24; (d) Nilsson, K. P.; Inganas, O., "Chip and Solution Detection of DNA Hybridization Using a Luminescent Zwitterionic Polythiophene Derivative" *Nat. Mater.* **2003**, *2*(*6*), 419–424; (e) Doré, K.; Dubus, S.; Ho, H.-A.; Lévesque, I.; Brunette, M.; Corbeil, G.; Boissinot, M.; Boivin, G.; Bergeron, M. G.; Boudreau, D.; Leclerc, M., "Fluorescent Polymeric Transducer for the Rapid, Simple, and Specific Detection of Nucleic Acids at the Zeptomole Level" *J. Am. Chem. Soc.* **2004**, *126*(*13*), 4240–4244; (f) Ho, H.-A.; Leclerc, M., "Optical Sensors Based on Hybrid Aptamer/Conjugated Polymer Complexes" *J. Am. Chem. Soc.* **2004**, *126*(*5*), 1384–1387; (g) Li, C.; Numata, M.; Takeuchi, M.; Shinkai, S., "A Sensitive Colorimetric and Fluorescent Probe Based on a Polythiophene Derivative for the Detection of ATP" *Angew. Chem. Int. Ed.* **2005**, *44*(*39*), 637–6374; (h) Béra Abérem, M.; Najari, A.; Ho, H. A.; Gravel, J. F.; Nobert, P.; Boudreau, D.; Leclerc, M., "Protein Detecting Arrays Based on Cationic Polythiophene–DNA-Aptamer Complexes" *Adv. Mater.* **2006**, *18*(*20*), 2703–2707; (i) Fan, L.-J.; Jones, W. E., "A Highly Selective and Sensitive Inorganic/Organic Hybrid Polymer Fluorescence “Turn-On” Chemosensory System for Iron Cations" *J. Am. Chem. Soc.* **2006**, *128*(*21*), 6784–6785; (j) Li, B.; Santhanam, S.; Schultz, L.; Jeffries-El, M.; Iovu, M. C.; Sauvé, G.; Cooper, J.; Zhang, R.; Revelli, J. C.; Kusne, A. G.; Snyder, J. L.; Kowalewski,

T.; Weiss, L. E.; McCullough, R. D.; Fedder, G. K.; Lambeth, D. N., "Inkjet Printed Chemical Sensor Array Based on Polythiophene Conductive Polymers" *Sensors Actuators B: Chem.* **2007**, *123*(*2*), 651–660; (k) Wang, F.; Gu, H.; Swager, T. M., "Carbon Nanotube/Polythiophene Chemiresistive Sensors for Chemical Warfare Agents" *J. Am. Chem. Soc.* **2008**, *130*(*16*), 5392–5393.

10. Walter, M. G.; Rudine, A. B.; Wamser, C. C., "Porphyrins and Phthalocyanines in Solar Photovoltaic Cells" *J. Porphyrins Phthalocyanines* **2010**, *14*(*09*), 759–792.

11. Cavaleiro, J. A. S.; Smith, K., "Porphyrin Synthesis" *Rev. Port. Quím.* **1989**, *31*, 29–41.

12. Anderson, H., L., "Building Molecular Wires from the Colours of Life: Conjugated Porphyrin Oligomers" *Chem. Commun.* **1999**, *23*, 2323–2330.

13. Selected publications: (a) Manassen, J.; Bar-Ilan, A., "Metal Complexes of Phthalocyanine and α,β,γ,δ-Tetraphenyl Porphyrin as Heterogeneous Catalysts in Oxidative Dehydrogenation. Correlation between Catalytic Activity and Redox Potential" *J. Catal.* **1970**, *17*(*1*), 86–92; (b) Collman, J. P.; Denisevich, P.; Konai, Y.; Marrocco, M.; Koval, C.; Anson, F. C., "Electrode Catalysis of the Four-Electron Reduction of Oxygen to Water by Dicobalt Face-to-Face Porphyrins" *J. Am. Chem. Soc.* **1980**, *102*(*19*), 6027–6036; (c) Aida, T.; Ishikawa, M.; Inoue, S., "Alternating Copolymerization of Carbon Dioxide and Epoxide Catalyzed by the Aluminum Porphyrin-quaternary Organic Salt or -Triphenylphosphine System. Synthesis of Polycarbonate with Well-Controlled Molecular Weight" *Macromolecules* **1986**, *19*(*1*), 8–13; (d) Bhugun, I.; Lexa, D.; Savéant, J.-M., "Homogeneous Catalysis of Electrochemical Hydrogen Evolution by Iron(0) Porphyrins" *J. Am. Chem. Soc.* **1996**, *118*(*16*), 3982–3983; (e) Mang, S.; Cooper, A. I.; Colclough, M. E.; Chauhan, N.; Holmes, A. B., "Copolymerization of CO_2 and 1,2-Cyclohexene Oxide Using a CO_2-Soluble Chromium Porphyrin Catalyst" *Macromolecules* **2000**, *33*(*2*), 303–308; (f) Yu, X.-Q.; Huang, J.-S.; Zhou, X.-G.; Che, C.-M., "Amidation of Saturated C–H Bonds Catalyzed by Electron-Deficient Ruthenium and Manganese Porphyrins. A Highly Catalytic Nitrogen Atom Transfer Process" *Org. Lett.* **2000**, *2*(*15*), 2233–2236; (g) Lefèvre, M.; Dodelet, J. P.; Bertrand, P., "Molecular Oxygen Reduction in PEM Fuel Cells: Evidence for the

Simultaneous Presence of Two Active Sites in Fe-Based Catalysts" *J. Phys. Chem. B* **2002**, *106*(*34*), 8705–8713; (h) Liang, J.-L.; Yuan, S.-X.; Huang, J.-S.; Yu, W.-Y.; Che, C.-M., "Highly Diastereo- and Enantioselective Intramolecular Amidation of Saturated C-H Bonds Catalyzed by Ruthenium Porphyrins" *Angew. Chem.* **2002**, *114*(*18*), 3615–3618; (i) Zhou, C.-Y.; Chan, P. W. H.; Che, C.-M., "Gold(III) Porphyrin-Catalyzed Cycloisomerization of Allenones" *Org. Lett.* **2006**, *8*(*2*), 325–328; (j) Alkordi, M. H.; Liu, Y.; Larsen, R. W.; Eubank, J. F.; Eddaoudi, M., "Zeolite-like Metal–Organic Frameworks as Platforms for Applications: On Metalloporphyrin-Based Catalysts" *J. Am. Chem. Soc.* **2008**, *130*(*38*), 12639–12641; (k) Lin, S.; Diercks, C. S.; Zhang, Y.-B.; Kornienko, N.; Nichols, E. M.; Zhao, Y.; Paris, A. R.; Kim, D.; Yang, P.; Yaghi, O. M.; Chang, C. J., "Covalent Organic Frameworks Comprising Cobalt Porphyrins for Catalytic CO_2 Reduction in Water" *Science* **2015**, *349*(*6253*), 1208; (l) Shen, J.; Kortlever, R.; Kas, R.; Birdja, Y. Y.; Diaz-Morales, O.; Kwon, Y.; Ledezma-Yanez, I.; Schouten, K. J. P.; Mul, G.; Koper, M. T. M., "Electrocatalytic Reduction of Carbon Dioxide to Carbon Monoxide and Methane at an Immobilized Cobalt Protoporphyrin" *Nat. Commun.* **2015**, *6*, 8177; (m) Kou, Y.; Nakatani, S.; Sunagawa, G.; Tachikawa, Y.; Masui, D.; Shimada, T.; Takagi, S.; Tryk, D. A.; Nabetani, Y.; Tachibana, H.; Inoue, H., "Visible Light-Induced Reduction of Carbon Dioxide Sensitized by a Porphyrin–Rhenium Dyad Metal Complex on p-Type Semiconducting NiO as the Reduction Terminal end of an Artificial Photosynthetic System" *J. Catal.* **2014**, *310*, 57–66.

14. Selected publications: (a) Smith, A.; Nuiry, I.; Awasthi, Y. C., "Interactions with Glutathione *S*-transferases of Porphyrins Used in Photodynamic Therapy and Naturally Occurring Porphyrins" *Biochem. J* **1985**, *229*(*3*), 823–831; (b) Maziere, J. C.; Santus, R.; Morliere, P.; Reyftmann, J. P.; Candide, C.; Mora, L.; Salmon, S.; Maziere, C.; Gatt, S.; Dubertret, L., "Cellular Uptake and Photosensitizing Properties of Anticancer Porphyrins in Cell Membranes and Low and High Density Lipoproteins" *J. Photochem. Photobiol. B: Biol.* **1990**, *6*(*1*), 61–68; (c) Sternberg, E. D.; Dolphin, D.; Brückner, C., "Porphyrin-Based Photosensitizers for Use in Photodynamic Therapy" *Tetrahedron* **1998**, *54*(*17*), 4151–4202; (d) Mody, T. D., "Pharmaceutical Development and Medical Applications of Porphyrin-Type Macrocycles" *J. Porphyrins Phthalocyanines* **2000**, *4*(*4*), 362–367; (e) Banfi, S.; Caruso, E.; Caprioli, S.; Mazzagatti, L.; Canti, G.; Ravizza, R.; Gariboldi, M.; Monti,

E., "Photodynamic Effects of Porphyrin and Chlorin Photosensitizers in Human Colon Adenocarcinoma Cells" *Biorg. Med. Chem.* **2004**, *12*(*18*), 4853–4860; (f) Davia, K.; King, D.; Hong, Y.; Swavey, S., "A Porphyrin–Ruthenium Photosensitizer as a Potential Photodynamic Therapy Agent" *Inorg. Chem. Commun.* **2008**, *11*(*5*), 584–586; (g) O'Connor, A. E.; Gallagher, W. M.; Byrne, A. T., "Porphyrin and Nonporphyrin Photosensitizers in Oncology: Preclinical and Clinical Advances in Photodynamic Therapy" *Photochem. Photobiol.* **2009**, *85*(*5*), 1053–1074; (h) Schwiertz, J.; Wiehe, A.; Gräfe, S.; Gitter, B.; Epple, M., "Calcium Phosphate Nanoparticles as Efficient Carriers for Photodynamic Therapy against Cells and Bacteria" *Biomaterials* **2009**, *30*(*19*), 3324–3331; (i) Králová, J.; Kejík, Z.; Bříza, T.; Poučková, P.; Král, A.; Martásek, P.; Král, V., "Porphyrin–Cyclodextrin Conjugates as a Nanosystem for Versatile Drug Delivery and Multimodal Cancer Therapy" *J. Med. Chem.* **2010**, *53*(*1*), 128–138; (j) Ethirajan, M.; Chen, Y.; Joshi, P.; Pandey, R. K., "The Role of Porphyrin Chemistry in Tumor Imaging and Photodynamic Therapy" *Chem. Soc. Rev.* **2011**, *40*(*1*), 340–362.

15. Selected publications: (a) Kwong, R. C.; Sibley, S.; Dubovoy, T.; Baldo, M.; Forrest, S. R.; Thompson, M. E., "Efficient, Saturated Red Organic Light Emitting Devices Based on Phosphorescent Platinum(II) Porphyrins" *Chem. Mater.* **1999**, *11*(*12*), 3709–3713; (b) Lupton, J. M.; Samuel, I. D. W.; Frampton, M. J.; Beavington, R.; Burn, P. L., "Control of Electrophosphorescence in Conjugated Dendrimer Light-Emitting Diodes" *Adv. Funct. Mater.* **2001**, *11*(*4*), 287–294; (c) Montes, V. A.; Pérez-Bolívar, C.; Agarwal, N.; Shinar, J.; Anzenbacher, P., "Molecular-Wire Behavior of OLED Materials: Exciton Dynamics in Multichromophoric Alq3-Oligofluorene-Pt(II)porphyrin Triads" *J. Am. Chem. Soc.* **2006**, *128*(*38*), 12436–12438; (d) Endo, A.; Ogasawara, M.; Takahashi, A.; Yokoyama, D.; Kato, Y.; Adachi, C., "Thermally Activated Delayed Fluorescence From Sn^{4+}-Porphyrin Complexes and Their Application to Organic Light Emitting Diodes-A Novel Mechanism for Electroluminescence" *Adv. Mater.* **2009**, *21*(*47*), 4802–4806; (e) Hoang, M. H.; Choi, D. H.; Lee, S. J., "Organic Field-Effect Transistors Based on Semiconducting Porphyrin Single Crystals" *Synth. Met.* **2012**, *162*(*5–6*), 419–425; (f) Imahori, H.; Umeyama, T.; Kurotobi, K.; Takano, Y., "Self-Assembling Porphyrins and Phthalocyanines for Photoinduced Charge Separation and Charge Transport" *Chem. Commun. (Camb.)*

2012, *48*(*34*), 4032–4045; (g) Lee, J. T.; Chae, D.-H.; Yao, Z.; Sessler, J. L., "High-Order Tunneling Processes in Single-Porphyrin Transistors" *Chem. Commun.* **2012**, *48*(*37*), 4420–4422; (h) Mol, J. A.; Lau, C. S.; Lewis, W. J. M.; Sadeghi, H.; Roche, C.; Cnossen, A.; Warner, J. H.; Lambert, C. J.; Anderson, H. L.; Briggs, G. A. D., "Graphene-Porphyrin Single-Molecule Transistors" *Nanoscale* **2015**, *7*(*31*), 13181–13185; (i) Wang, C.-L.; Chang, Y.-C.; Lan, C.-M.; Lo, C.-F.; Wei-Guang Diau, E.; Lin, C.-Y., "Enhanced Light Harvesting with π-Conjugated Cyclic Aromatic Hydrocarbons for Porphyrin-Sensitized Solar Cells" *Energy Environ. Sci.* **2011**, *4*(*5*), 1788–1795; (j) Yella, A.; Lee, H.-W.; Tsao, H. N.; Yi, C.; Chandiran, A. K.; Nazeeruddin, M. K.; Diau, E. W.-G.; Yeh, C.-Y.; Zakeeruddin, S. M.; Grätzel, M., "Porphyrin-Sensitized Solar Cells with Cobalt (II/III)–Based Redox Electrolyte Exceed 12 Percent Efficiency" *Science* **2011**, *334*(*6056*), 629; (k) Mathew, S.; Yella, A.; Gao, P.; Humphry-Baker, R.; CurchodBasile, F. E.; Ashari-Astani, N.; Tavernelli, I.; Rothlisberger, U.; NazeeruddinMd, K.; Grätzel, M., "Dye-Sensitized Solar Cells with 13% Efficiency Achieved through the Molecular Engineering of Porphyrin Sensitizers" *Nat. Chem.* **2014**, *6*(*3*), 242-247.

16. Mitsubishi Chemical Corporation Organic Photovoltaic Modules and Materials. http://www.mitsubishichem-hd.co.jp/english/discover_kaiteki/kaiteki_value/detail01.html (accessed 9 January 2017).

17. Chen, H.; Zeng, J.; Deng, F.; Luo, X.; Lei, Z.; Li, H., "Synthesis and Photophysical Properties of Porphyrin-Containing Polymers" *J. Polym. Res.* **2012**, *19*(*6*), 9880.

18. Horowitz, G., Organic Transistors. In *Org. Electron.*, Wiley-VCH Verlag GmbH & Co. KGaA: 2006; pp 1–32.

19. Bundgaard, E.; Krebs, F. C., "Low Band Gap Polymers for Organic Photovoltaics" *Sol. Energy Mater. Sol. Cells* **2007**, *91*(*11*), 954–985.

20. Kitai, A., *Principles of Solar Cells, LEDs and Diodes: The role of the PN junction*. Wiley: 2011.

21. Spanggaard, H.; Krebs, F. C., "A Brief History of the Development of Organic and Polymeric Photovoltaics" *Sol. Energy Mater. Sol. Cells* **2004**, *83*, 125–146.

22. Lee, J.-H.; Kim, J. W.; Kim, S.-Y.; Yoo, S.-J.; Lee, J.-H.; Kim, J.-J., "An Organic P–N Junction as an Efficient and Cathode Independent Electron Injection Layer for Flexible Inverted Organic Light Emitting Diodes" *Org. Electron.* **2012**, *13*(*4*), 545–549.

23. Farchioni, R.; Grosso, G., *Organic Electronic Materials: Conjugated Polymers and Low Molecular Weight Organic Solids*. Springer-Verlag Berlin Heidelberg: 2001.

24. Ostroverkhova, O., "Organic Optoelectronic Materials: Mechanisms and Applications" *Chem. Rev.* **2016**, *116*(*22*), 13279–13412.

25. Heeger, A. J., "Nobel Lecture: Semiconducting and Metallic Polymers: The Fourth Generation of Polymeric Materials" *Rev. Mod. Phys.* **2001**, *73*(*3*), 681–700.

26. Scharber, M. C.; Sariciftci, N. S., "Efficiency of Bulk-Heterojunction Organic Solar Cells" *Prog. Polym. Sci.* **2013**, *38*(*12*), 1929–1940.

27. Selected publications: (a) Jones, J.-P.; Prakash, G. K. S.; Olah, G. A., "Electrochemical CO_2 Reduction: Recent Advances and Current Trends" *Isr. J. Chem.* **2014**, *54*(*10*), 1451–1466; (b) Lim, R. J.; Xie, M.; Sk, M. A.; Lee, J.-M.; Fisher, A.; Wang, X.; Lim, K. H., "A review on the electrochemical reduction of CO_2 in fuel cells, metal electrodes and molecular catalysts" *Catal. Today* **2014**, *233*, 169-180; (c) Kortlever, R.; Shen, J.; Schouten, K. J. P.; Calle-Vallejo, F.; Koper, M. T. M., "Catalysts and Reaction Pathways for the Electrochemical Reduction of Carbon Dioxide" *The Journal of Physical Chemistry Letters* **2015**, *6*(*20*), 4073–4082; (d) Wang, W.-H.; Himeda, Y.; Muckerman, J. T.; Manbeck, G. F.; Fujita, E., "CO_2 Hydrogenation to Formate and Methanol as an Alternative to Photo- and Electrochemical CO_2 Reduction" *Chem. Rev.* **2015**, *115*(*23*), 12936–12973.

28. Kossmehl, G.; Engelmann, G., Application of Electrically Conductive Polythiophenes. In *Handbook of Oligo- and Polythiophenes*, Wiley-VCH Verlag GmbH: 1998; pp 491–524.

29. Nobelprize.org The Nobel Prize in Chemistry 2000. https://www.nobelprize.org/nobel_prizes/chemistry/laureates/2000/ (accessed 10 February).

30. Roncali, J., "Electrogenerated Functional Conjugated Polymers as Advanced Electrode Materials" *J. Mater. Chem.* **1999**, *9*(*9*), 1875–1893.

31. Roncali, J., "Conjugated Poly(thiophenes): Synthesis, Functionalization, and Applications" *Chem. Rev.* **1992**, *92*(*4*), 711–738.

32. Chen, T.-A.; Wu, X.; Rieke, R. D., "Regiocontrolled Synthesis of Poly(3-alkylthiophenes) Mediated by Rieke Zinc: Their Characterization and Solid-State Properties" *J. Am. Chem. Soc.* **1995**, *117*(*1*), 233–244.

33. Loewe, R. S.; Khersonsky, S. M.; McCullough, R. D., "A Simple Method to Prepare Head-to-Tail Coupled, Regioregular Poly(3-alkylthiophenes) Using Grignard Metathesis" *Adv. Mater.* **1999**, *11*(*3*), 250–253.

34. Blanchard, P.; Cravino, A.; Levillain, E., Electrochemistry of Oligothiophenes and Polythiophenes. In *Handbook of Thiophene-Based Materials*, John Wiley & Sons, Ltd: 2009; pp 419–453.

35. Yamamoto, T., "Molecular Assembly and Properties of Polythiophenes" *NPG Asia Materials* **2010**, *2*(*2*), 54–60.

36. Selected publications: (a) Turut, A.; Koleli, F., "Semiconductive Polymer-Based Schottky Diode" *J. Appl. Phys.* **1992**, *72*(*2*), 818–19; (b) Zotti, G.; Schiavon, G.; Berlin, A.; Pagani, G., "Thiophene Oligomers as Polythiophene Models. 3. Conductive and Capacitive Behavior of End-Capped Oligothienyls as Thin Films. A Contribution to the Conduction Mechanism and to the Faradaic-Capacitive Debate of Conducting Polymers" *Adv. Mater. (Weinheim, Fed. Repub. Ger.)* **1993**, *5*(*7–8*), 551–554; (c) Rudge, A.; Davey, J.; Raistrick, I.; Gottesfeld, S.; Ferraris, J. P., "Conducting Polymers as Active Materials in Electrochemical Capacitors" *J. Power Sources* **1994**, *47*(*1–2*), 89-107; (d) Laforgue, A.; Simon, P.; Sarrazin, C.; Fauvarque, J.-F., "Polythiophene-Based Supercapacitors" *J. Power Sources* **1999**, *80*(*1–2*), 142–148; (e) Tang, J.; Kong, L.; Zhang, J.; Zhan, L.; Zhan, H.; Zhou, Y.; Zhan, C., "Solvent-Free, Oxidatively Prepared Polythiophene: High Specific Capacity as a Cathode Active Material for Lithium Batteries" *React. Funct. Polym.* **2008**, *68*(*9*), 1408–1413; (f) Aydin, M.; Esat, B.; Kilic, C.; Koese, M. E.; Ata, A.; Yilmaz, F., "A Polythiophene Derivative Bearing TEMPO as a Cathode Material for Rechargeable Batteries" *Eur. Polym. J.* **2011**, *47*(*12*), 2283–2294; (g) Fu, C.; Zhou, H.; Liu, R.; Huang, Z.; Chen, J.; Kuang, Y., "Supercapacitor Based on Electropolymerized Polythiophene and Multi-Walled Carbon Nanotubes Composites" *Mater. Chem. Phys.* **2012**, *132*(*2-3*), 596–600.

37. Selected publications: (a) Tsumura, A.; Koezuka, H.; Ando, T., "Macromolecular Electronic Device: Field-Effect Transistor with a Polythiophene Thin Film" *Appl. Phys. Lett.* **1986**, *49*(*18*), 1210–12; (b) Koezuka, H.; Tsumura, A.; Ando, T., "Field-Effect Transistor with Polythiophene Thin Film" *Synth. Met.* **1987**, *18*(*1-3*), 699–704; (c) Tsumura, A.; Koezuka, H.; Ando, T., "Polythiophene Field-Effect Transistor: Its Characteristics and Operation Mechanism" *Synth. Met.* **1988**, *25*(*1*), 11–23; (d) Osaka, I.; Sauve, G.; Zhang, R.; Kowalewski, T.; McCullough, R. D., "Novel Thiophene-Thiazolothiazole Copolymers for Organic Field-Effect Transistors" *Adv. Mater. (Weinheim, Ger.)* **2007**, *19*(*23*), 4160–4165; (e) Lan, Y.-K.; Yang, C. H.; Yang, H.-C., "Theoretical Investigations of Electronic Structure and Charge Transport Properties in Polythiophene-Based Organic Field-Effect Transistors" *Polym. Int.* **2010**, *59*(*1*), 16–21; (f) Voigt, M. M.; Guite, A.; Chung, D.-Y.; Khan, R. U. A.; Campbell, A. J.; Bradley, D. D. C.; Meng, F.; Steinke, J. H. G.; Tierney, S.; McCulloch, I.; Penxten, H.; Lutsen, L.; Douheret, O.; Manca, J.; Brokmann, U.; Soennichsen, K.; Huelsenberg, D.; Bock, W.; Barron, C.; Blanckaert, N.; Springer, S.; Grupp, J.; Mosley, A., "Polymer Field-Effect Transistors Fabricated by the Sequential Gravure Printing of Polythiophene, Two Insulator Layers, and a Metal Ink Gate" *Adv. Funct. Mater.* **2010**, *20*(*2*), 239–246.

38. Selected publications: (a) Garnier, F.; Tourillon, G.; Gazard, M.; Dubois, J. C., "Organic Conducting Polymers Derived from Substituted Thiophenes as Electrochromic Material" *J. Electroanal. Chem. Interfacial Electrochem.* **1983**, *148*(*2*), 299–303; (b) Kumar, A.; Welsh, D. M.; Morvant, M. C.; Piroux, F.; Abboud, K. A.; Reynolds, J. R., "Conducting Poly(3,4-alkylenedioxythiophene) Derivatives as Fast Electrochromics with High-Contrast Ratios" *Chem. Mater.* **1998**, *10*(*3*), 896–902; (c) Lu, W.; Fadeev, A. G.; Qi, B.; Smela, E.; Mattes, B. R.; Ding, J.; Spinks, G. M.; Mazurkiewicz, J.; Zhou, D.; Wallace, G. G.; MacFarlane, D. R.; Forsyth, S. A.; Forsyth, M., "Use of Ionic Liquids for **π**-Conjugated Polymer Electrochemical Devices" *Science (Washington, DC, U. S.)* **2002**, *297*(*5583*), 983–987; (d) Meng, H.; Tucker, D.; Chaffins, S.; Chen, Y.; Helgeson, R.; Dunn, B.; Wudl, F., "An Unusual Electrochromic Device Based on a New Low-Bandgap Conjugated Polymer" *Adv. Mater. (Weinheim, Ger.)* **2003**, *15*(*2*), 146–149; (e) Nicho, M. E.; Hu, H.; Lopez-Mata, C.; Escalante, J., "Synthesis of Derivatives of Polythiophene and Their Application in an Electrochromic Device" *Sol. Energy Mater. Sol. Cells* **2004**, *82*(*1-2*),

105–118; (f) Thompson, B. C.; Kim, Y.-G.; McCarley, T. D.; Reynolds, J. R., "Soluble Narrow Band Gap and Blue Propylenedioxythiophene-Cyanovinylene Polymers as Multifunctional Materials for Photovoltaic and Electrochromic Applications" *J. Am. Chem. Soc.* **2006**, *128*(*39*), 12714–12725; (g) Beaujuge, P. M.; Ellinger, S.; Reynolds, J. R., "The Donor-Acceptor Approach Allows a Black-to-Transmissive Switching Polymeric Electrochrome" *Nat. Mater.* **2008**, *7*(*10*), 795–799; (h) Zhang, X.; Steckler, T. T.; Dasari, R. R.; Ohira, S.; Potscavage, W. J., Jr.; Tiwari, S. P.; Coppee, S.; Ellinger, S.; Barlow, S.; Bredas, J.-L.; Kippelen, B.; Reynolds, J. R.; Marder, S. R., "Dithienopyrrole-Based Donor-Acceptor Copolymers: Low Band-Gap Materials for Charge Transport, Photovoltaics and Electrochromism" *J. Mater. Chem.* **2010**, *20*(*1*), 123–134.

39. Milgrom, L. R., *The Colours of Life: An Introduction to the Chemistry of Porphyrins and Related Compounds*. Oxford University Press: 1997.

40. Bonkovsky, H. L.; Guo, J.-T.; Hou, W.; Li, T.; Narang, T.; Thapar, M., Porphyrin and Heme Metabolism and the Porphyrias. In *Comprehensive Physiology*, John Wiley & Sons, Inc.: 2013; pp 365–401.

41. Mauzerall, D., Porphyrins, Chlorophyll, and Photosynthesis. In *Photosynthesis I: Photosynthetic Electron Transport and Photophosphorylation*, Trebst, A.; Avron, M., Eds. Springer Berlin Heidelberg: Berlin, Heidelberg, 1977; pp 117–124.

42. Moss, G. P., "Nomenclature of Tetrapyrroles" *Eur. J. Biochem.* **1988**, *178*(*2*), 277–328.

43. Lash, T. D.; AbuSalim, D. I.; Ferrence, G. M., "*adj*-Dicarbachlorin, The First Free Base Carbaporphyrinoid System with an Internal Methylene Unit" *Chem. Commun.* **2015**, *51*(*88*), 15952–15955.

44. Selected publications: (a) Malinski, T.; Bailey, F.; Fish, J. R.; Kiechle, F., "Determination of Nickel Accumulation in Single Biological Cells using Porphyrinic Microsensors" *Anal. Chim. Acta* **1991**, *249*(*1*), 35–41; (b) Malinski, T.; Taha, Z.; Grunfeld, S.; Burewicz, A.; Tomboulian, P.; Kiechle, F., "Measurements of Nitric Oxide in Biological Materials Using a Porphyrinic Microsensor" *Anal. Chim. Acta* **1993**, *279*(*1*), 135–40; (c) Yang, R.; Li, K. a.; Wang, K.; Zhao, F.; Li, N.; Liu, F., "Porphyrin Assembly on *β*-Cyclodextrin for Selective Sensing and Detection of a Zinc Ion Based on the Dual Emission Fluorescence Ratio" *Anal. Chem.* **2003**, *75*(*3*), 612–621; (d) Brinas, R. P.; Troxler,

T.; Hochstrasser, R. M.; Vinogradov, S. A., "Phosphorescent Oxygen Sensor with Dendritic Protection and Two-Photon Absorbing Antenna" *J. Am. Chem. Soc.* **2005**, *127*(*33*), 11851–11862; (e) Park, E. J.; Reid, K. R.; Tang, W.; Kennedy, R. T.; Kopelman, R., "Ratiometric Fiber Optic Sensors for the Detection of Inter- and Intra-Cellular Dissolved Oxygen" *J. Mater. Chem.* **2005**, *15*(*27–28*), 2913–2919; (f) Zhang, X.-a.; Lovejoy, K. S.; Jasanoff, A.; Lippard, S. J., "Water-Soluble Porphyrins as a Dual-Function Molecular Imaging Platform for MRI and Fluorescence Zinc Sensing" *Proc. Natl. Acad. Sci. U. S. A.* **2007**, *104*(*26*), 10780–10785; (g) Wu, C.; Bull, B.; Christensen, K.; McNeill, J., "Ratiometric Single-Nanoparticle Oxygen Sensors for Biological Imaging" *Angew. Chem., Int. Ed.* **2009**, *48*(*15*), 2741–2745; (h) Cheng, S.-H.; Lee, C.-H.; Chen, M.-C.; Souris, J. S.; Tseng, F.-G.; Yang, C.-S.; Mou, C.-Y.; Chen, C.-T.; Lo, L.-W., "Tri-Functionalization of Mesoporous Silica Nanoparticles for Comprehensive Cancer Theranostics-The Trio of Imaging, Targeting and Therapy" *J. Mater. Chem.* **2010**, *20*(*29*), 6149–6157; (i) Tu, W.-W.; Lei, J.-P.; Wang, P.; Ju, H.-X., "Photoelectrochemistry of Free-Base-Porphyrin-Functionalized Zinc Oxide Nanoparticles and Their Applications in Biosensing" *Chem. - Eur. J.* **2011**, *17*(*34*), 9440–9447.

45. Selected publications: (a) Becker, R. S.; Allison, J. B., "Metalloporphyrins. Electronic Spectra and Nature of Perturbations. II. Group II-A, II-B, and IV-A Derivatives" *J. Phys. Chem.* **1963**, *67*(*12*), 2669-75; (b) Slobodkin, G.; Fan, E.; Hamilton, A. D., "Molecular Recognition: Porphyrin-Containing Receptors as Analogs of Barbiturate-Induced Cytochrome P450" *New J. Chem.* **1992**, *16*(*5*), 643–5; (c) Kuroda, Y.; Hatakeyama, H.; Inakoshi, N.; Ogoshi, H., "Nucleotide Recognition in Aqueous Media with Artificial Receptor Based on Porphyrin" *Tetrahedron Lett.* **1993**, *34*(*51*), 828–8; (d) Mizutani, T.; Ema, T.; Tomita, T.; Kuroda, Y.; Ogoshi, H., "Design and Synthesis of a Trifunctional Chiral Porphyrin with C_2 Symmetry as a Chiral Recognition Host for Amino Acid Esters" *J. Am. Chem. Soc.* **1994**, *116*(*10*), 4240–4250; (e) Tsukube, H.; Shinoda, S.; Tamiaki, H., "Recognition and Sensing of Chiral Biological Substrates *via* Lanthanide Coordination Chemistry" *Coord. Chem. Rev.* **2002**, *226*(*1–2*), 227–234; (f) Bender, G. M.; Lehmann, A.; Zou, H.; Cheng, H.; Fry, H. C.; Engel, D.; Therien, M. J.; Blasie, J. K.; Roder, H.; Saven, J. G.; DeGrado, W. F., "De Novo Design of a Single-Chain Diphenylporphyrin Metalloprotein" *J. Am. Chem. Soc.* **2007**, *129*(*35*), 10732–10740; (g) Stefan-van Staden,

R.-I.; Moldoveanu, I.; Stanciu Gavan, C., "Pattern Recognition of HER-1 in Biological Fluids Using Stochastic Sensing" *J. Enzyme Inhib. Med. Chem.* **2015**, *30*(*2*), 283–285.

46. Selected publications: (a) Henderson, B. W.; Waldow, S. M.; Mang, T. S.; Potter, W. R.; Malone, P. B.; Dougherty, T. J., "Tumor Destruction and Kinetics of Tumor Cell Death in Two Experimental Mouse Tumors following Photodynamic Therapy" *Cancer Res.* **1985**, *45*(*2*), 572–6; (b) Bonnett, R., "Photosensitizers of the Porphyrin and Phthalocyanine Series for Photodynamic Therapy" *Chem. Soc. Rev.* **1995**, *24*(*1*), 19–33; (c) Oleinick, N. L.; Evans, H. H., "The Photobiology of Photodynamic Therapy: Cellular Targets and Mechanisms" *Radiat. Res.* **1998**, *150*(*5, Suppl.*), S146–S156; (d) Sternberg, E. D.; Dolphin, D.; Bruckner, C., "Porphyrin-Based Photosensitizers for Use in Photodynamic Therapy" *Tetrahedron* **1998**, *54*(*17*), 4151–4202; (e) Pandey, R. K.; Zheng, G. In *Porphyrins as Photosensitizers in Photodynamic Therapy*, Academic Press: 2000; pp 157–230; (f) Dichtel, W. R.; Serin, J. M.; Edder, C.; Frechet, J. M. J.; Matuszewski, M.; Tan, L.-S.; Ohulchanskyy, T. Y.; Prasad, P. N., "Singlet Oxygen Generation *via* Two-Photon Excited FRET" *J. Am. Chem. Soc.* **2004**, *126*(*17*), 5380–5381; (g) Drobizhev, M.; Stepanenko, Y.; Dzenis, Y.; Karotki, A.; Rebane, A.; Taylor, P. N.; Anderson, H. L., "Understanding Strong Two-Photon Absorption in **π**-Conjugated Porphyrin Dimers *via* Double-Resonance Enhancement in a Three-Level Model" *J. Am. Chem. Soc.* **2004**, *126*(*47*), 15352–15353; (h) Lang, K.; Mosinger, J.; Wagnerova, D. M., "Photophysical Properties of Porphyrinoid Sensitizers Non-Covalently Bound to Host Molecules; Models for Photodynamic Therapy" *Coord. Chem. Rev.* **2004**, *248*(*3–4*), 321–350; (i) Schmitt, F.; Govindaswamy, P.; Suess-Fink, G.; Ang, W. H.; Dyson, P. J.; Juillerat-Jeanneret, L.; Therrien, B., "Ruthenium Porphyrin Compounds for Photodynamic Therapy of Cancer" *J. Med. Chem.* **2008**, *51*(*6*), 1811–1816; (j) Ethirajan, M.; Chen, Y.; Joshi, P.; Pandey, R. K., "The Role of Porphyrin Chemistry in Tumor Imaging and Photodynamic Therapy" *Chem. Soc. Rev.* **2011**, *40*(*1*), 340–362.

47. Selected publications: (a) Kahl, S. B.; Joel, D. D.; Finkel, G. C.; Micca, P. L.; Nawrocky, M. M.; Coderre, J. A.; Slatkin, D. N., "A Carboranyl Porphyrin for Boron Neutron Capture Therapy of Brain Tumors" *Basic Life Sci.* **1989**, *50*, 193–203; (b) Miura, M.; Gabel, D.; Oenbrink, G.; Fairchild, R. G., "Preparation of Carboranyl Porphyrins for Boron Neutron-Capture Therapy" *Tetrahedron Lett.* **1990**, *31*(*16*), 2247–50; (c) Hill, J. S.; Kahl,

S. B.; Stylli, S. S.; Nakamura, Y.; Koo, M.-S.; Kaye, A. H., "Selective Tumor Kill of Cerebral Glioma by Photodynamic Therapy Using a Boronated Porphyrin Photosensitizer" *Proc. Natl. Acad. Sci. U. S. A.* **1995**, *92*(*26*), 12126–12130; (d) Miura, M.; Micca, P. L.; Fisher, C. D.; Gordon, C. R.; Heinrichs, J. C.; Slatkin, D. N., "Evaluation of Carborane-Containing Porphyrins as Tumor Targeting Agents for Boron Neutron Capture Therapy" *Br. J. Radiol.* **1998**, *71*(*July*), 773–781; (e) Mody, T. D., "Pharmaceutical Development and Medical Applications of Porphyrin-Type Macrocycles" *J. Porphyrins Phthalocyanines* **2000**, *4*(*4*), 362–367; (f) Vicente, M. G. H., "Porphyrin-Based Sensitizers in the Detection and Treatment of Cancer: Recent Progress" *Curr. Med. Chem.: Anti-Cancer Agents* **2001**, *1*(*2*), 175–194; (g) Kreimann, E. L.; Miura, M.; Itoiz, M. E.; Heber, E.; Garavaglia, R. N.; Batistoni, D.; Rebagliati, R. J.; Roberti, M. J.; Micca, P. L.; Coderre, J. A.; Schwint, A. E., "Biodistribution of a Carborane-Containing Porphyrin as a Targeting Agent for Boron Neutron Capture Therapy of Oral Cancer in the Hamster Cheek Pouch" *Arch. Oral Biol.* **2003**, *48*(*3*), 223–232; (h) Luguya, R.; Fronczek, F. R.; Smith, K. M.; Vicente, M. G. H., "Synthesis of Novel Carboranylchlorins with Dual Application in Boron Neutron Capture Therapy (BNCT) and Photodynamic Therapy (PDT)" *Appl. Radiat. Isot.* **2004**, *61*(*5*), 1117–1123; (i) Gottumukkala, V.; Luguya, R.; Fronczek, F. R.; Vicente, M. G. H., "Synthesis and Cellular Studies of an Octa-Anionic 5,10,15,20-Tetra[3,5-(nido-carboranylmethyl)phenyl]porphyrin (H2OCP) for Application in BNCT" *Bioorg. Med. Chem.* **2005**, *13*(*5*), 1633–1640; (j) Renner, M. W.; Miura, M.; Easson, M. W.; Vicente, M. G. H., "Recent Progress in the Syntheses and Biological Evaluation of Boronated Porphyrins for Boron Neutron-Capture Therapy" *Anti-Cancer Agents Med. Chem.* **2006**, *6*(*2*), 145–157.

48. Selected publications: (a) Georgiou, G. N.; Ahmet, M. T.; Houlton, A.; Silver, J.; Cherry, J., "Measurement of the Rate of Uptake and Subcellular Localization of Porphyrins in Cells Using Fluorescence Digital Imaging Microscopy" *Photochem. Photobiol.* **1994**, *59*(*4*), 419–422; (b) Guo, M.; Chen, J.; Zhang, Y.; Chen, K.; Pan, C.; Yao, S., "Enhanced Adhesion/Spreading and Proliferation of Mammalian Cells on Electropolymerized Porphyrin Film for Biosensing Applications" *Biosens. Bioelectron.* **2008**, *23*(*6*), 865–871; (c) Lee, T.; Zhang, X.-a.; Dhar, S.; Faas, H.; Lippard, S. J.; Jasanoff, A., "*In vivo* Imaging with a Cell-Permeable Porphyrin-Based MRI Contrast Agent" *Chem.*

Biol. (Cambridge, MA, U. S.) **2010**, *17*(*6*), 665–673; (d) Zhao, T.; Wu, H.; Yao, S. Q.; Xu, Q.-H.; Xu, G. Q., "Nanocomposites Containing Gold Nanorods and Porphyrin-Doped Mesoporous Silica with Dual Capability of Two-Photon Imaging and Photosensitization" *Langmuir* **2010**, *26*(*18*), 14937–14942; (e) Mazzaglia, A.; Valerio, A.; Micali, N.; Villari, V.; Quaglia, F.; Castriciano, M. A.; Scolaro, L. M.; Giuffre, M.; Siracusano, G.; Sciortino, M. T., "Effective Cell Uptake of Nanoassemblies of a Fluorescent Amphiphilic Cyclodextrin and an Anionic Porphyrin" *Chem. Commun. (Cambridge, U. K.)* **2011**, *47*(*32*), 9140–9142; (f) Nowostawska, M.; Corr, S. A.; Byrne, S. J.; Conroy, J.; Volkov, Y.; Gun'ko, Y. K., "Porphyrin-Magnetite Nanoconjugates for Biological Imaging" *J. Nanobiotechnol.* **2011**, *9*, 13; (g) Eggenspiller, A.; Michelin, C.; Desbois, N.; Richard, P.; Barbe, J.-M.; Denat, F.; Licona, C.; Gaiddon, C.; Sayeh, A.; Choquet, P.; Gros, C. P., "Design of Porphyrin-dota-Like Scaffolds as All-in-One Multimodal Heterometallic Complexes for Medical Imaging" *Eur. J. Org. Chem.* **2013**, *2013*(*29*), 6629–6643; (h) Lu, J.; Zhang, W.; Yuan, L.; Ma, W.; Li, X.; Lu, W.; Zhao, Y.; Chen, G., "One-Pot Synthesis of Glycopolymer-Porphyrin Conjugate as Photosensitizer for Targeted Cancer Imaging and Photodynamic Therapy" *Macromol. Biosci.* **2014**, *14*(*3*), 340–346; (i) Mauriello-Jimenez, C.; Croissant, J.; Maynadier, M.; Cattoen, X.; Wong Chi Man, M.; Vergnaud, J.; Chaleix, V.; Sol, V.; Garcia, M.; Gary-Bobo, M.; Raehm, L.; Durand, J.-O., "Porphyrin-Functionalized Mesoporous Organosilica Nanoparticles for Two-Photon Imaging of Cancer Cells and Drug Delivery" *J. Mater. Chem. B* **2015**, *3*(*18*), 3681–3684.

49. Selected publications: (a) Hong, F. T.; Mauzerall, D., "Photoemf at a Single Membrane-Solution Interface Specific to Lipid Bilayers Containing Magnesium Porphyrins" *Nature (London), New Biol.* **1972**, *240*(*100*), 154–5; (b) Imahori, H.; Fukuzumi, S., "Porphyrin- and Fullerene-Based Molecular Photovoltaic Devices" *Adv. Funct. Mater.* **2004**, *14*(*6*), 525–536; (c) Hasobe, T.; Imahori, H.; Kamat, P. V.; Ahn, T. K.; Kim, S. K.; Kim, D.; Fujimoto, A.; Hirakawa, T.; Fukuzumi, S., "Photovoltaic Cells Using Composite Nanoclusters of Porphyrins and Fullerenes with Gold Nanoparticles" *J. Am. Chem. Soc.* **2005**, *127*(*4*), 1216–1228; (d) Wang, Q.; Campbell, W. M.; Bonfantani, E. E.; Jolley, K. W.; Officer, D. L.; Walsh, P. J.; Gordon, K.; Humphry-Baker, R.; Nazeeruddin, M. K.; Graetzel, M., "Efficient Light Harvesting by Using Green Zn-Porphyrin-Sensitized Nanocrystalline TiO_2 Films" *J. Phys. Chem. B* **2005**, *109*(*32*), 15397–15409; (e) Campbell,

W. M.; Jolley, K. W.; Wagner, P.; Wagner, K.; Walsh, P. J.; Gordon, K. C.; Schmidt-Mende, L.; Nazeeruddin, M. K.; Wang, Q.; Graetzel, M.; Officer, D. L., "Highly Efficient Porphyrin Sensitizers for Dye-Sensitized Solar Cells" *J. Phys. Chem. C* **2007**, *111*(*32*), 11760–11762; (f) Imahori, H.; Umeyama, T.; Ito, S., "Large **π**-Aromatic Molecules as Potential Sensitizers for Highly Efficient Dye-Sensitized Solar Cells" *Acc. Chem. Res.* **2009**, *42*(*11*), 1809–1818; (g) Lee, C.-W.; Lu, H.-P.; Lan, C.-M.; Huang, Y.-L.; Liang, Y.-R.; Yen, W.-N.; Liu, Y.-C.; Lin, Y.-S.; Diau, R. W.-G.; Yeh, C.-Y., "Novel Zinc Porphyrin Sensitizers for Dye-Sensitized Solar Cells: Synthesis and Spectral, Electrochemical, and Photovoltaic Properties" *Chem. - Eur. J.* **2009**, *15*(*6*), 1403–1412; (h) Bessho, T.; Zakeeruddin, S. M.; Yeh, C.-Y.; Diau, E. W.-G.; Graetzel, M., "Highly Efficient Mesoscopic Dye-Sensitized Solar Cells Based on Donor-Acceptor-Substituted Porphyrins" *Angew. Chem., Int. Ed.* **2010**, *49*(*37*), 6646–6649; (i) Yella, A.; Lee, H.-W.; Tsao, H. N.; Yi, C.; Chandiran, A. K.; Nazeeruddin, M. K.; Diau, E. W.-G.; Yeh, C.-Y.; Zakeeruddin, S. M.; Graetzel, M., "Porphyrin-Sensitized Solar Cells with Cobalt (II/III)-Based Redox Electrolyte Exceed 12% Efficiency" *Science (Washington, DC, U. S.)* **2011**, *334*(*6056*), 629–634; (j) Mathew, S.; Yella, A.; Gao, P.; Humphry-Baker, R.; Curchod, B. F. E.; Ashari-Astani, N.; Tavernelli, I.; Rothlisberger, U.; Nazeeruddin, M. K.; Graetzel, M., "Dye-Sensitized Solar Cells with 13% Efficiency Achieved through the Molecular Engineering of Porphyrin Sensitizers" *Nat. Chem.* **2014**, *6*(*3*), 242–247.

50. Selected publications: (a) Lamansky, S.; Kwong, R. C.; Nugent, M.; Djurovich, P. I.; Thompson, M. E., "Molecularly Doped Polymer Light Emitting Diodes Utilizing Phosphorescent Pt(II) and Ir(III) Dopants" *Org. Electron.* **2001**, *2*(*1*), 53–62; (b) Lupton, J. M.; Samuel, I. D. W.; Frampton, M. J.; Beavington, R.; Burn, P. L., "Control of Electrophosphorescence in Conjugated Dendrimer Light-Emitting Diodes" *Adv. Funct. Mater.* **2001**, *11*(*4*), 287–294; (c) Higgins, R. W. T.; Monkman, A. P.; Nothofer, H. G.; Scherf, U., "Energy Transfer to Porphyrin Derivative Dopants in Polymer Light-Emitting Diodes" *J. Appl. Phys.* **2002**, *91*(*1*), 99–105; (d) Noh, Y.-Y.; Lee, C.-L.; Kim, J.-J.; Yase, K., "Energy Transfer and Device Performance in Phosphorescent Dye Doped Polymer Light Emitting Diodes" *J. Chem. Phys.* **2003**, *118*(*6*), 2853–2864; (e) Li, B.; Li, J.; Fu, Y.; Bo, Z., "Porphyrins with Four Monodisperse Oligofluorene Arms as Efficient Red Light-Emitting Materials" *J. Am. Chem. Soc.* **2004**, *126*(*11*), 3430–3431; (f) Li, B.; Xu, X.; Sun, M.; Fu, Y.; Yu, G.; Liu,

Y.; Bo, Z., "Porphyrin-Cored Star Polymers as Efficient Nondoped Red Light-Emitting Materials" *Macromolecules* **2006**, *39*(*1*), 456–461; (g) Endo, A.; Ogasawara, M.; Takahashi, A.; Yokoyama, D.; Kato, Y.; Adachi, C., "Thermally Activated Delayed Fluorescence from $Sn4^{+}$-Porphyrin Complexes and Their Application to Organic Light Emitting Diodes - A Novel Mechanism for Electroluminescence" *Adv. Mater. (Weinheim, Ger.)* **2009**, *21*(*47*), 4802–4806; (h) Sommer, J. R.; Farley, R. T.; Graham, K. R.; Yang, Y.; Reynolds, J. R.; Xue, J.; Schanze, K. S., "Efficient Near-Infrared Polymer and Organic Light-Emitting Diodes Based on Electrophosphorescence from (Tetraphenyltetranaphtho[2,3]porphyrin)platinum(II)" *ACS Appl. Mater. Interfaces* **2009**, *1*(*2*), 274–278; (i) Fenwick, O.; Sprafke, J. K.; Binas, J.; Kondratuk, D. V.; Di Stasio, F.; Anderson, H. L.; Cacialli, F., "Linear and Cyclic Porphyrin Hexamers as Near-Infrared Emitters in Organic Light-Emitting Diodes" *Nano Lett.* **2011**, *11*(*6*), 2451–2456; (j) Graham, K. R.; Yang, Y.; Sommer, J. R.; Shelton, A. H.; Schanze, K. S.; Xue, J.; Reynolds, J. R., "Extended Conjugation Platinum(II) Porphyrins for use in Near-Infrared Emitting Organic Light Emitting Diodes" *Chem. Mater.* **2011**, *23*(*24*), 5305–5312.

51. Selected publications: (a) Irie, R.; Li, X.; Saito, Y., "Reaction Mechanism of Photocatalysis for the Liquid-Phase Dehydrogenation of 2-Propanol with Rhodium Porphyrin Complex" *J. Mol. Catal.* **1984**, *23*(*1*), 17–22; (b) Barley, M. H.; Takeuchi, K. J.; Meyer, T. J., "Electrocatalytic Reduction of Nitrite to Ammonia Based on a Water-Soluble Iron Porphyrin" *J. Am. Chem. Soc.* **1986**, *108*(*19*), 5876–85; (c) Zak, J.; Yuan, H.; Ho, M.; Woo, L. K.; Porter, M. D., "Thiol-Derivatized Metalloporphyrins: Monomolecular Films for the Electrocatalytic Reduction of Dioxygen at Gold Electrodes" *Langmuir* **1993**, *9*(*11*), 2772–2774; (d) Maldotti, A.; Bartocci, C.; Varani, G.; Molinari, A.; Battioni, P.; Mansuy, D., "Oxidation of Cyclohexane by Molecular Oxygen Photoassisted by *meso*-Tetraarylporphyrin Iron(III)-Hydroxo Complexes" *Inorg. Chem.* **1996**, *35*(*5*), 1126–1131; (e) Gojkovic, S. L.; Gupta, S.; Savinell, R. F., "Heat-Treated Iron(III) Tetramethoxyphenyl Porphyrin Supported on High-Area Carbon as an Electrocatalyst for Oxygen Reduction. I. Characterization of the Electrocatalyst" *J. Electrochem. Soc.* **1998**, *145*(*10*), 3493–3499; (f) Mele, G.; Del Sole, R.; Vasapollo, G.; Garcia-Lopez, E.; Palmisano, L.; Schiavello, M., "Photocatalytic Degradation of 4-Nitrophenol in Aqueous Suspension by Using Polycrystalline TiO_2 Impregnated with Functionalized Cu(II)-Porphyrin or Cu(II)-

Phthalocyanine" *J. Catal.* **2003**, *217*(*2*), 334–342; (g) Rosenthal, J.; Luckett, T. D.; Hodgkiss, J. M.; Nocera, D. G., "Photocatalytic Oxidation of Hydrocarbons by a Bis-iron(III)-μ-oxo Pacman Porphyrin Using O_2 and Visible Light" *J. Am. Chem. Soc.* **2006**, *128*(*20*), 6546–6547; (h) Koslowski, U. I.; Abs-Wurmbach, I.; Fiechter, S.; Bogdanoff, P., "Nature of the Catalytic Centers of Porphyrin-Based Electrocatalysts for the ORR: A Correlation of Kinetic Current Density with the Site Density of Fe-N_4 Centers" *J. Phys. Chem. C* **2008**, *112*(*39*), 15356–15366; (i) Fateeva, A.; Chater, P. A.; Ireland, C. P.; Tahir, A. A.; Khimyak, Y. Z.; Wiper, P. V.; Darwent, J. R.; Rosseinsky, M. J., "A Water-Stable Porphyrin-Based Metal-Organic Framework Active for Visible-Light Photocatalysis" *Angew. Chem. Int. Ed.* **2012**, *51*(*30*), 7440–7444,; (j) Wu, Z.-S.; Chen, L.; Liu, J.; Parvez, K.; Liang, H.; Shu, J.; Sachdev, H.; Graf, R.; Feng, X.; Muellen, K., "High-Performance Electrocatalysts for Oxygen Reduction Derived from Cobalt Porphyrin-Based Conjugated Mesoporous Polymers" *Adv. Mater. (Weinheim, Ger.)* **2014**, *26*(*9*), 1450–1455.

52. Nobelprize.org Nobel Lecture: On Haemin and the Relationships between Haemin and Chlorophyll. http://www.nobelprize.org/nobel_prizes/chemistry/laureates/1930/fischer-lecture.html (accessed 4 February).

53. Rothemund, P., "Formation of Porphyrins from Pyrrole and Aldehydes" *J. Am. Chem. Soc.* **1935**, *57*(*10*), 2010–2011.

54. Rothemund, P., "A New Porphyrin Synthesis. The Synthesis of Porphin" *J. Am. Chem. Soc.* **1936**, *58*(*4*), 625–627.

55. Rothemund, P., "Porphyrin Studies. III. The Structure of the Porphine Ring System" *J. Am. Chem. Soc.* **1939**, *61*(*10*), 2912–2915.

56. Adler, A. D.; Longo, F. R.; Finarelli, J. D.; Goldmacher, J.; Assour, J.; Korsakoff, L., "A Simplified Synthesis for *meso*-Tetraphenylporphine" *The Journal of Organic Chemistry* **1967**, *32*(*2*), 476-476.

57. Lindsey, J. S.; Schreiman, I. C.; Hsu, H. C.; Kearney, P. C.; Marguerettaz, A. M., "Rothemund and Adler-Longo Reactions Revisited: Synthesis of Tetraphenylporphyrins under Equilibrium Conditions" *The Journal of Organic Chemistry* **1987**, *52*(*5*), 827–836.

58. Geier, G. R.; Ciringh, Y.; Li, F.; Haynes, D. M.; Lindsey, J. S., "A Survey of Acid Catalysts for Use in Two-Step, One-Flask Syntheses of Meso-Substituted Porphyrinic Macrocycles" *Org. Lett.* **2000**, *2*(*12*), 1745–1748.

59. Geier Iii, G. R.; Lindsey, J. S., "Effects of Aldehyde or Dipyrromethane Substituents on the Reaction Course Leading to *meso*-Substituted Porphyrins" *Tetrahedron* **2004**, *60*(*50*), 11435–11444.

60. Rao, P. D.; Dhanalekshmi, S.; Littler, B. J.; Lindsey, J. S., "Rational Syntheses of Porphyrins Bearing up to Four Different Meso Substituents" *J. Org. Chem.* **2000**, *65*(*22*), 7323–7344.

61. Littler, B. J.; Ciringh, Y.; Lindsey, J. S., "Investigation of Conditions Giving Minimal Scrambling in the Synthesis of *trans*-Porphyrins from Dipyrromethanes and Aldehydes" *J. Org. Chem.* **1999**, *64*(*8*), 2864–2872.

62. Filatov, M. A.; Lebedev, A. Y.; Vinogradov, S. A.; Cheprakov, A. V., "Synthesis of 5,15-Diaryltetrabenzoporphyrins" *J. Org. Chem.* **2008**, *73*(*11*), 4175–4185.

63. Jaboski, A., "Efficiency of Anti-Stokes Fluorescence in Dyes" *Nature* **1933**, *131*, 839–840.

64. Segawa, H.; Nakayama, N.; Shimidzu, T., "Electrochemical Synthesis of One-Dimensional Donor-Acceptor Polymers Containing Oligothiophenes and Phosphorus Porphyrins" *J. Chem. Soc., Chem. Commun.* **1992**, (*10*), 784–786.

65. Shimidzu, T.; Segawa, H.; Wu, F.; Nakayama, N., "Approaches to Conducting Polymer Devices with Nanostructures: Photoelectrochemical Function of One-Dimensional and Two-Dimensional Porphyrin Polymers with Oligothienyl Molecular Wire" *J. Photochem. Photobiol. A: Chem.* **1995**, *92*(*1*), 121–127.

66. Cho, E. H.; Chae, S. H.; Kim, K.; Lee, S. J.; Joo, J., "Photovoltaic Characteristics of Organic Solar Cells Using Zn–Porphyrin Derivatives with Controlled **π**-Conjugation Structures" *Synth. Met.* **2012**, *162*(*9–10*), 813–819.

67. Keawsongsaeng, W.; Gasiorowski, J.; Denk, P.; Oppelt, K.; Apaydin, D. H.; Rojanathanes, R.; Hingerl, K.; Scharber, M.; Sariciftci, N. S.; Thamyongkit, P., "Systematic Investigation of Porphyrin-Thiophene Conjugates for Ternary Bulk Heterojunction Solar Cells" *Adv. Energy Mater.* **2016**, *6*(*20*), 1600957.

68. Rohand, T.; Dolusic, E.; Ngo, T. H.; Maes, W.; Dehaen, W., "Efficient Synthesis of Aryldipyrromethanes in Water and Their Application in the Synthesis of Corroles and Dipyrromethenes" *ARKIVOC* **2007**, *10*, 307–324.

69. Lee, C.-H.; S. Lindsey, J., "One-Flask Synthesis of *meso*-Substituted Dipyrromethanes and Their Application in the Synthesis of *trans*-Substituted Porphyrin Building Blocks" *Tetrahedron* **1994**, *50*(*39*), 11427–11440.

70. Jiao, J.; Thamyongkit, P.; Schmidt, I.; Lindsey, J. S.; Bocian, D. F., "Characterization of Porphyrin Surface Orientation in Monolayers on Au(111) and Si(100) Using Spectroscopically Labeled Molecules" *J. Phys. Chem. C* **2007**, *111*(*34*), 12693–12704.

71. Ono, N.; Maruyama, K., "Synthesis of Octaalkyl- and Octaarylporphyrins from Nitroalkenes" *Chem. Lett.* **1988**, *17*(*9*), 1511–1514.

72. Finikova, O. S.; Cheprakov, A. V.; Beletskaya, I. P.; Carroll, P. J.; Vinogradov, S. A., "Novel Versatile Synthesis of Substituted Tetrabenzoporphyrins" *J. Org. Chem.* **2004**, *69*(*2*), 522–535.

73. Uppal, T.; Hu, X.; Fronczek, F. R.; Maschek, S.; Bobadova-Parvanova, P.; Vicente, M. G. H., "Synthesis, Computational Modeling, and Properties of Benzo-Appended BODIPYs" *Chemistry – A European Journal* **2012**, *18*(*13*), 3893–3905.

74. Filatov, M. A.; Cheprakov, A. V.; Beletskaya, I. P., "A Facile and Reliable Method for the Synthesis of Tetrabenzoporphyrin from 4,7-Dihydroisoindole" *Eur. J. Org. Chem.* **2007**, *2007*(*21*), 3468–3475.

75. Smith, T. J.; Stevenson, K. J., Reference Electrodes. In *Handbook of Electrochemistry*, Elsevier: Amsterdam, 2007; pp 73–110.

76. (a) Cardona, C. M.; Li, W.; Kaifer, A. E.; Stockdale, D.; Bazan, G. C., "Electrochemical Considerations for Determining Absolute Frontier Orbital Energy Levels of Conjugated Polymers for Solar Cell Applications" *Adv. Mater.* **2011**, *23*(*20*), 2367–2371; (b) Baran, D.; Balan, A.; Celebi, S.; Meana Esteban, B.; Neugebauer, H.; Sariciftci, N. S.; Toppare, L., "Processable Multipurpose Conjugated Polymer for Electrochromic and Photovoltaic Applications" *Chem. Mater.* **2010**, *22*(*9*), 2978–2987.

77. Geier Iii, G. R.; Littler, B. J.; Lindsey, J. S., "Investigation of Porphyrin-Forming Reactions. Part 3.1 The Origin of Scrambling in Dipyrromethane + Aldehyde

Condensations Yielding *trans*-A_2B_2-Tetraarylporphyrins" *J. Chem. Soc., Perkin Trans. 2* **2001**, (*5*), 701–711.

78. Shustareva, T. K.; Druzhinina, V. E., "Study of Kinetics and Mechanism of Sulfonation of Thiophene and Its Derivatives by Complex Compounds of Sulfuric Anhydride" *Chemistry of Heterocyclic Compounds* **1986**, *22*(*1*), 28–33.

79. Rochford, J.; Botchway, S.; McGarvey, J. J.; Rooney, A. D.; Pryce, M. T., "Photophysical and Electrochemical Properties of *meso*-Substituted Thien-2-yl Zn(II) Porphyrins" *The Journal of Physical Chemistry A* **2008**, *112*(*46*), 11611–11618.

80. Jintanalert, P. Development of Benzoporphyrinic Compounds as Electrocatalysts for Carbon Dioxide Reduction. Chulalongkorn, Bangkok, 2014.

81. (a) Bruckner, C.; Foss, P. C. D.; Sullivan, J. O.; Pelto, R.; Zeller, M.; Birge, R. R.; Crundwell, G., "Origin of the Bathochromically Shifted Optical Spectra of *meso*-Tetrathien-2'- and 3'-ylporphyrins as Compared to *meso*-Tetraphenylporphyrin" *PCCP* **2006**, *8*(*20*), 2402–2412; (b) Gupta, I.; Ravikanth, M., "Spectroscopic Properties of *meso*-Thienylporphyrins with Different Porphyrin Cores" *J. Photochem. Photobiol. A: Chem.* **2006**, *177*, 156–163.

82. Scheidt, W. R.; Kastner, M. E.; Hatano, K., "Stereochemistry of the Toluene Solvate of α,β,γ,δ-Tetraphenylporphinatozinc(II)" *Inorg. Chem.* **1978**, *17*(*3*), 706–710.

83. (a) Luechai, A.; Gasiorowski, J.; Petsom, A.; Neugebauer, H.; Sariciftci, N. S.; Thamyongkit, P., "Photosensitizing Porphyrin-Triazine Compound for Bulk Heterojunction Solar Cells" *J. Mater. Chem.* **2012**, *22*(*43*), 23030–23037; (b) Kengthanomma, T.; Thamyongkit, P.; Gasiorowski, J.; Ramil, A. M.; Sariciftci, N. S., "On the Potential of Porphyrin-Spiked Triarylamine Stars for Bulk Heterojunction Solar Cells" *J. Mater. Chem. A* **2013**, *1*(*35*), 10524–10531.

84. Denden, Z.; Ezzayani, K.; Saint-Aman, E.; Loiseau, F.; Najmudin, S.; Bonifácio, C.; Daran, J.-C.; Nasri, H., "Insights on the UV/Vis, Fluorescence, and Cyclic Voltammetry Properties and the Molecular Structures of ZnII Tetraphenylporphyrin Complexes with Pseudohalide Axial Azido, Cyanato-N, Thiocyanato-N, and Cyanido Ligands" *Eur. J. Inorg. Chem.* **2015**, *2015*(*15*), 2596–2610.

85. Zanotti, G.; Angelini, N.; Mattioli, G.; Paoletti, A. M.; Pennesi, G.; Rossi, G.; Caschera, D.; de Marco, L.; Gigli, G., "Metal-Organic Green Dye: Chemical and Physical

Insight into a Modified Zn-Benzoporphyrin for Dye-Sensitized Solar Cells" *RSC Advances* **2016**, *6*(*6*), 5123–5133.

APPENDIX

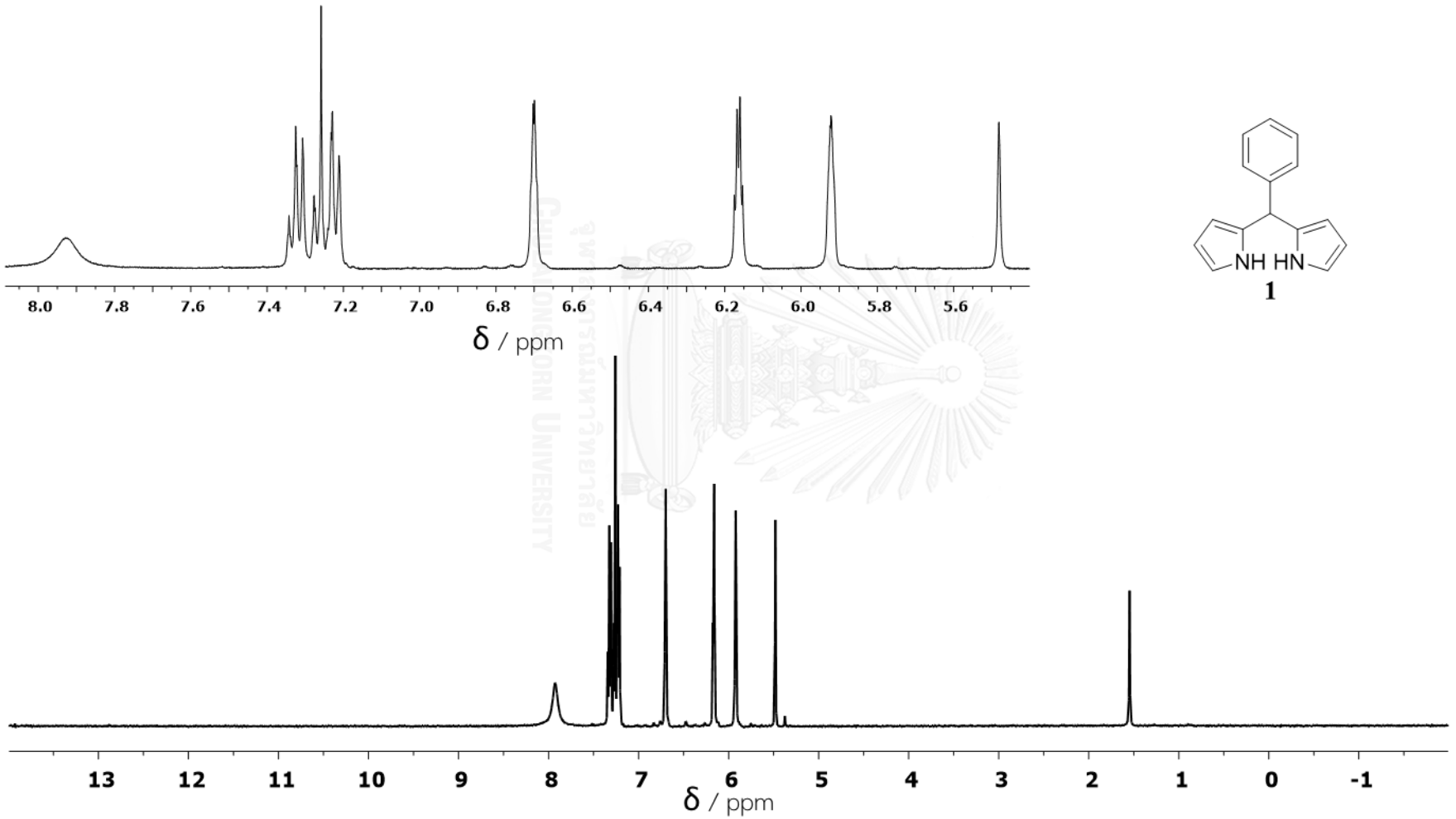

Figure A–1: ^{1}H-NMR spectrum of compound **1** in $CDCl_3$.

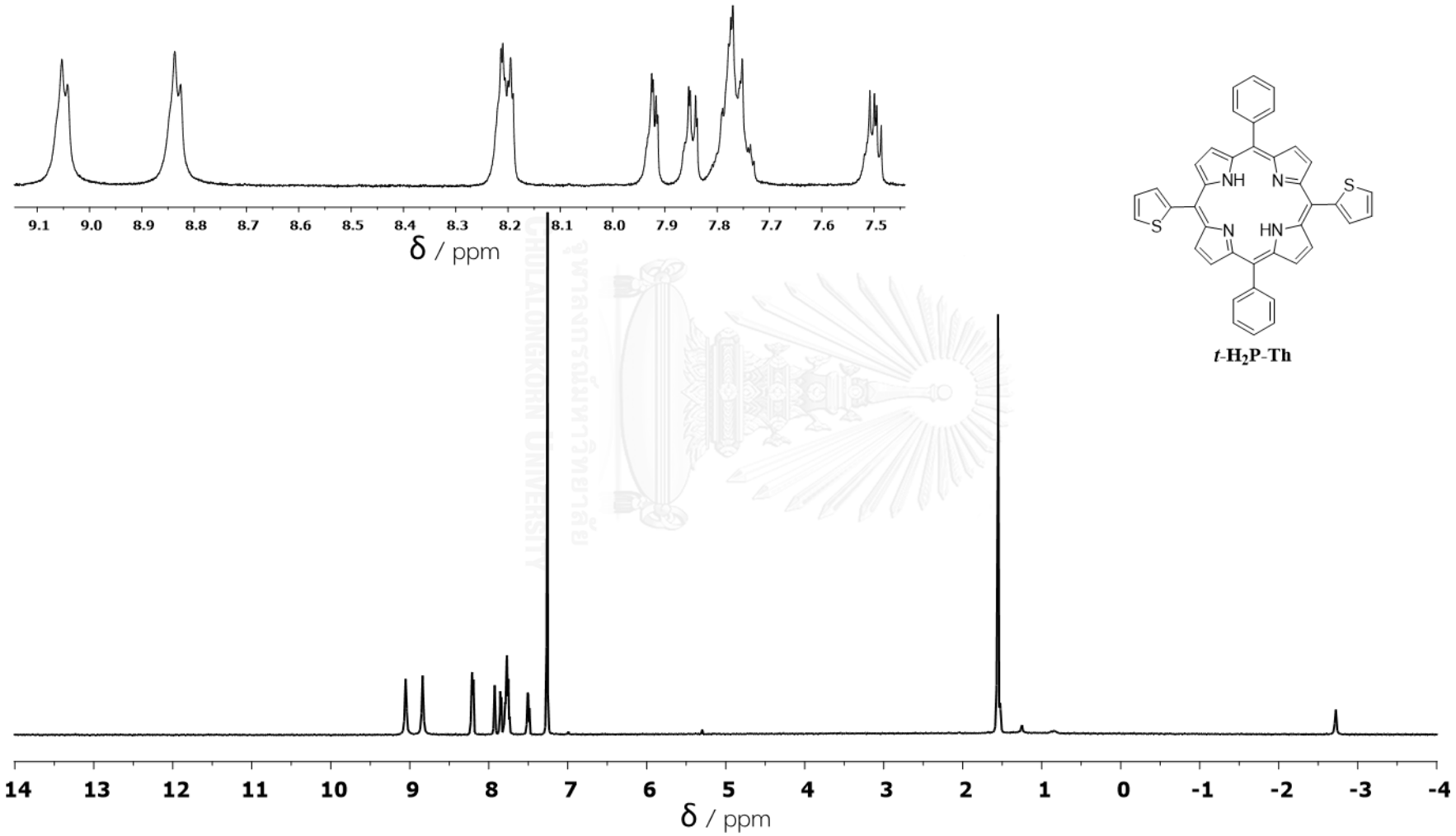

Figure A–2: ^{1}H-NMR spectrum of ***t*-H_2P-Th** in $CDCl_3$.

Mass Spectrum List Report

Analysis Info

Analysis Name	OSCUHS580727005.d	Acquisition Date	7/28/2015 3:28:35 PM
Method	MKE_tune_wide_20130204.m	Operator	Administrator
Sample Name	Por-1 Por-1	Instrument	micrOTOF 72

Acquisition Parameter

Source Type	ESI	Ion Polarity	Positive	Set Corrector Fill	79 V
Scan Range	n/a	Capillary Exit	180.0 V	Set Pulsar Pull	406 V
Scan Begin	50 m/z	Hexapole RF	400.0 V	Set Pulsar Push	388 V
Scan End	3000 m/z	Skimmer 1	54.4 V	Set Reflector	1300 V
		Hexapole 1	21.4 V	Set Flight Tube	9000 V
				Set Detector TOF	1910 V

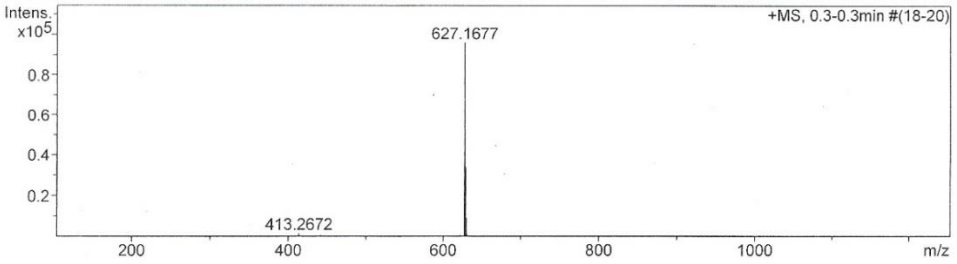

#	m/z	I	I %	S/N	FWHM	Res.
1	53.7384	127	0.1	19.1	0.0052	10283
2	56.1487	204	0.2	30.9	0.0052	10876
3	58.6166	180	0.2	27.3	0.0056	10402
4	69.0062	142	0.1	21.4	0.0060	11551
5	74.5182	111	0.1	16.6	0.0064	11607
6	145.0665	115	0.1	17.3	0.0078	18498
7	145.1766	106	0.1	15.9	0.0083	17494
8	297.7730	153	0.2	27.1	0.0117	25470
9	413.2672	1501	1.6	238.6	0.0560	7386
10	414.2702	346	0.4	54.7	0.0573	7224
11	429.2467	152	0.2	23.0	0.0479	8965
12	441.2992	620	0.6	92.7	0.0484	9123
13	442.3033	135	0.1	19.8	0.0605	7316
14	482.9375	104	0.1	14.0	0.0157	30740
15	621.2103	505	0.5	68.6	0.0798	7788
16	622.2113	215	0.2	28.9	0.0605	10279
17	627.1677	95817	100.0	13188.2	0.0802	7820
18	628.1702	34248	35.7	4719.0	0.0765	8214
19	629.1685	8988	9.4	1239.5	0.0728	8641
20	630.1654	1236	1.3	170.3	0.0673	9370
21	631.1618	265	0.3	36.2	0.0532	11870
22	791.1396	199	0.2	32.0	0.1028	7696
23	792.1432	118	0.1	18.9	0.0833	9509
24	1305.6079	102	0.1	20.3	0.0256	51014
25	1389.2393	103	0.1	20.9	0.0261	53137
26	1616.1765	115	0.1	24.2	0.0273	59127
27	2061.9888	103	0.1	22.3	0.0338	61074
28	2352.1975	268	0.3	57.5	0.0311	75626
29	2867.1611	107	0.1	22.9	0.0371	77313
30	2972.6793	107	0.1	22.8	0.0369	80497

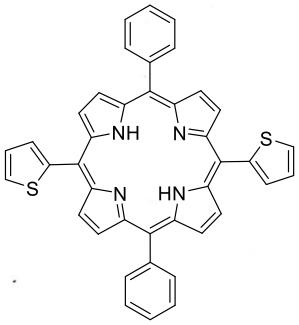

***t*-H_2P-Th**

Chemical Formula: $C_{40}H_{26}N_4S_2$

Exact Mass: 626.1599

Molecular Weight: 626.7960

$[M+H]^+$: 627.1672

Bruker Daltonics DataAnalysis 3.3 printed: 7/28/2015 3:51:24 PM Page 1 of 1

Figure A–3: HR-ESI mass spectrum of ***t*-H_2P-Th**.

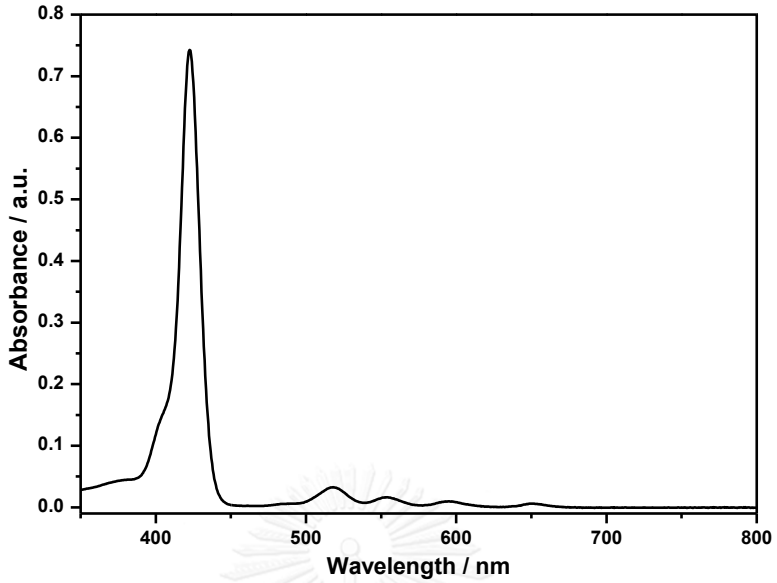

Figure A–4: Absorption spectrum of ***t*-H_2P-Th** in toluene.

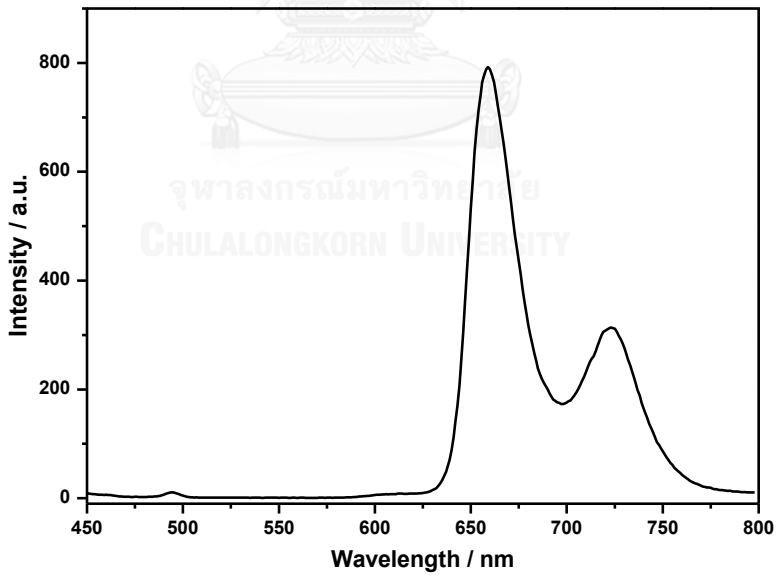

Figure A–5: Emission spectrum of ***t*-H_2P-Th** in toluene (λ_{ex} = 422 nm).

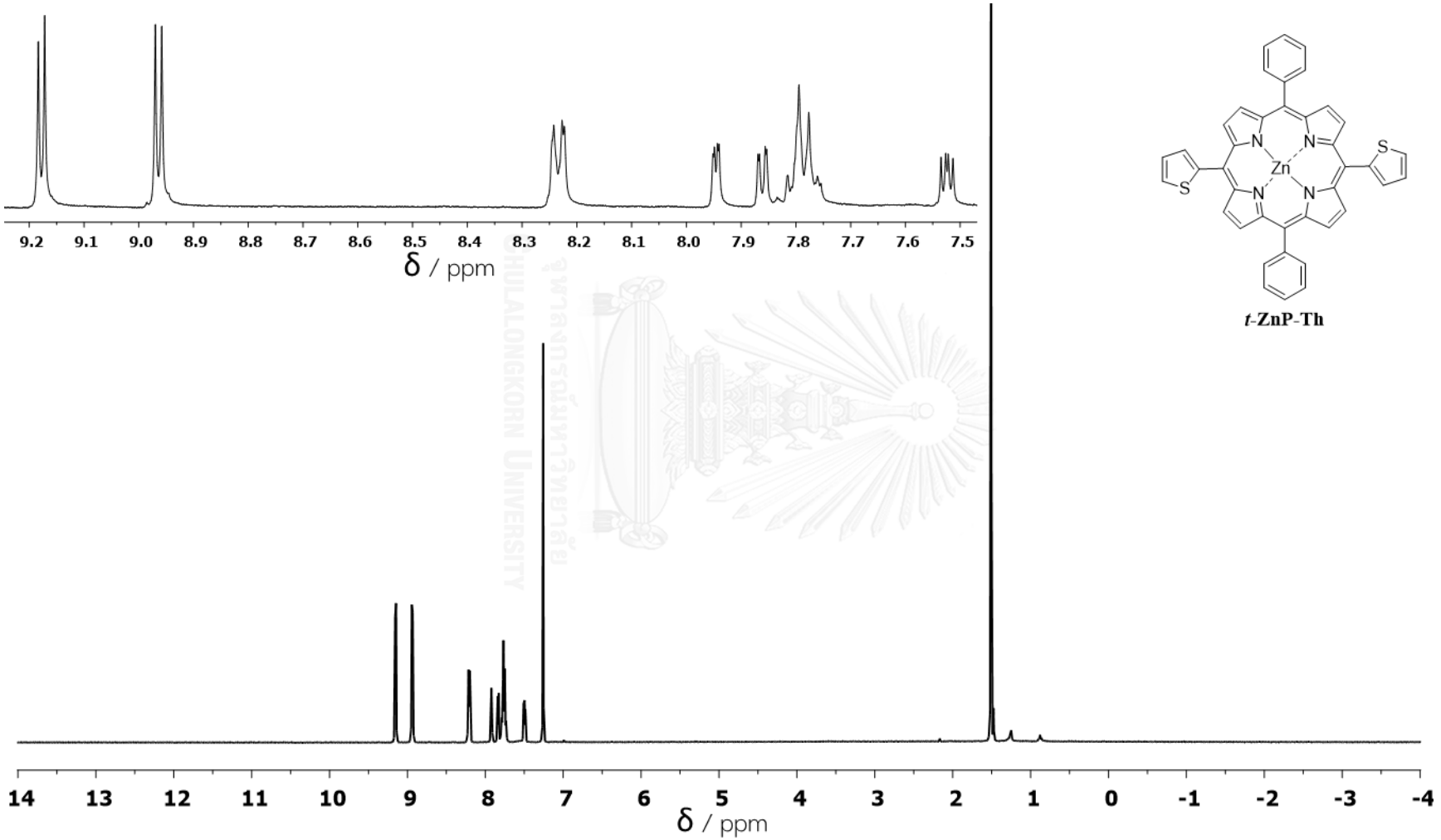

Figure A–6: ^{1}H-NMR spectrum of ***t*-ZnP-Th** in $CDCl_3$.

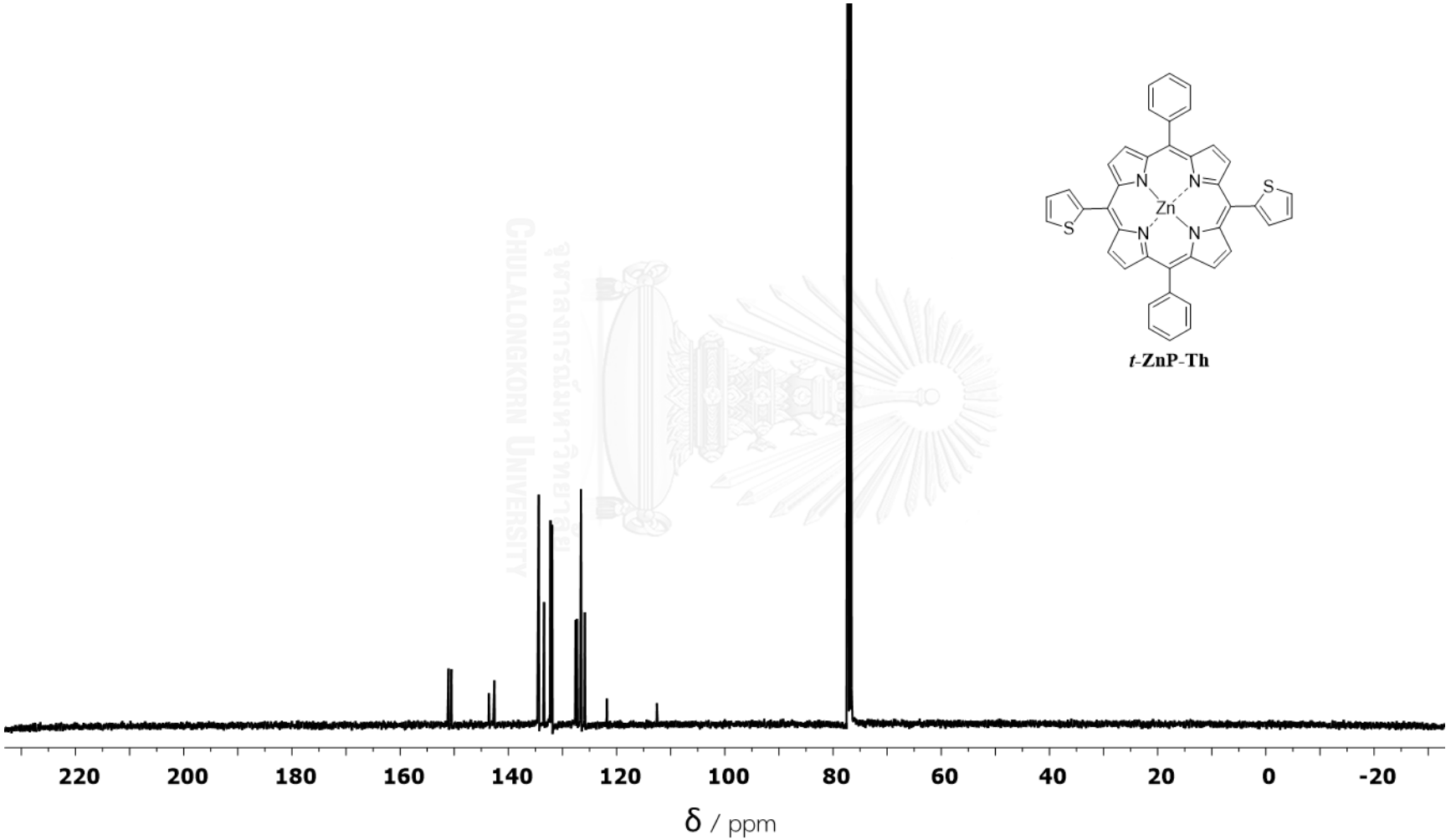

Figure A–7: ^{13}C-NMR spectrum of ***t*-ZnP-Th** in $CDCl_3$

Mass Spectrum List Report

Analysis Info

Analysis Name	OSCUAT590405003.d	Acquisition Date	4/5/2016 12:36:24 PM
Method	Tune_wide_POS_Tawatchai_05Feb2016.m	Operator	Administrator
Sample Name	t-ZnP-Th	Instrument	micrOTOF 72
	t-ZnP-Th		

Acquisition Parameter

Source Type	ESI	Ion Polarity	Positive	Set Corrector Fill	50 V
Scan Range	n/a	Capillary Exit	180.0 V	Set Pulsar Pull	337 V
Scan Begin	50 m/z	Hexapole RF	400.0 V	Set Pulsar Push	337 V
Scan End	3000 m/z	Skimmer 1	70.0 V	Set Reflector	1300 V
		Hexapole 1	25.0 V	Set Flight Tube	9000 V
				Set Detector TOF	2295 V

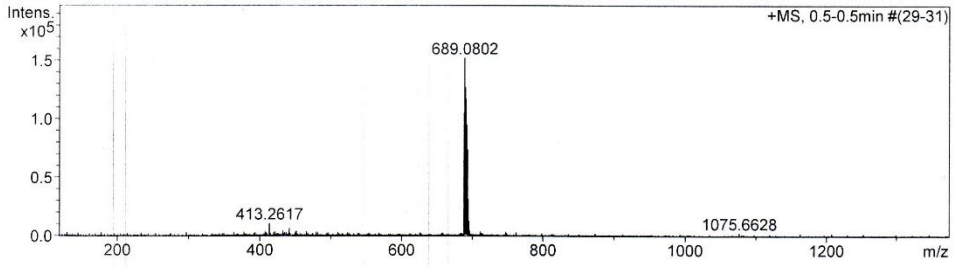

#	m/z	I	I %	S/N	FWHM	Res.
1	129.7642	3088	2.0	12.6	0.0094	13801
2	296.8551	3380	2.2	14.9	0.0119	25022
3	363.1880	3225	2.1	14.3	0.0816	4450
4	377.1989	3447	2.3	15.2	0.0949	3973
5	393.2063	3156	2.1	13.7	0.0936	4203
6	407.2125	3808	2.5	16.6	0.0870	4681
7	413.2617	10795	7.1	48.2	0.0752	5497
8	421.2274	3989	2.6	17.3	0.0970	4343
9	432.1537	4300	2.8	18.6	0.1069	4041
10	435.2245	3053	2.0	13.0	0.1090	3994
11	441.2924	6817	4.5	29.8	0.0900	4902
12	450.2208	3651	2.4	15.5	0.0918	4905
13	451.2346	4183	2.8	17.9	0.1038	4347
14	465.2493	3834	2.5	16.2	0.1094	4253
15	479.2599	3305	2.2	13.8	0.1167	4108
16	495.2717	3189	2.1	13.1	0.1556	3184
17	509.2830	3332	2.2	13.7	0.1279	3982
18	688.0734	104683	68.9	479.8	0.1286	5352
19	689.0802	151884	100.0	697.1	0.1267	5439
20	690.0770	126963	83.6	582.7	0.1278	5400
21	691.0778	117158	77.1	537.8	0.1259	5488
22	692.0751	94840	62.4	435.2	0.1285	5386
23	693.0768	73760	48.6	338.2	0.1299	5335
24	694.0759	31530	20.8	143.7	0.1300	5340
25	695.0755	12476	8.2	56.0	0.1298	5353
26	696.0803	4362	2.9	18.5	0.1183	5884
27	711.0606	3403	2.2	14.2	0.1297	5481
28	747.3228	3414	2.2	14.6	0.1560	4791
29	1442.9522	4013	2.6	21.2	0.0265	54489
30	2339.1215	3800	2.5	19.3	0.0322	72534

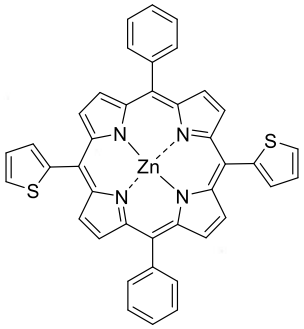

***t*-ZnP-Th**

Chemical Formula: $C_{40}H_{24}N_4S_2Zn$

Exact Mass: 688.0734

Molecular Weight: 690.1600

$[M+H]^+$: 689.0807

Bruker Daltonics DataAnalysis 3.3 printed: 4/19/2016 1:19:38 PM Page 1 of 1

Figure A–8: HR-ESI mass spectrum of ***t*-ZnP-Th**.

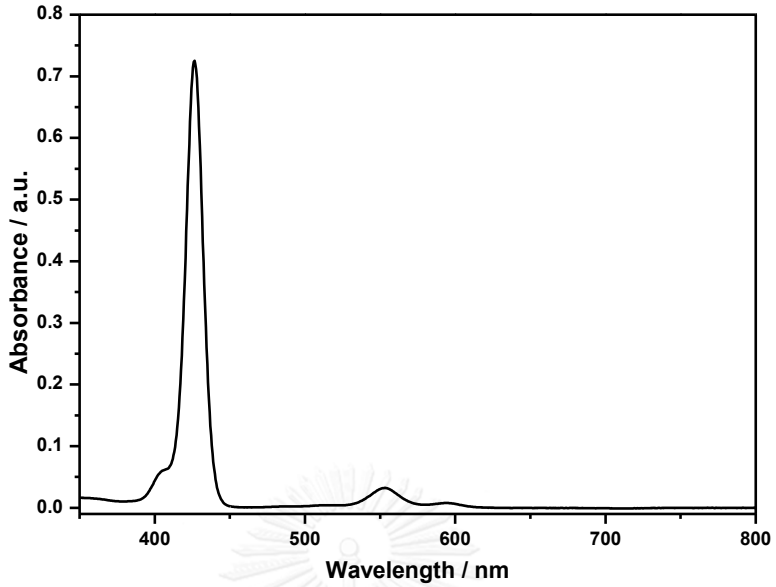

Figure A–9: Absorption spectrum of ***t*-ZnP-Th** in toluene.

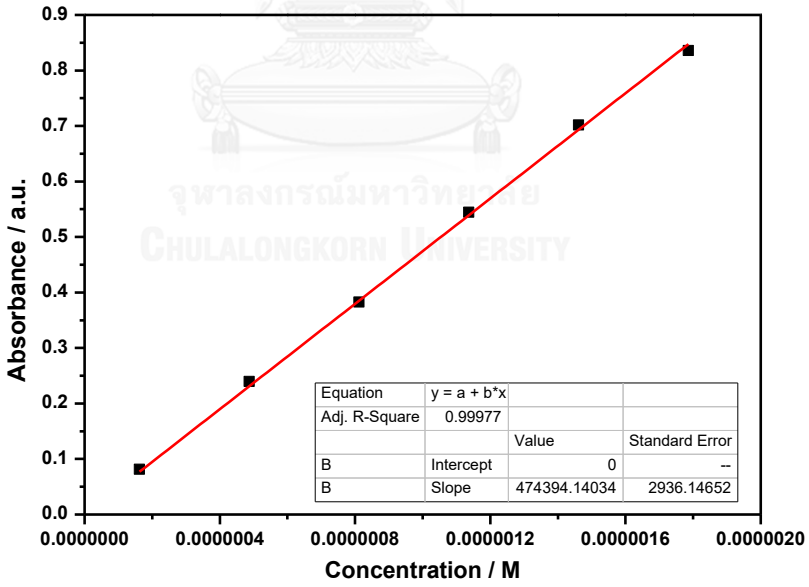

Figure A–10: Calibration curve for quantitative determination of ***t*-ZnP-Th** in toluene (λ_{abs} = 426 nm).

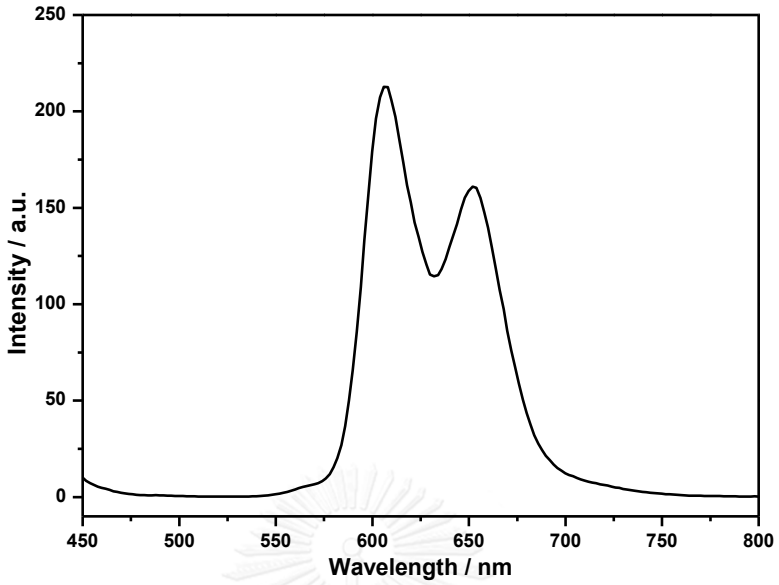

Figure A–11: Emission spectrum of ***t*-ZnP-Th** in toluene (λ_{ex} = 426 nm).

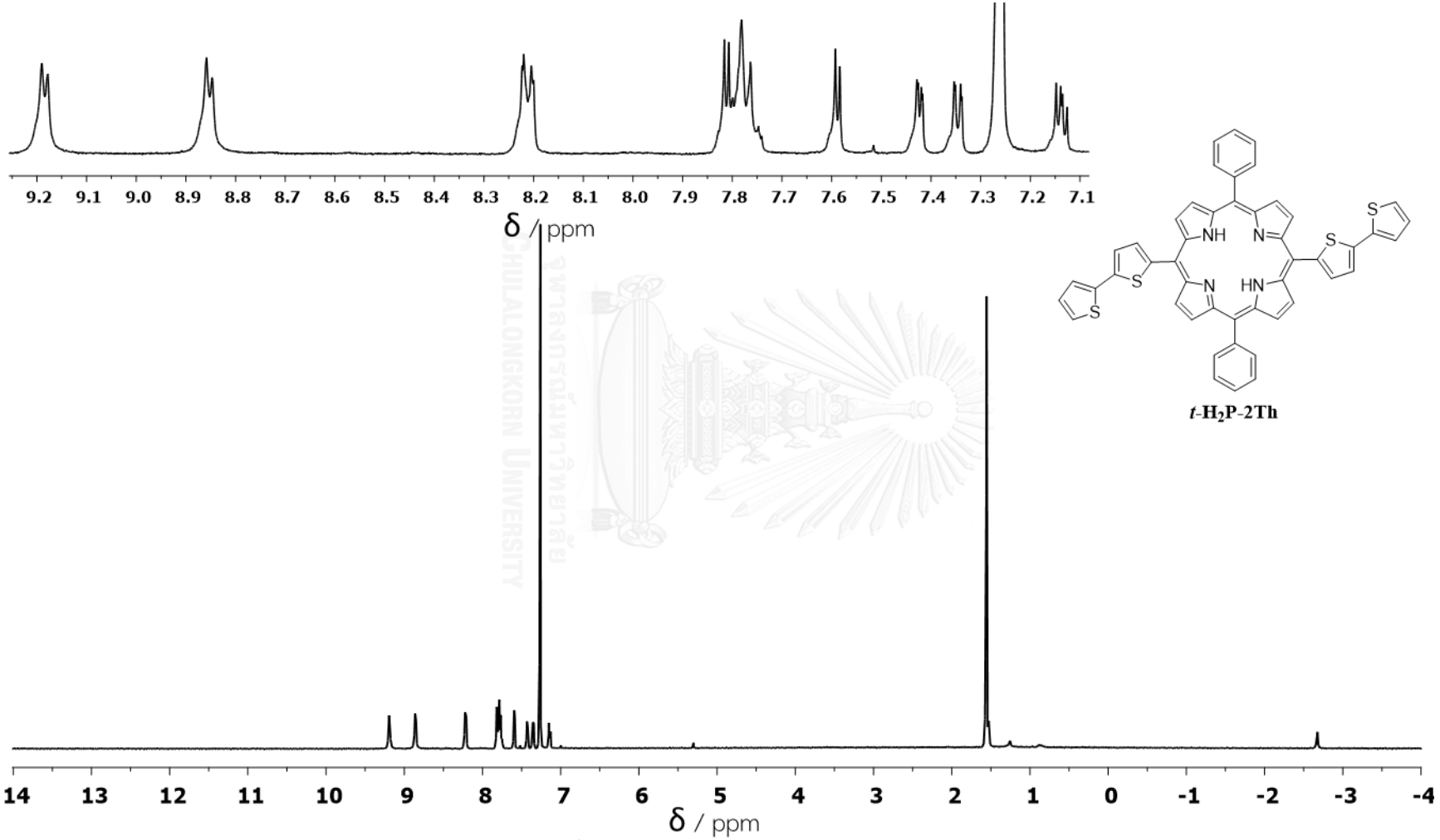

Figure A–12: ^{1}H-NMR spectrum of ***t*-H_2P-2Th** in $CDCl_3$.

Mass Spectrum List Report

Analysis Info

Analysis Name	OSCUHS580727004.d	Acquisition Date	7/28/2015 3:25:16 PM
Method	MKE_tune_wide_20130204.m	Operator	Administrator
Sample Name	Por-2	Instrument	micrOTOF 72
	Por-2		

Acquisition Parameter

Source Type	ESI	Ion Polarity	Positive	Set Corrector Fill	79 V
Scan Range	n/a	Capillary Exit	180.0 V	Set Pulsar Pull	406 V
Scan Begin	50 m/z	Hexapole RF	400.0 V	Set Pulsar Push	388 V
Scan End	3000 m/z	Skimmer 1	54.4 V	Set Reflector	1300 V
		Hexapole 1	21.4 V	Set Flight Tube	9000 V
				Set Detector TOF	1910 V

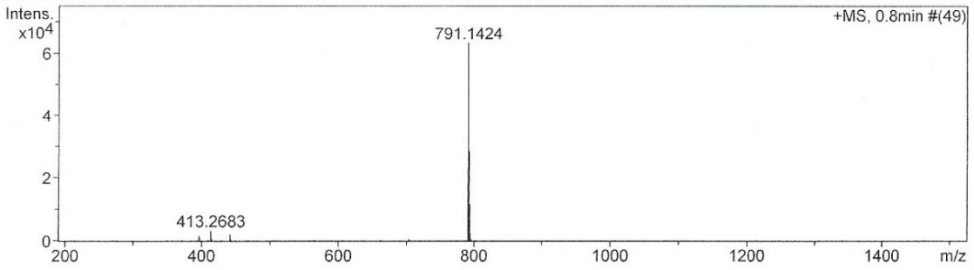

#	m/z	I	I %	S/N	FWHM	Res.
1	53.7398	188	0.3	28.8	0.0049	10944
2	56.1496	263	0.4	40.4	0.0050	11264
3	58.6165	195	0.3	29.9	0.0054	10796
4	69.0068	137	0.2	20.9	0.0057	12003
5	357.1365	162	0.3	24.7	0.0489	7303
6	371.1670	193	0.3	28.7	0.0593	6259
7	385.1839	189	0.3	27.3	0.0457	8437
8	393.3032	141	0.2	19.9	0.0555	7085
9	396.0780	1621	2.6	231.9	0.0485	8167
10	396.5799	761	1.2	108.5	0.0535	7410
11	397.0802	522	0.8	74.3	0.0500	7940
12	397.5824	200	0.3	28.2	0.0491	8095
13	409.1661	233	0.4	32.2	0.0530	7725
14	413.2683	3255	5.2	451.1	0.0567	7283
15	414.2699	657	1.0	90.6	0.0572	7248
16	441.2983	2023	3.2	266.4	0.0473	9333
17	442.3033	341	0.5	44.5	0.0644	6867
18	455.3186	131	0.2	16.4	0.0730	6235
19	565.1802	214	0.3	23.3	0.0465	12160
20	605.4818	142	0.2	15.0	0.1003	6034
21	661.5279	150	0.2	15.5	0.0922	7178
22	703.1976	478	0.8	49.8	0.0853	8241
23	704.1965	288	0.5	29.8	0.0679	10372
24	791.1424	63146	100.0	7241.8	0.0997	7936
25	792.1450	28504	45.1	3274.7	0.0891	8888
26	793.1423	11735	18.6	1350.3	0.0874	9074
27	794.1411	2552	4.0	293.8	0.0795	9983
28	795.1391	456	0.7	52.1	0.0932	8530
29	2151.6103	139	0.2	30.1	0.0313	68727
30	2352.2004	130	0.2	28.3	0.0313	75107

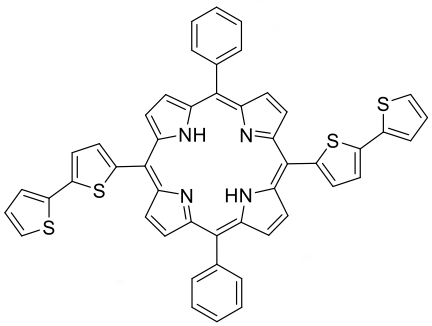

***t*-H_2P-2Th**

Chemical Formula: $C_{48}H_{30}N_4S_4$

Exact Mass: 790.1353

Molecular Weight: 791.0360

$[M+H]^+$: 791.1426

Bruker Daltonics DataAnalysis 3.3 printed: 7/28/2015 3:51:01 PM Page 1 of 1

Figure A–13: HR-ESI mass spectrum of ***t*-H_2P-2Th**.

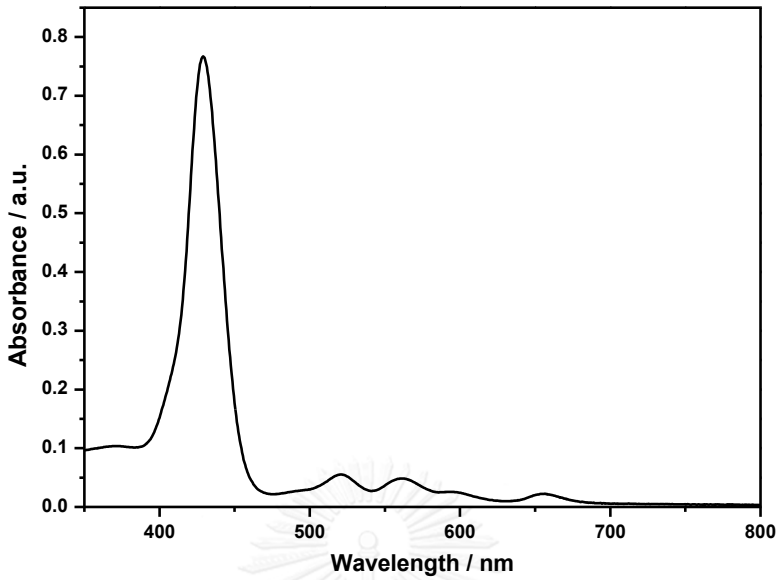

Figure A–14: Absorption spectrum of ***t*-H_2P-2Th** in toluene.

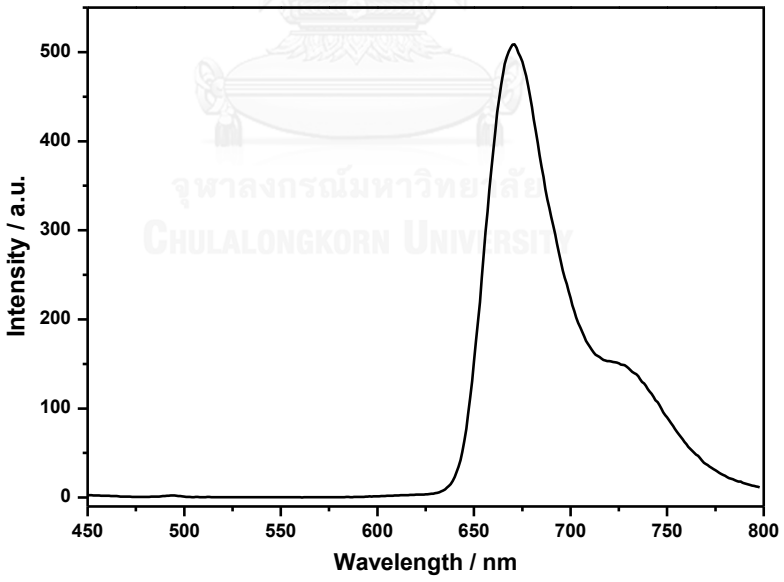

Figure A–15: Emission spectrum of ***t*-H_2P-2Th** in toluene (λ_{ex} = 429 nm).

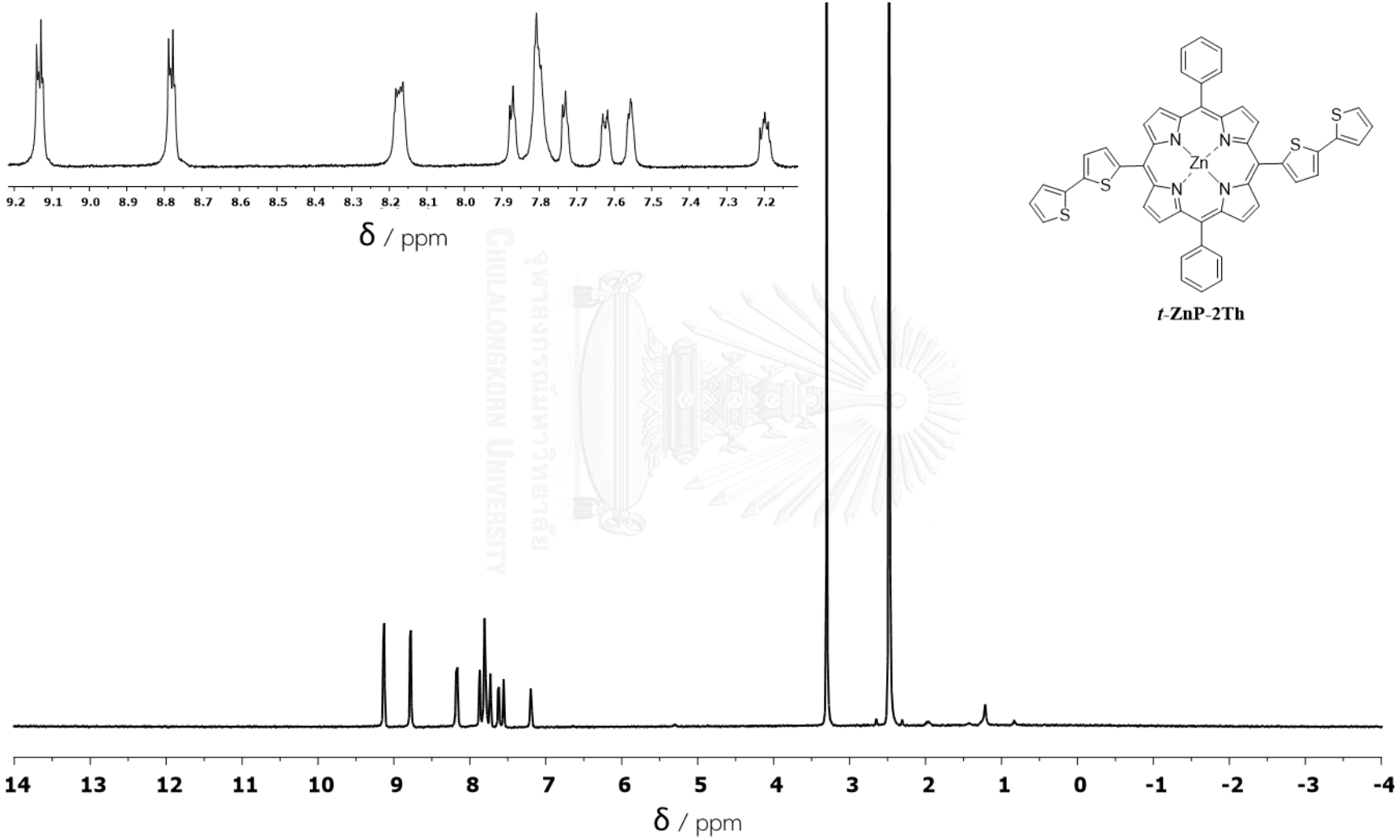

Figure A–16: ^{1}H-NMR spectrum of ***t*-ZnP-2Th** in DMSO-d_6.

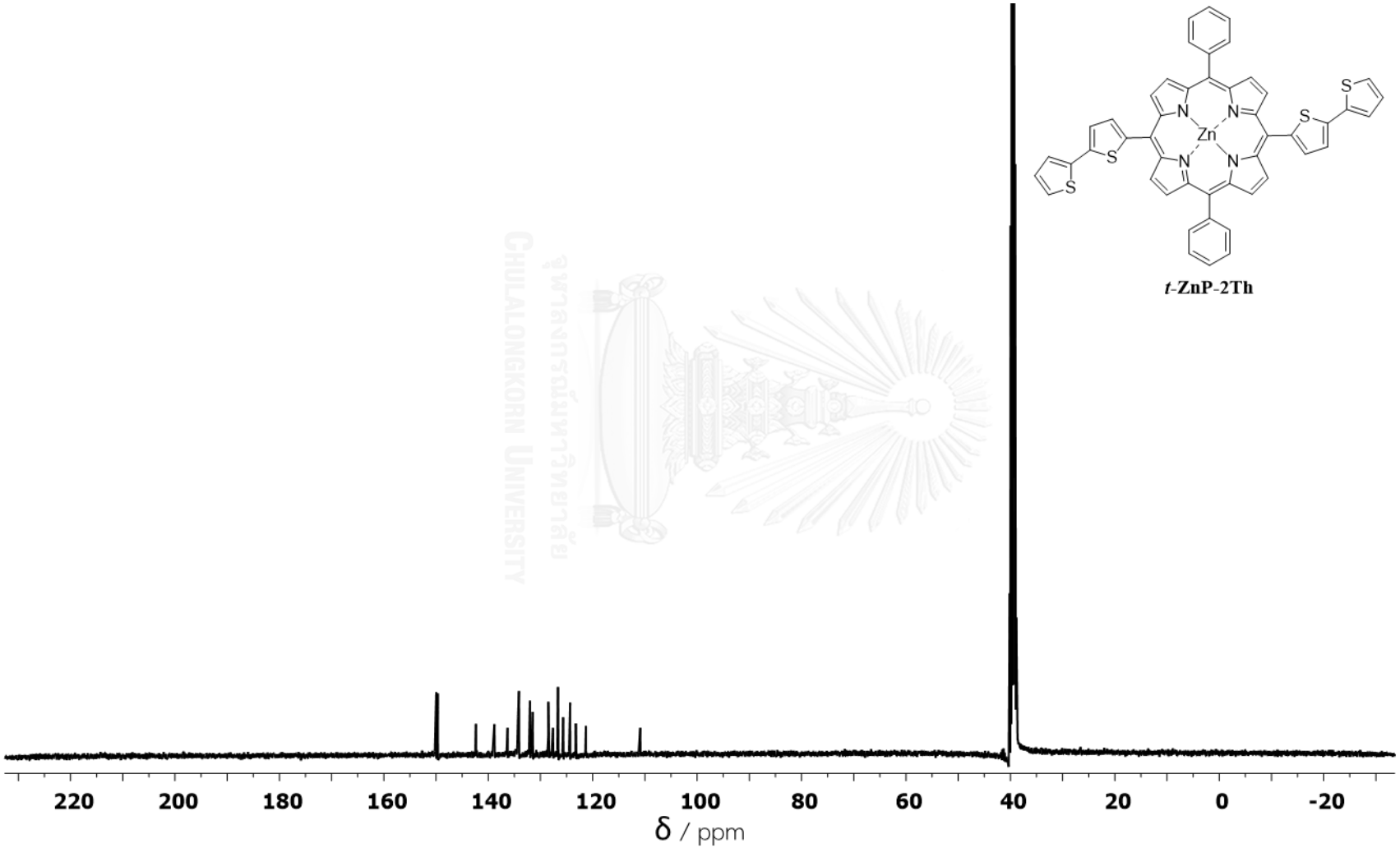

Figure A–17: ^{13}C-NMR spectrum of ***t*-ZnP-2Th** in DMSO-d_6.

Mass Spectrum List Report

Analysis Info

Analysis Name	OSCUHS600131001.d	Acquisition Date	1/31/2017 11:13:30 AM
Method	Tune_wide_POS_Natee20130403.m	Operator	Administrator
Sample Name	tZnP2th	Instrument	micrOTOF 72
	tZnP2th		

Acquisition Parameter

Source Type	ESI	Ion Polarity	Positive	Set Corrector Fill	50 V
Scan Range	n/a	Capillary Exit	350.0 V	Set Pulsar Pull	337 V
Scan Begin	50 m/z	Hexapole RF	600.0 V	Set Pulsar Push	337 V
Scan End	3000 m/z	Skimmer 1	70.0 V	Set Reflector	1300 V
		Hexapole 1	25.0 V	Set Flight Tube	9000 V
				Set Detector TOF	2295 V

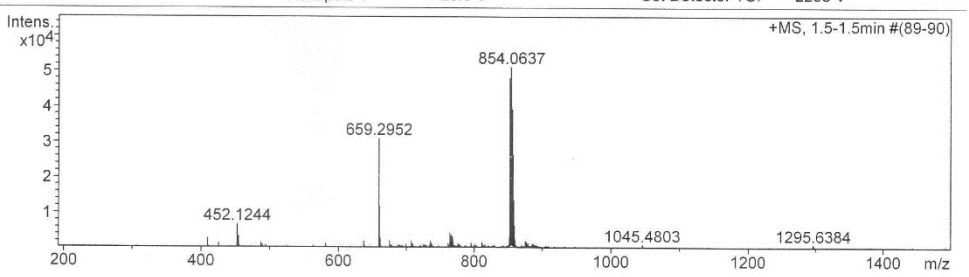

#	m/z	I	I %	S/N	FWHM	Res.
1	409.1679	2791	5.5	71.4	0.0773	5291
2	452.1244	6764	13.2	160.0	0.0855	5288
3	453.1276	2330	4.6	53.4	0.0908	4992
4	454.1235	3518	6.9	81.7	0.0879	5167
5	637.3110	2086	4.1	29.6	0.1242	5131
6	659.2952	31024	60.6	464.2	0.1286	5126
7	660.2979	11938	23.3	176.1	0.1222	5403
8	661.2983	2930	5.7	40.5	0.1284	5150
9	675.2758	2221	4.3	28.9	0.1480	4562
10	707.3571	2067	4.0	24.7	0.1281	5523
11	735.3877	2036	4.0	22.9	0.1564	4702
12	764.1199	4456	8.7	54.7	0.1569	4870
13	765.1176	3373	6.6	40.5	0.1374	5568
14	766.1172	3870	7.6	47.0	0.1527	5017
15	767.1143	2672	5.2	31.3	0.1463	5244
16	768.1095	3415	6.7	41.1	0.1251	6139
17	769.1181	1989	3.9	22.4	0.1264	6087
18	795.3448	1638	3.2	17.9	0.1804	4408
19	811.3245	1657	3.2	18.2	0.1533	5292
20	852.0644	48109	94.0	644.4	0.1677	5079
21	853.0680	44043	86.1	589.8	0.1660	5140
22	854.0637	51176	100.0	686.2	0.1718	4972
23	855.0646	40077	78.3	536.7	0.1682	5083
24	856.0627	39086	76.4	523.5	0.1683	5086
25	857.0635	26372	51.5	352.1	0.1627	5268
26	858.0620	13542	26.5	179.0	0.1703	5038
27	859.0592	6452	12.6	83.4	0.1731	4964
28	860.0641	2512	4.9	30.2	0.1823	4718
29	875.0539	2159	4.2	25.6	0.1609	5437
30	877.0496	1754	3.4	20.1	0.1704	5149

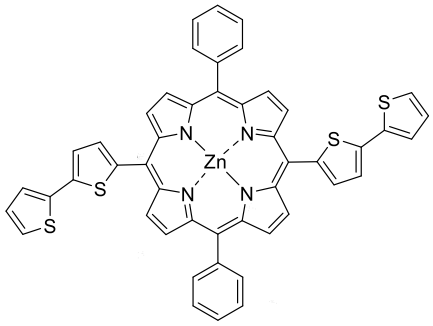

***t*-ZnP-2Th**

Chemical Formula: $C_{48}H_{28}N_4S_4Zn$

Exact Mass: 852.0488

Molecular Weight: 854.4000

$[M+H]^+$: 853.0561

$[M+2H]^+$: 854.0634

Bruker Daltonics DataAnalysis 3.3 printed: 1/31/2017 2:19:12 PM Page 1 of 1

Figure A–18: HR-ESI mass spectrum of ***t*-ZnP-2Th**.

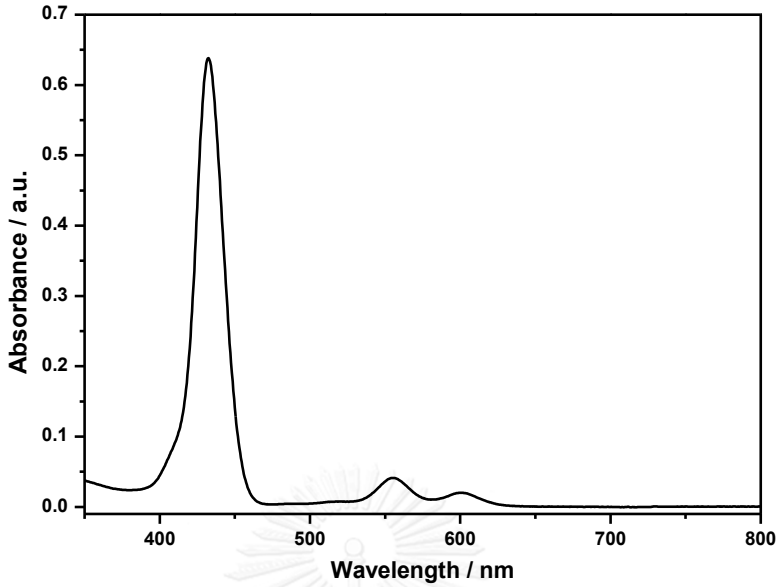

Figure A–19: Absorption spectrum of ***t*-ZnP-2Th** in toluene.

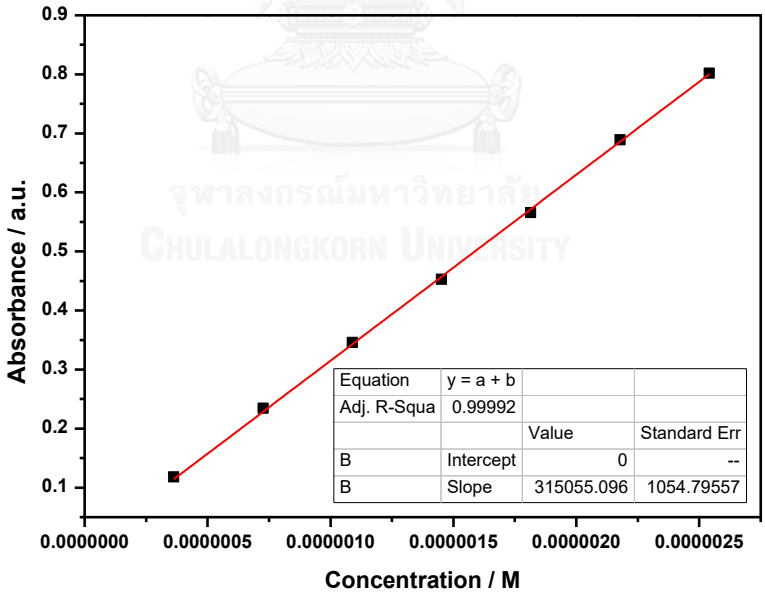

Figure A–20: Calibration curve for quantitative determination of ***t*-ZnP-2Th** in toluene (λ_{abs} = 432 nm).

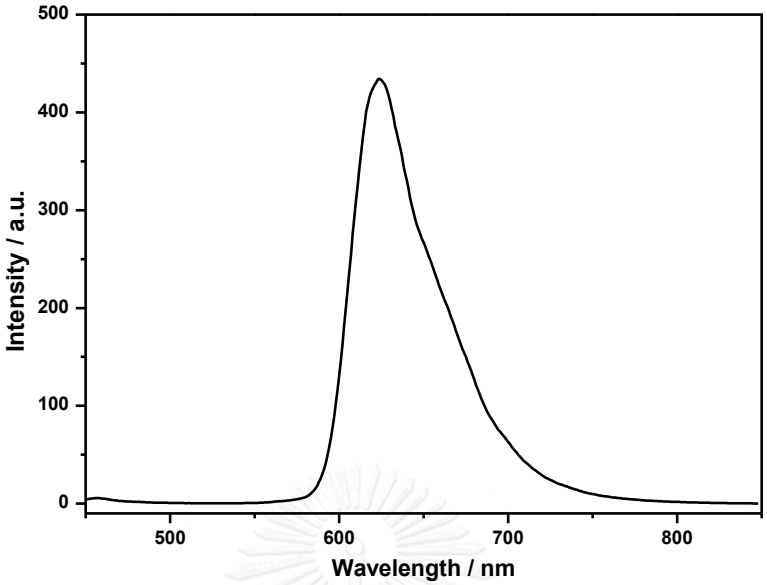

Figure A–21: Emission spectrum of ***t*-ZnP-2Th** in toluene (λ_{ex} = 432 nm).

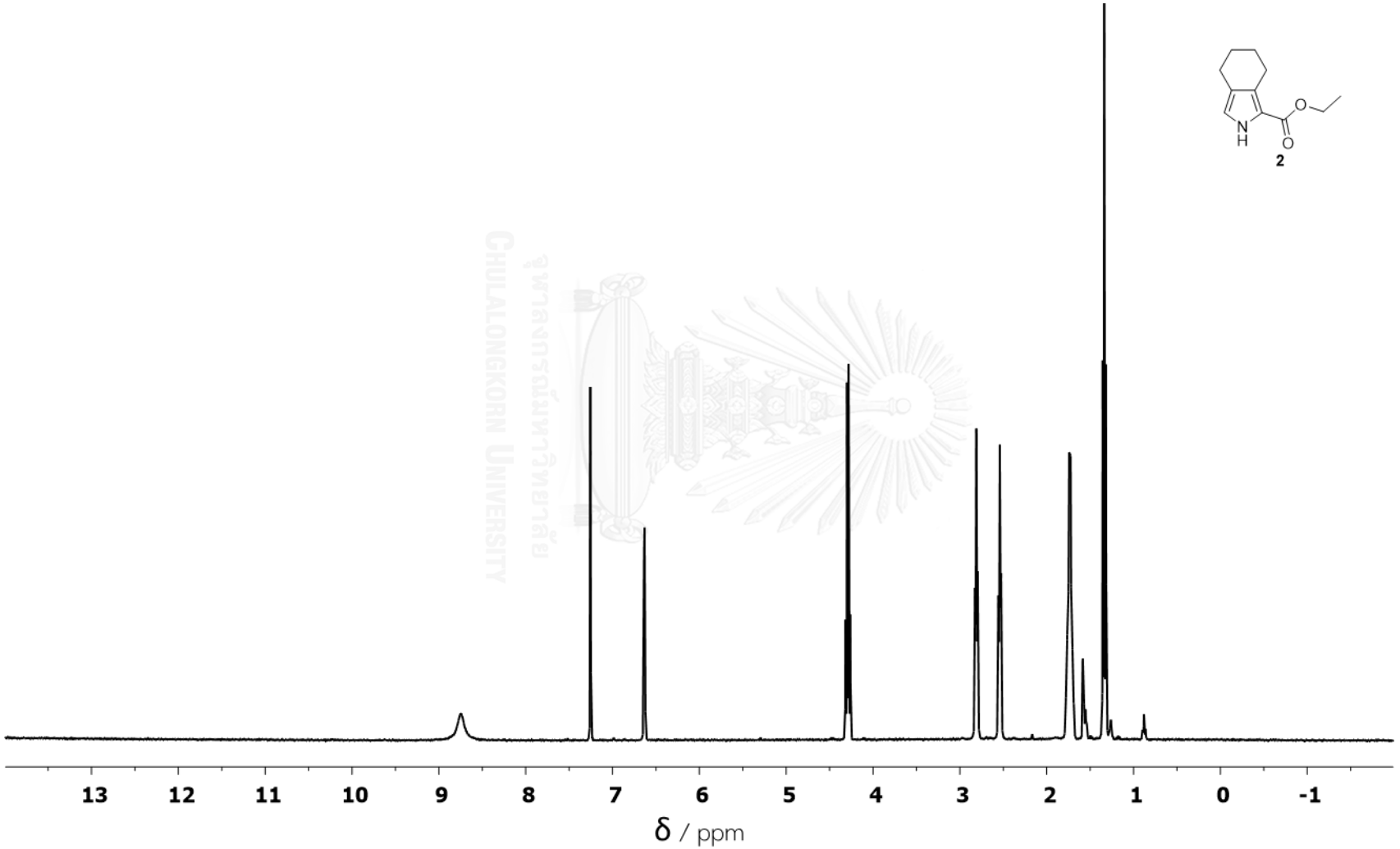

Figure A–22: ^{1}H-NMR spectrum of compound **2** in $CDCl_3$.

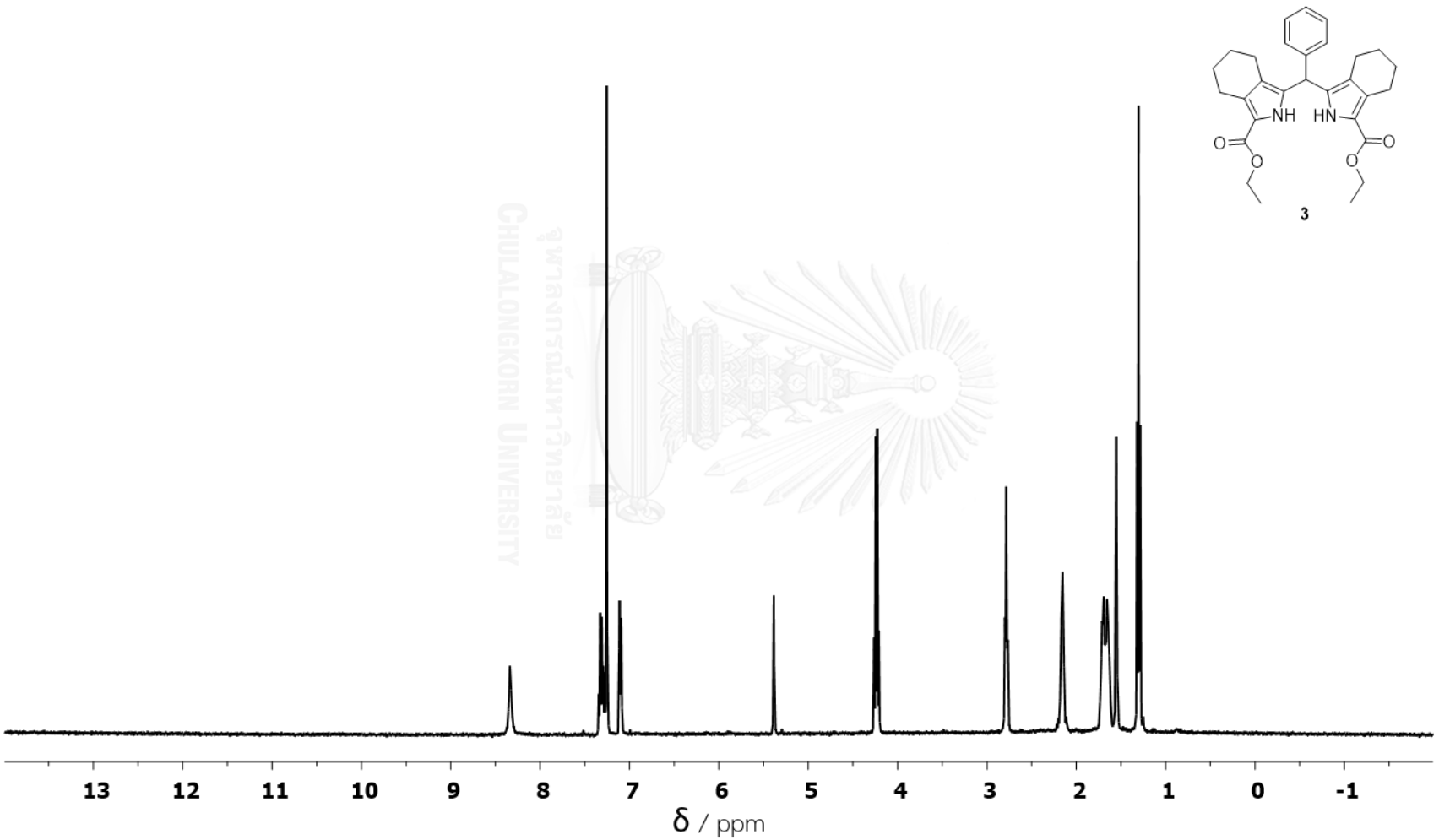

Figure A–23: ^{1}H-NMR spectrum of compound **3** in $CDCl_3$.

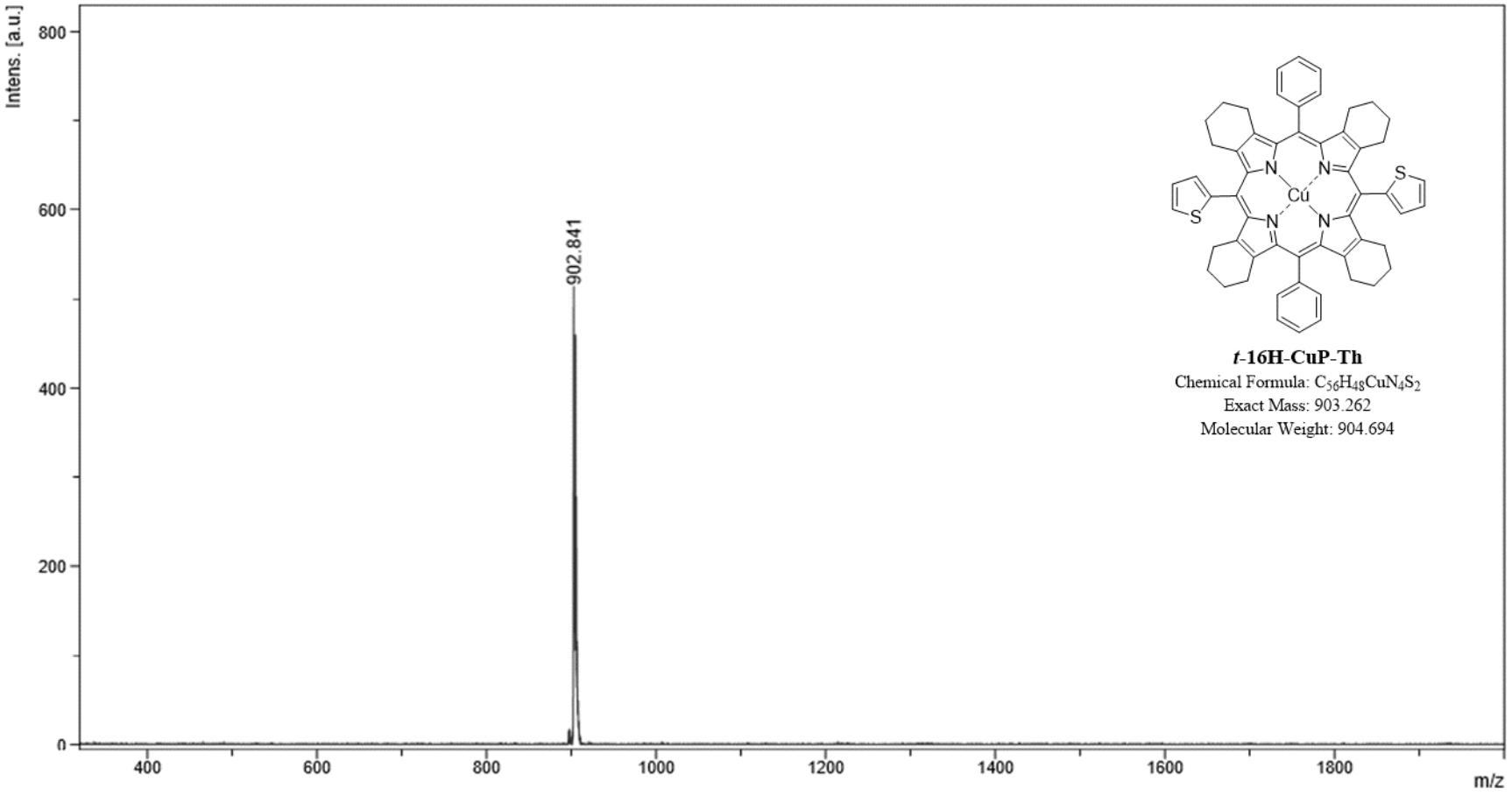

Figure A–24: MALDI-TOF mass spectrum of ***t*-16H-CuP-Th**.

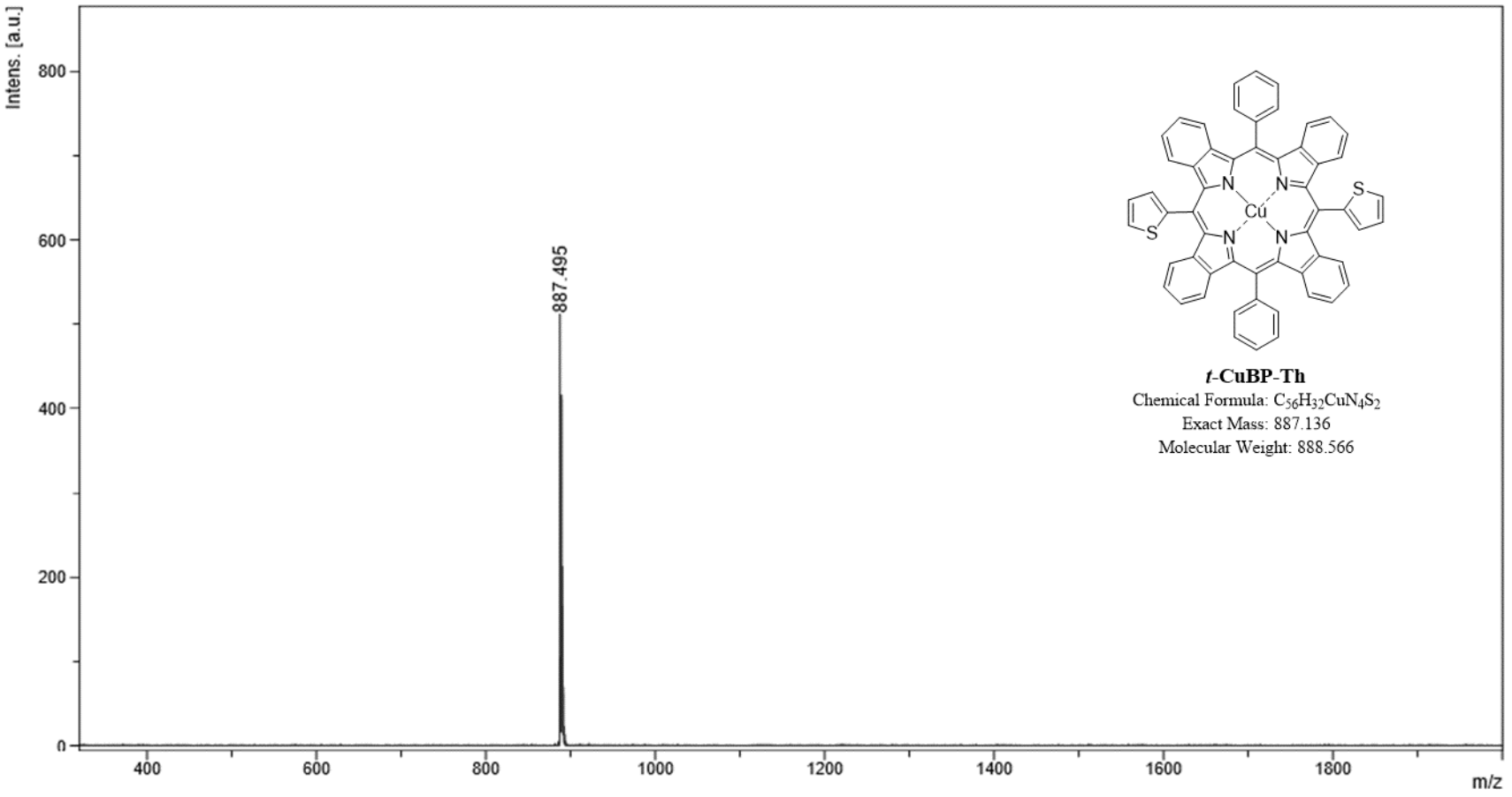

Figure A–25: MALDI-TOF mass spectrum of ***t*-CuBP-Th**.

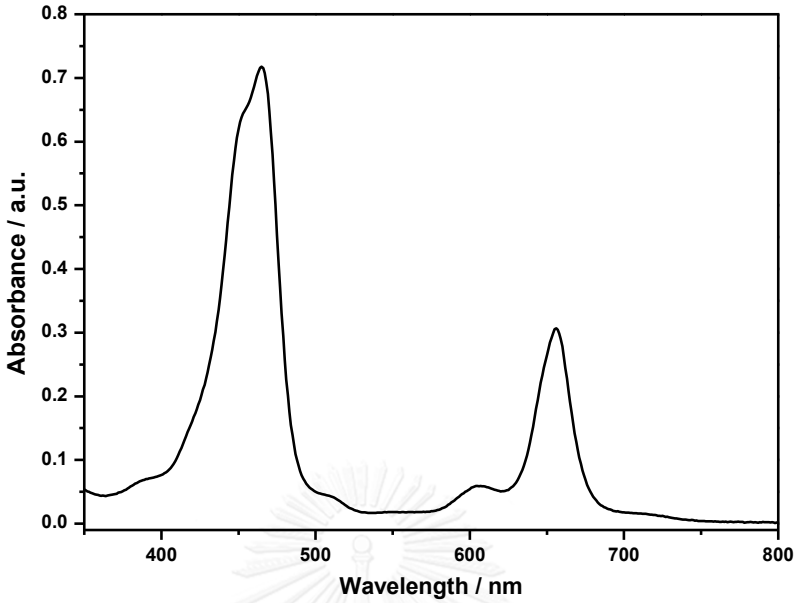

Figure A–26: Absorption spectrum of ***t*-CuBP-Th** in toluene.

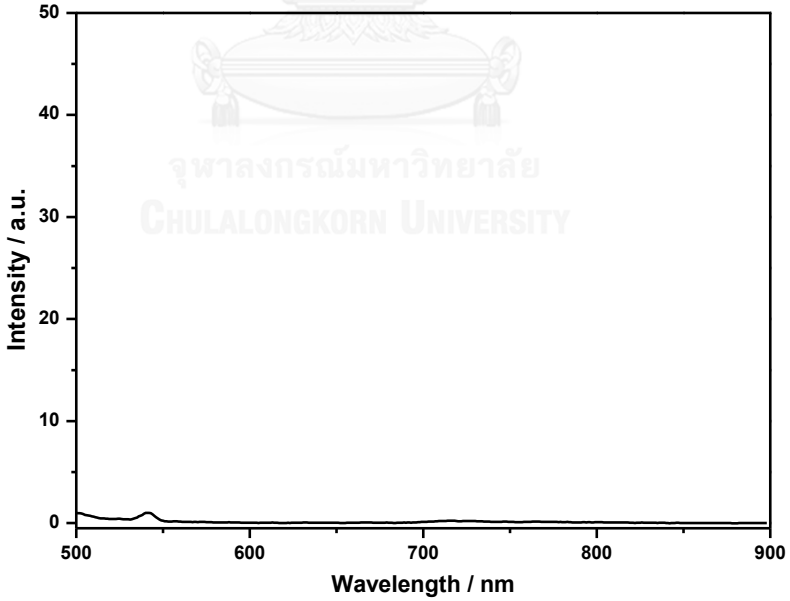

Figure A–27: Emission spectrum of ***t*-CuBP-Th** in toluene (λ_{ex} = 465 nm).

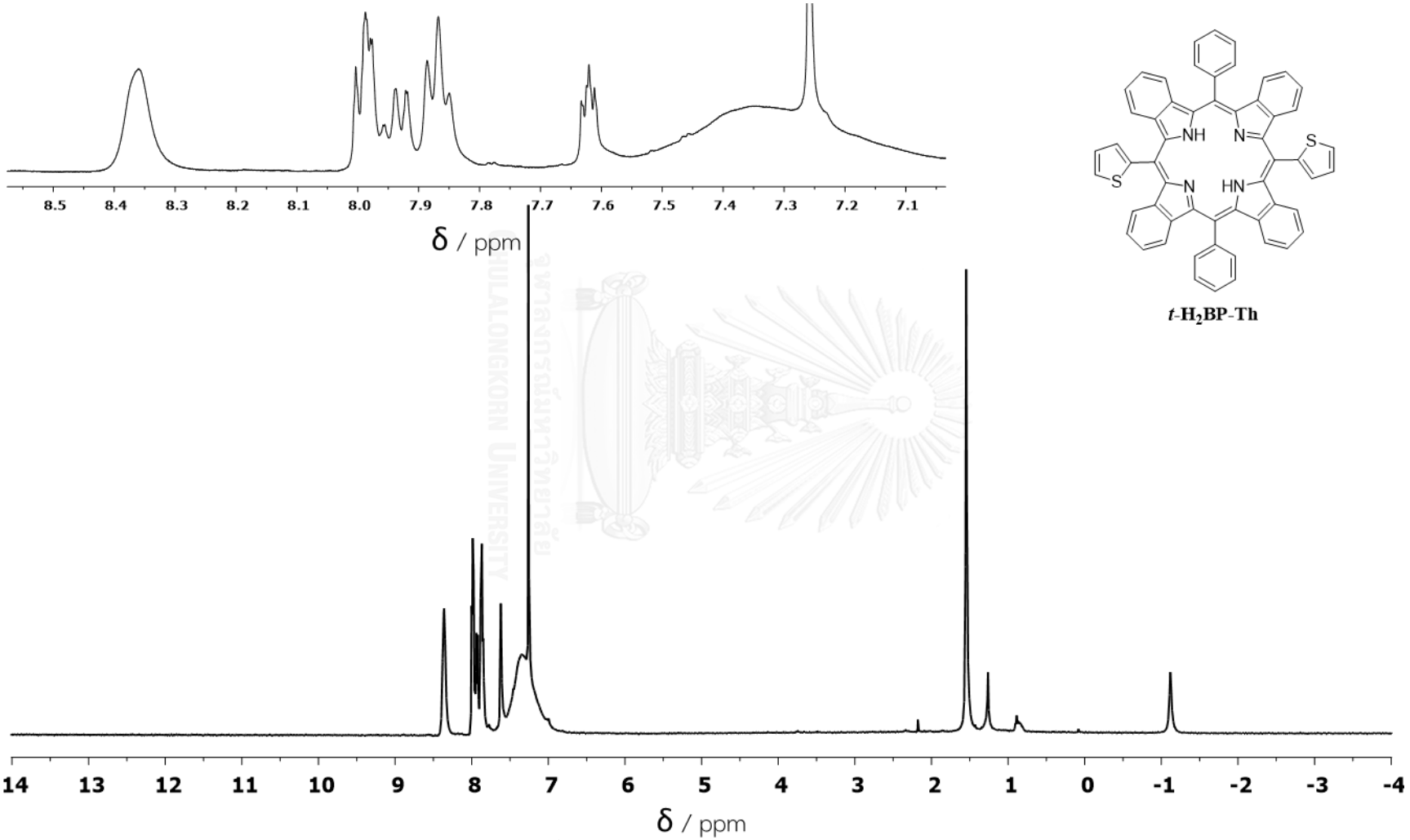

Figure A–28: ^{1}H-NMR spectrum of ***t*-H_2BP-Th** in $CDCl_3$.

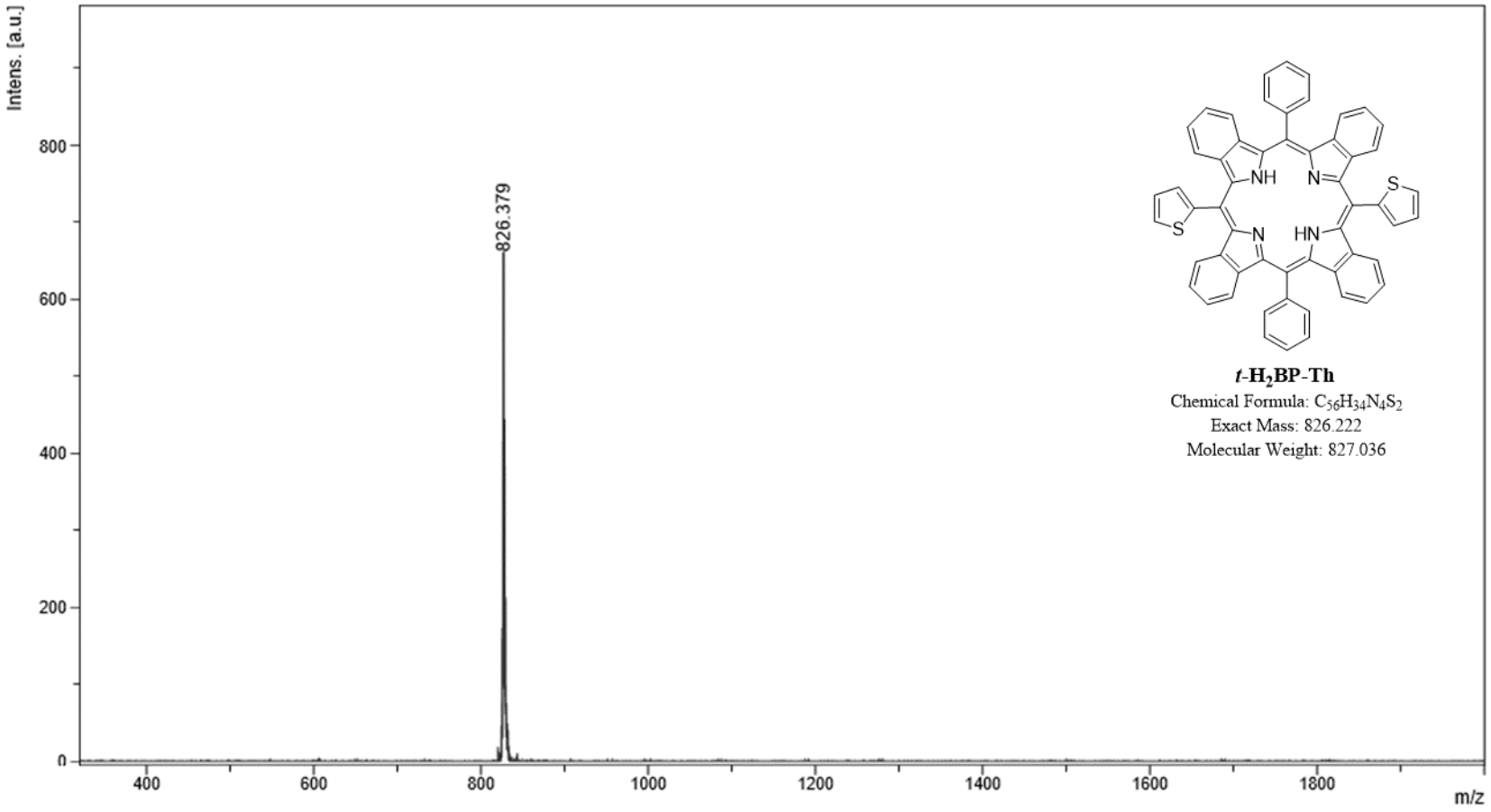

Figure A–29: MALDI-TOF mass spectrum of ***t*-H_2BP-Th**.

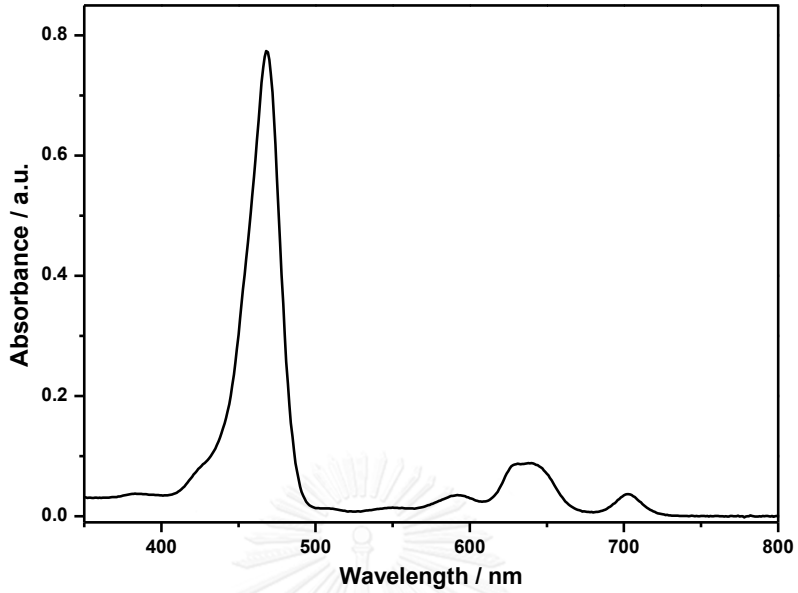

Figure A–30: Absorption spectrum of ***t*-H_2BP-Th** in toluene.

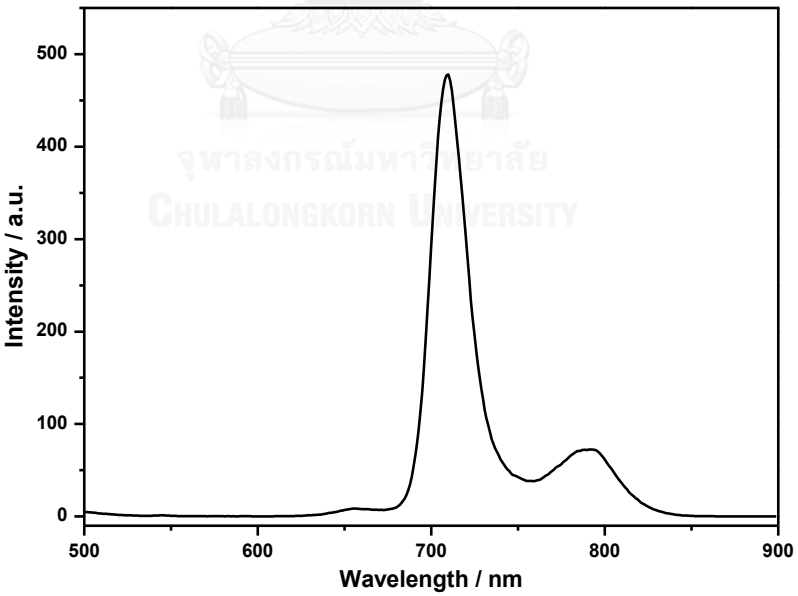

Figure A–31: Emission spectrum of ***t*-H_2BP-Th** in toluene (λ_{ex} = 468 nm).

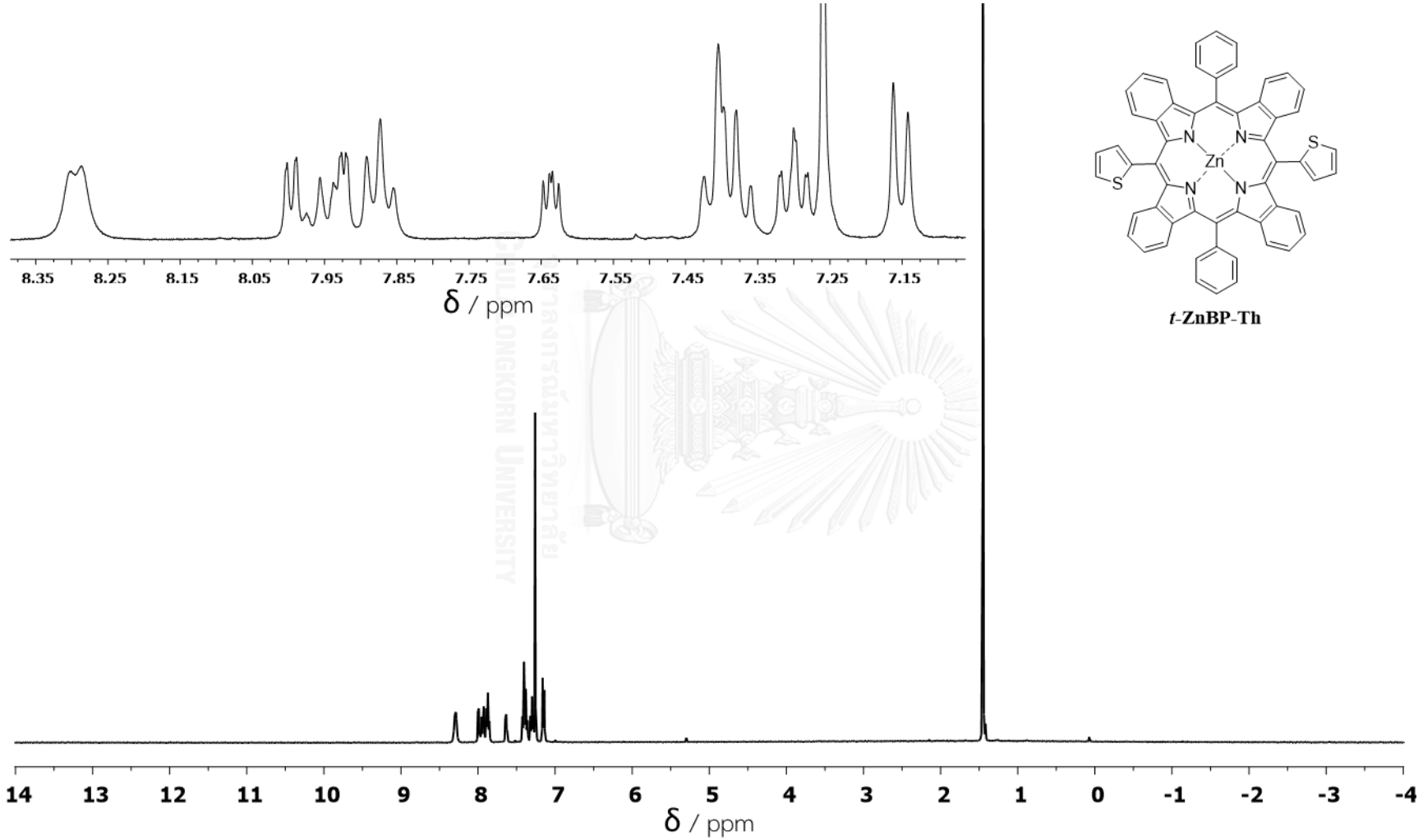

Figure A–32: ^{1}H-NMR spectrum of ***t*-ZnBP-Th** in $CDCl_3$.

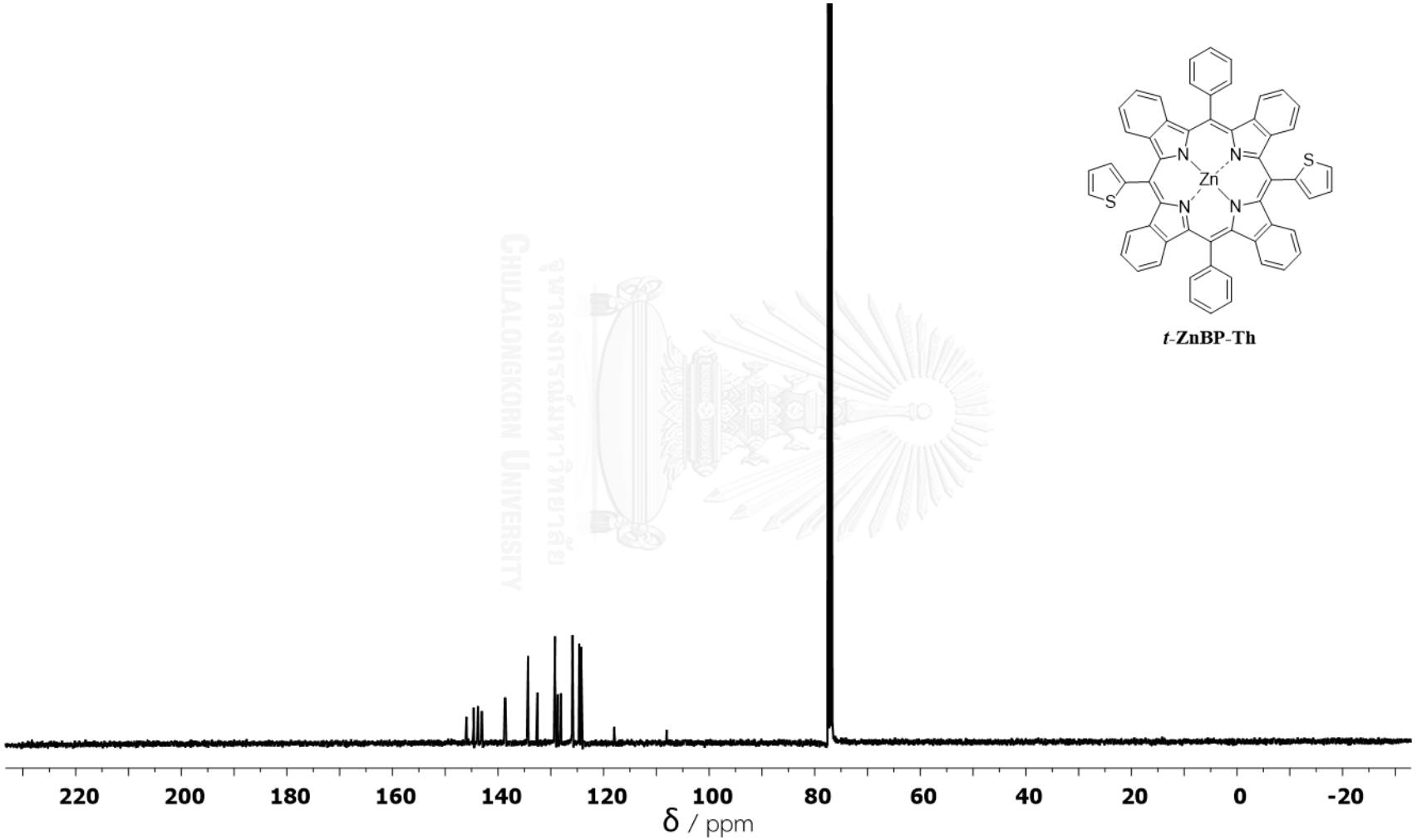

Figure A–33: ^{13}C-NMR spectrum of ***t*-ZnBP-Th** in $CDCl_3$.

Mass Spectrum List Report

Analysis Info

Analysis Name	OSCUHS591121001.d	Acquisition Date	11/22/2016 12:00:22 PM
Method	Tune_wide_POS_Tawatchai_05Feb2016.m	Operator	Administrator
Sample Name	tZnBPTh tZnBPTh	Instrument	micrOTOF 72

Acquisition Parameter

Source Type	ESI	Ion Polarity	Positive	Set Corrector Fill	50 V
Scan Range	n/a	Capillary Exit	300.0 V	Set Pulsar Pull	337 V
Scan Begin	50 m/z	Hexapole RF	400.0 V	Set Pulsar Push	337 V
Scan End	3000 m/z	Skimmer 1	70.0 V	Set Reflector	1300 V
		Hexapole 1	25.0 V	Set Flight Tube	9000 V
				Set Detector TOF	2295 V

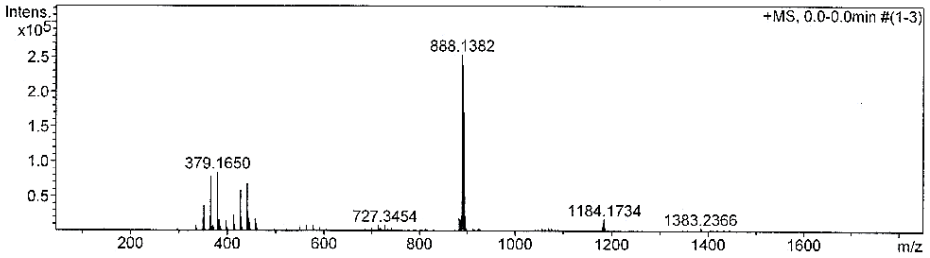

#	m/z	I	I %	S/N	FWHM	Res.
1	349.1698	19811	7.8	73.4	0.0631	5534
2	351.1375	36466	14.4	136.0	0.0696	5048
3	363.1866	21877	8.6	80.8	0.0673	5394
4	365.1515	78341	30.9	292.5	0.0678	5382
5	379.1650	84856	33.5	315.9	0.0655	5790
6	380.1679	17665	7.0	64.8	0.0715	5315
7	413.1714	23904	9.4	87.3	0.0794	5204
8	427.1856	59165	23.3	217.5	0.0725	5895
9	428.1869	20643	8.1	74.9	0.0774	5532
10	429.1794	19476	7.7	70.6	0.0867	4948
11	441.2005	68695	27.1	251.9	0.0750	5884
12	442.2041	24122	9.5	87.5	0.0809	5466
13	443.1875	28690	11.3	104.3	0.1005	4411
14	457.1796	18558	7.3	66.7	0.0794	5761
15	882.1809	19589	7.7	66.6	0.1397	6314
16	886.1494	23215	9.2	79.5	0.1787	4958
17	888.1382	253596	100.0	896.8	0.1447	6138
18	889.1422	208740	82.3	738.0	0.1495	5948
19	890.1382	237743	93.7	841.2	0.1465	6075
20	891.1391	173572	68.4	613.7	0.1443	6178
21	892.1370	169738	66.9	600.3	0.1445	6174
22	893.1386	101563	40.0	358.2	0.1465	6096
23	894.1354	51117	20.2	179.0	0.1537	5817
24	895.1338	22091	8.7	75.8	0.1562	5730
25	1184.1734	18190	7.2	62.4	0.1756	6745
26	2343.3585	29554	11.7	118.4	0.3886	6031
27	2344.3629	46002	18.1	185.9	0.3908	5999
28	2345.3557	49293	19.4	199.6	0.3928	5971
29	2346.3566	37679	14.9	152.0	0.4194	5594
30	2347.3533	24577	9.7	98.3	0.4201	5587

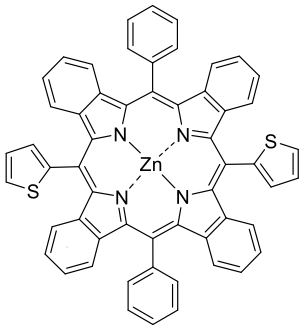

***t*-ZnBP-Th**

Chemical Formula: $C_{56}H_{32}N_4S_2Zn$

Exact Mass: 888.1360

Molecular Weight: 890.4000

$[M+H]^+$: 889.1433

Bruker Daltonics DataAnalysis 3.3 printed: 11/22/2016 1:25:51 PM Page 1 of 1

Figure A–34: HR-ESI mass spectrum of ***t*-ZnBP-Th**.

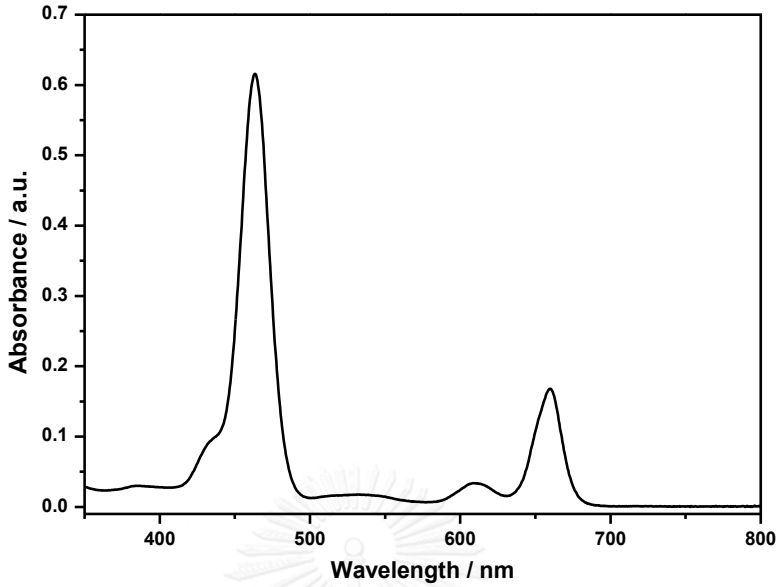

Figure A–35: Absorption spectrum of ***t*-ZnBP-Th** in toluene.

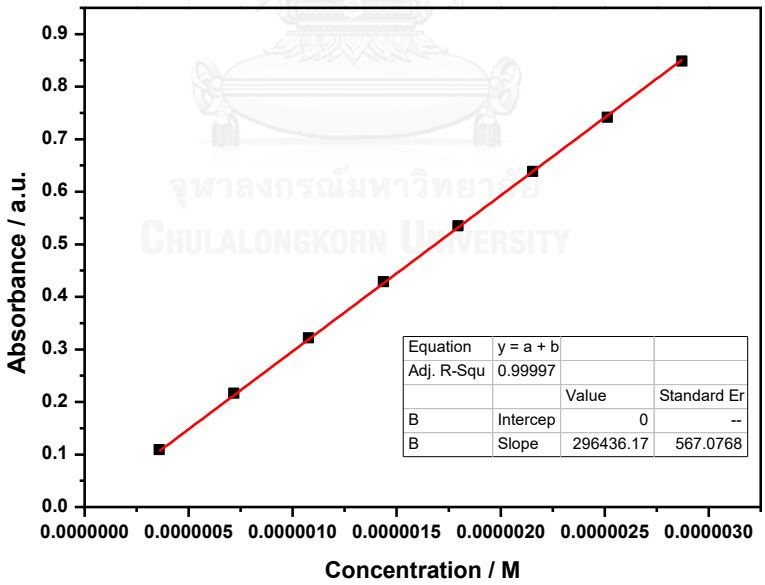

Figure A–36: Calibration curve for quantitative determination of ***t*-ZnBP-Th** in toluene (λ_{abs} = 463 nm).

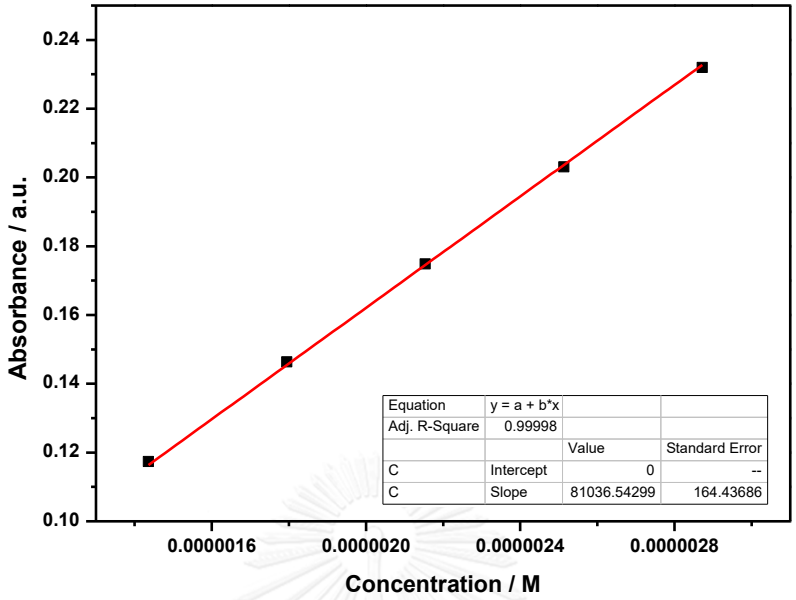

Figure A–37: Calibration curve for quantitative determination of ***t*-ZnBP-Th** in toluene (λ_{abs} = 660 nm).

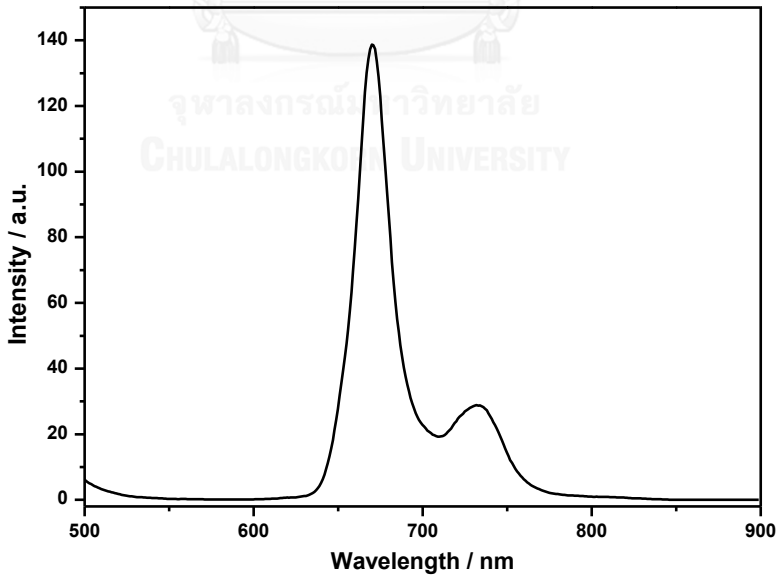

Figure A–38: Emission spectrum of ***t*-ZnBP-Th** in toluene (λ_{ex} = 463 nm).

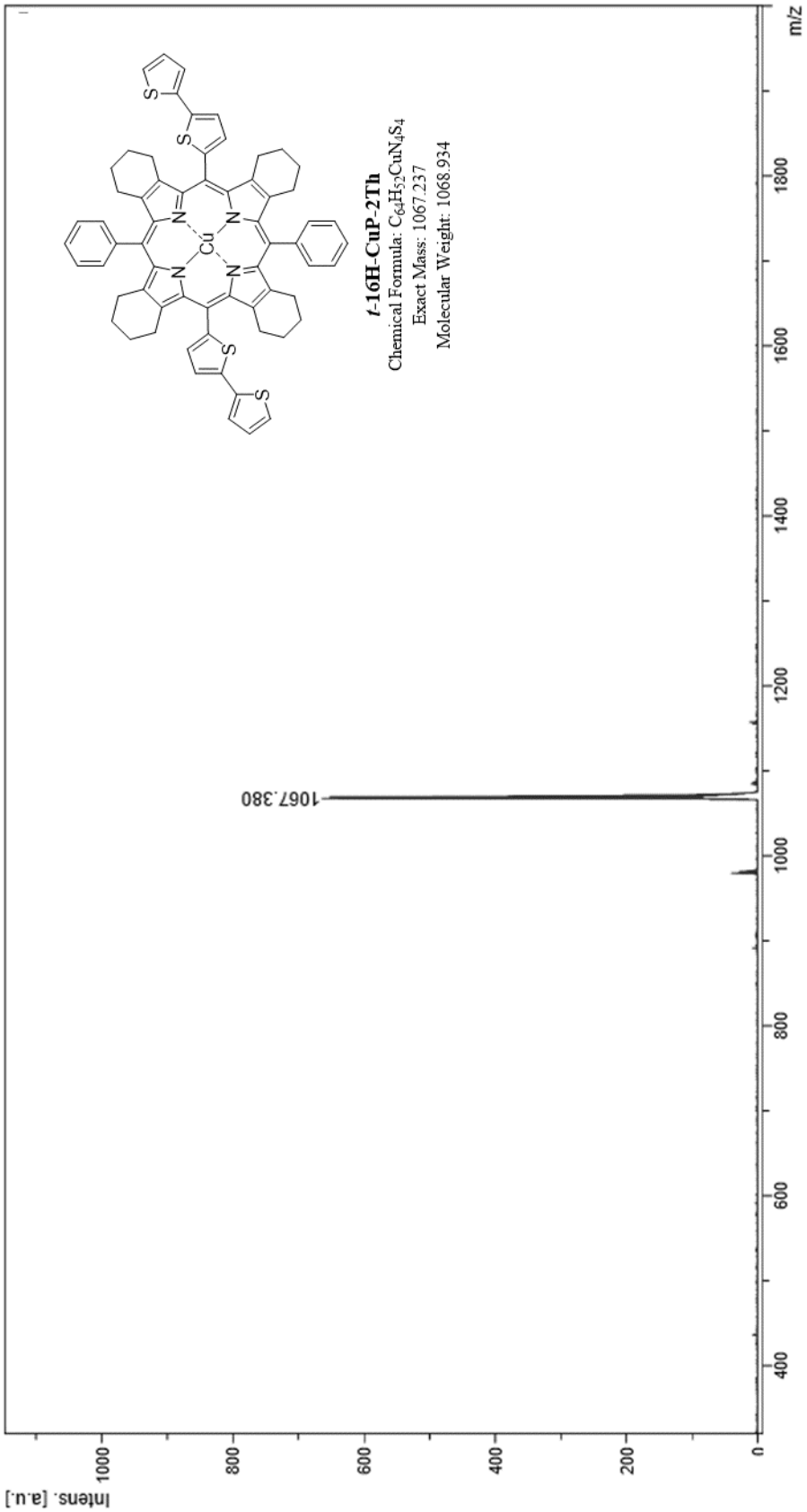

Figure A–39: MALDI-TOF mass spectrum of ***t*-16H-CuP-2Th**.

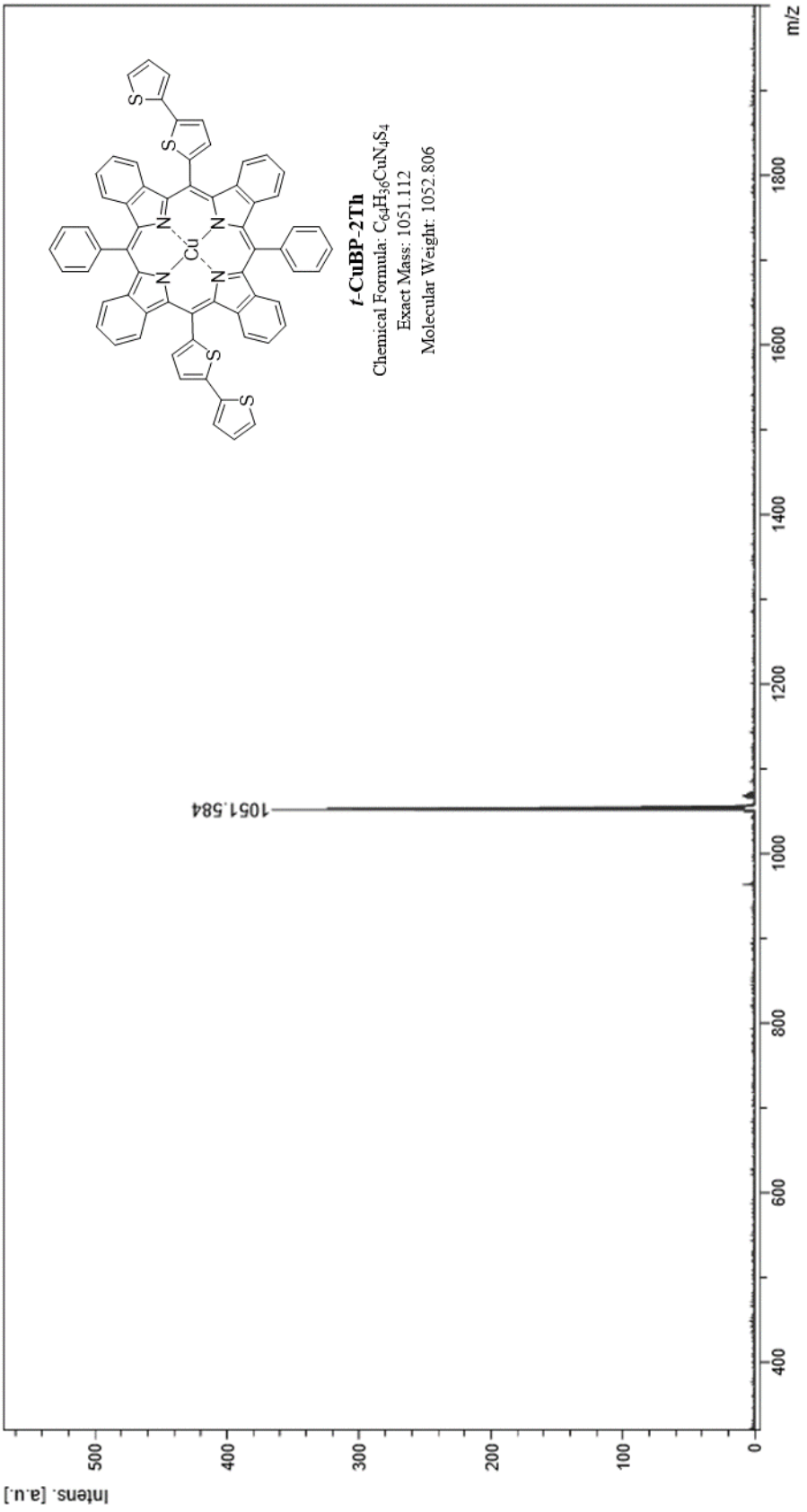

Figure A–40: MALDI-TOF mass spectrum of ***t*-CuBP-2Th**.

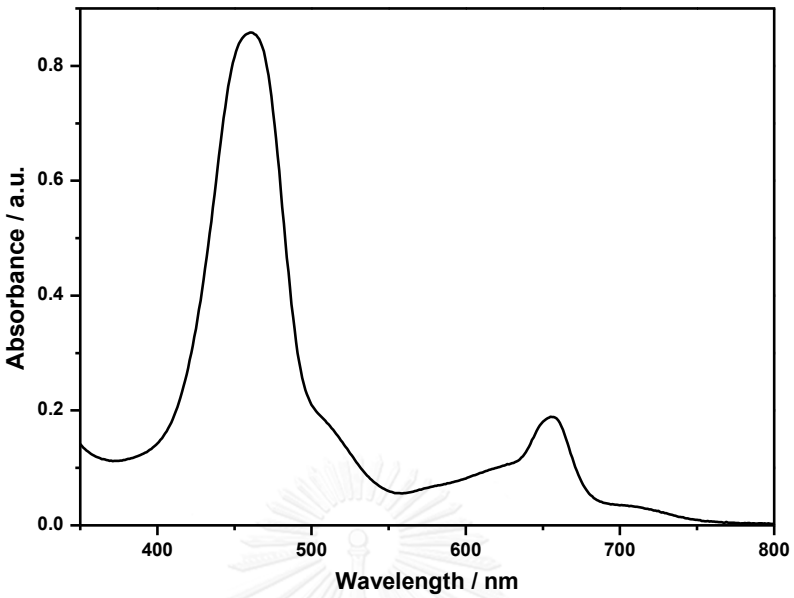

Figure A–41: Absorption spectrum of ***t*-CuBP-2Th** in toluene.

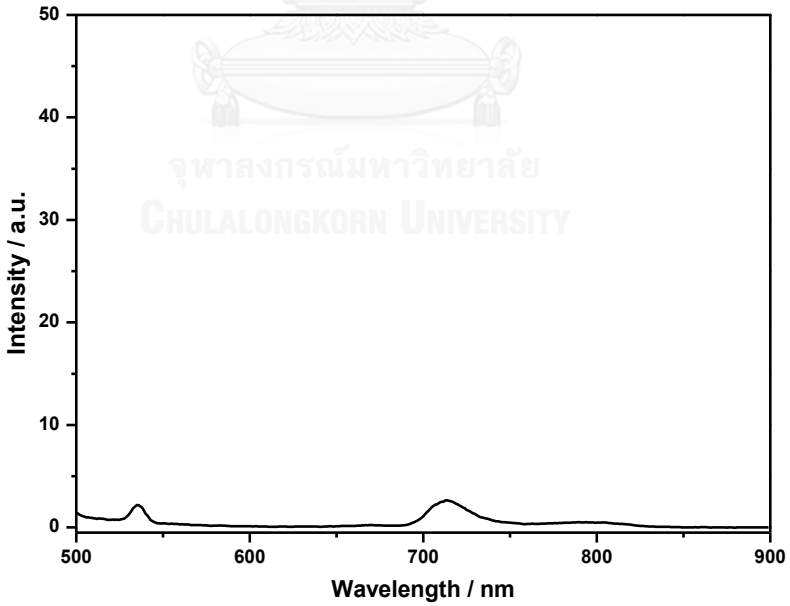

Figure A–42: Emission spectrum of ***t*-CuBP-2Th** in toluene (λ_{ex} = 461 nm).

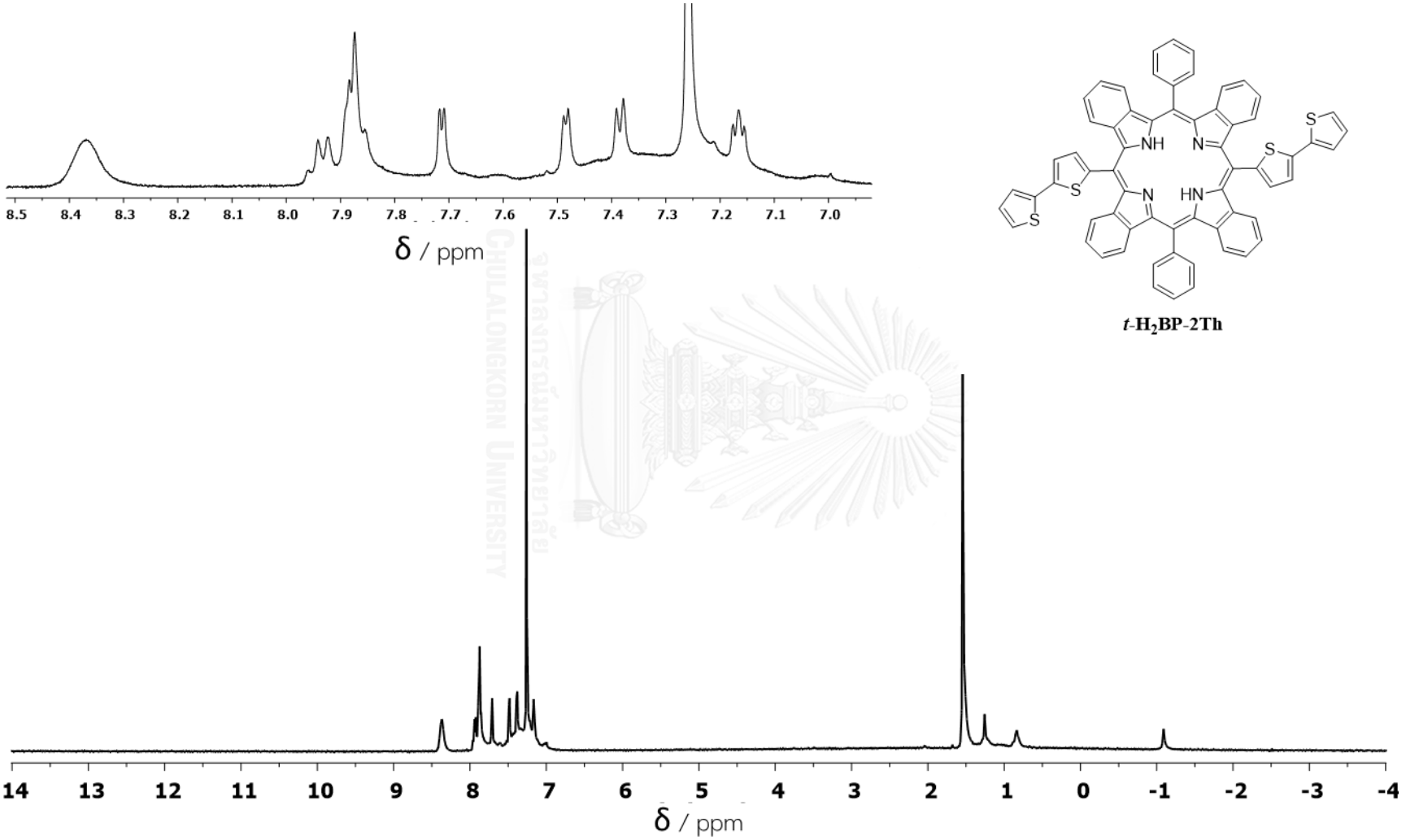

Figure A–43: ^{1}H-NMR spectrum of ***t*-H_2BP-2Th** in $CDCl_3$.

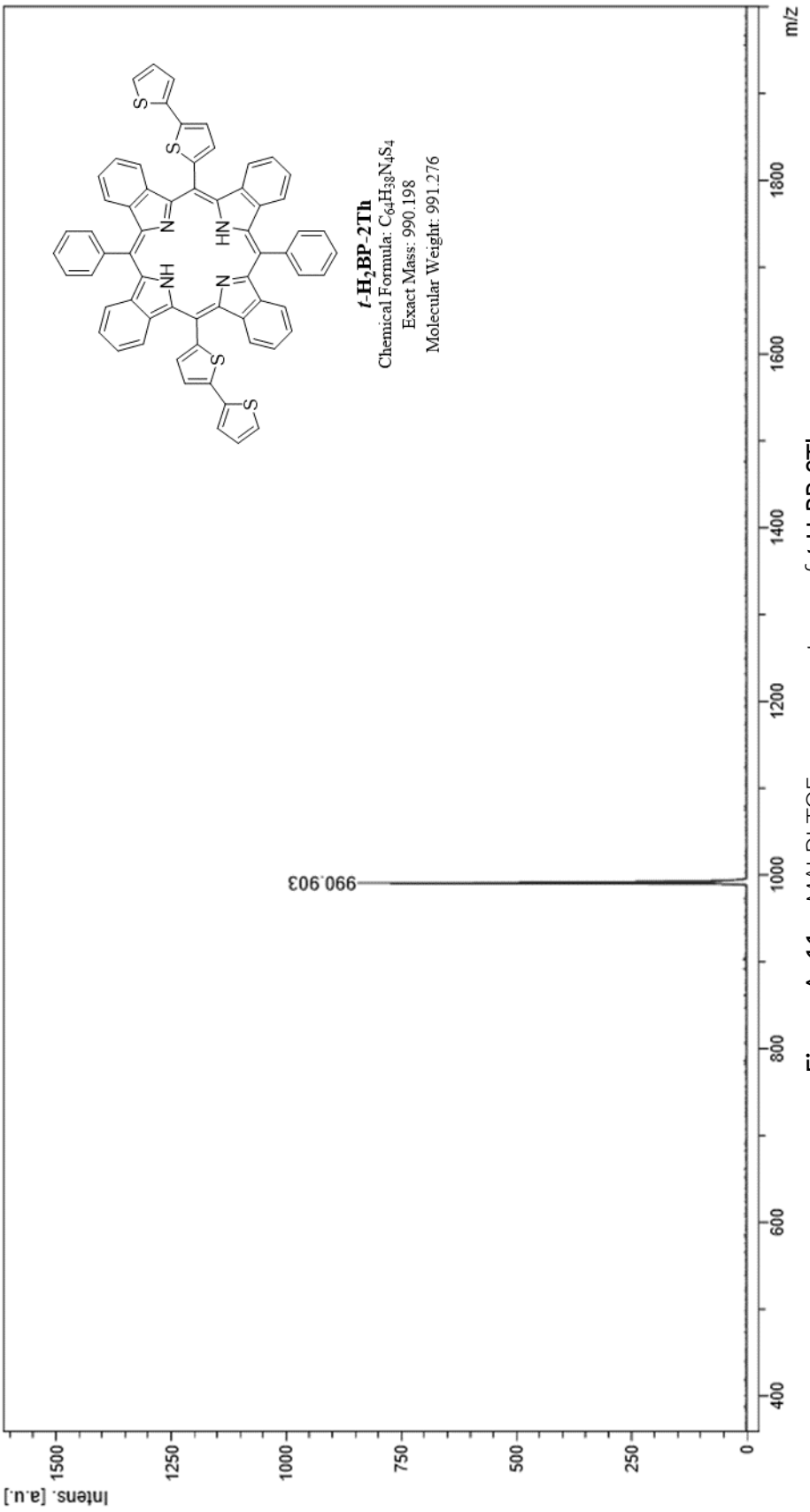

Figure A–44: MALDI-TOF mass spectrum of ***t*-H_2BP-2Th**.

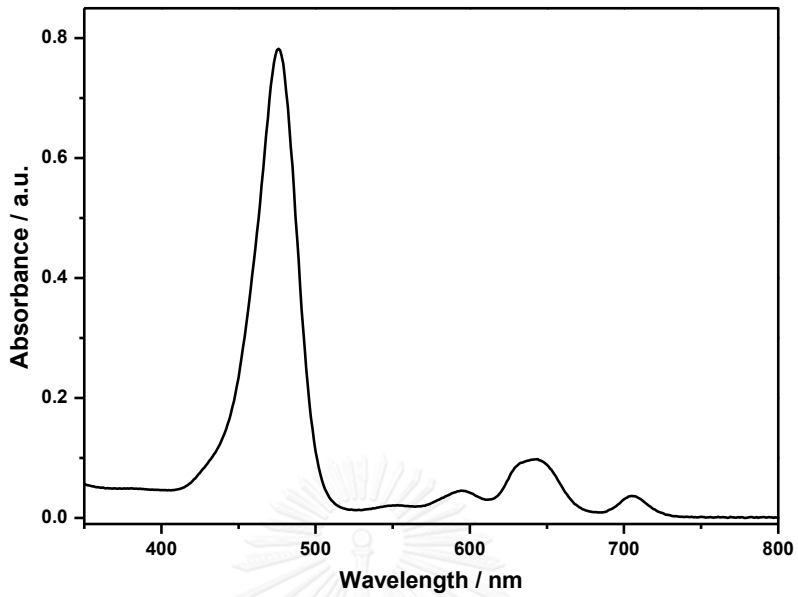

Figure A–45: Absorption spectrum of ***t*-H_2BP-2Th** in toluene.

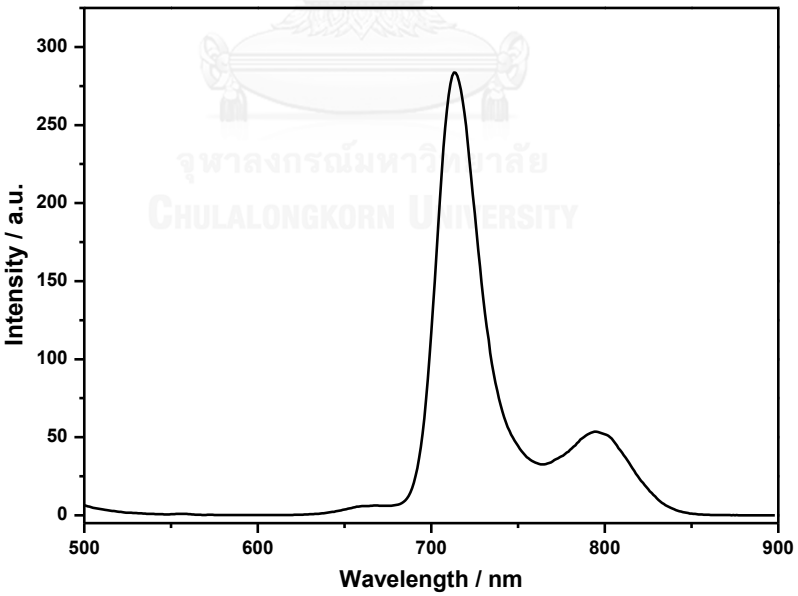

Figure A–46: Emission spectrum of ***t*-H_2BP-2Th** in toluene (λ_{ex} = 476 nm).

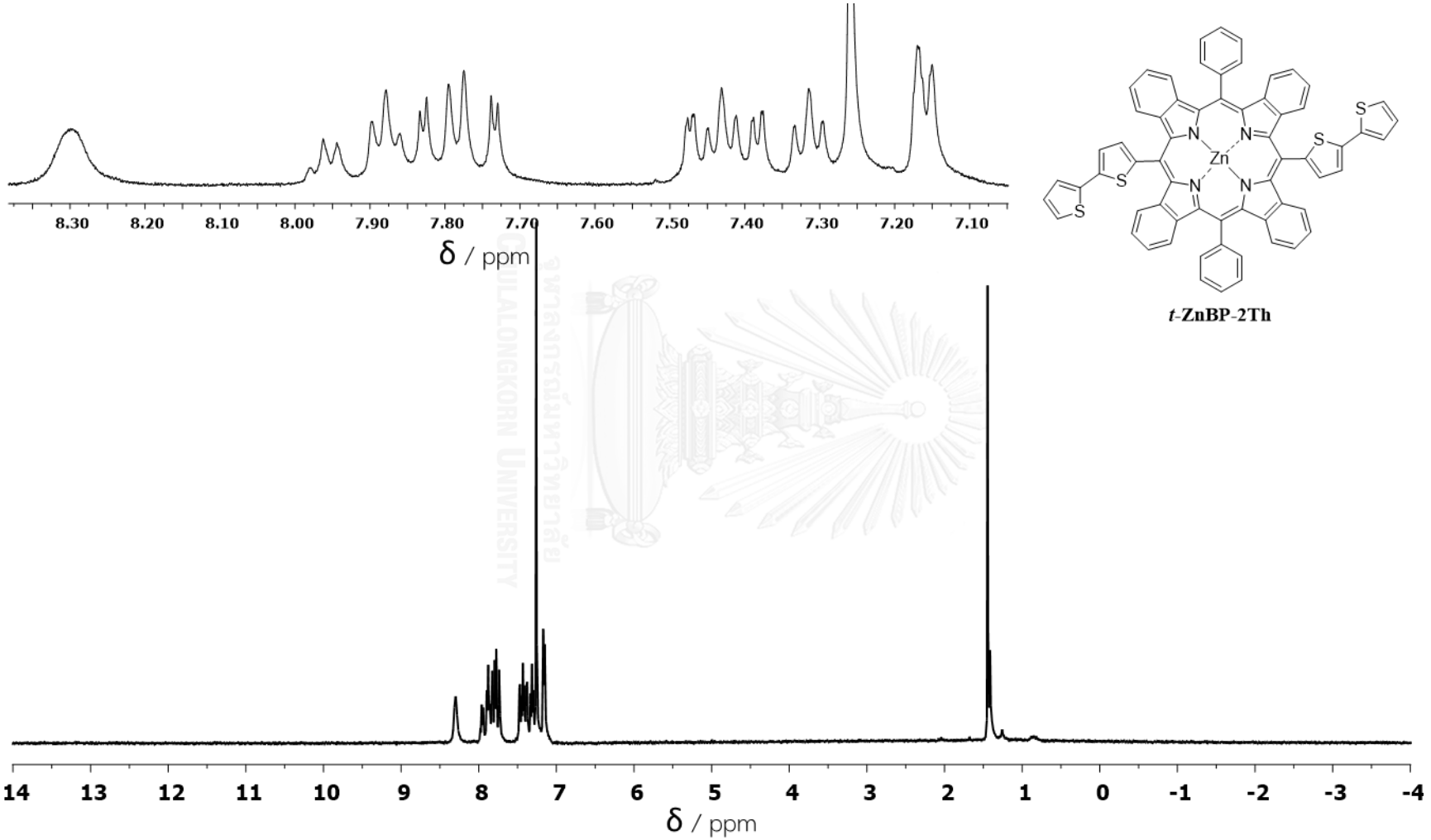

Figure A–47: ^{1}H-NMR spectrum of ***t*-ZnBP-2Th** in $CDCl_3$.

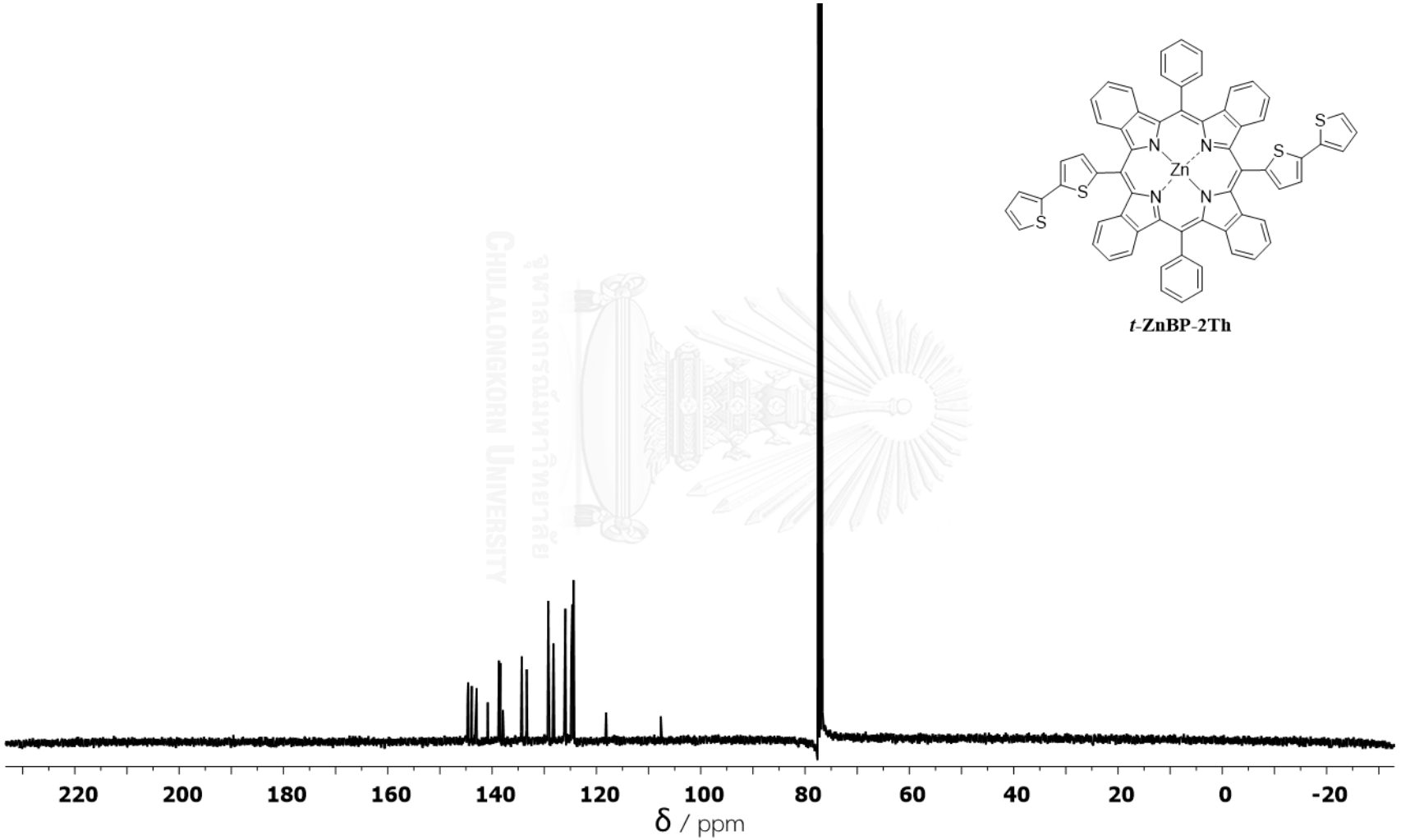

Figure A–48: ^{1}H-NMR spectrum of ***t*-ZnBP-2Th** in $CDCl_3$.

Mass Spectrum List Report

Analysis Info

Analysis Name	OSCUHS591121002_1.d	Acquisition Date	11/22/2016 12:06:19 PM
Method	Tune_wide_POS_Tawatchai_05Feb2016.m	Operator	Administrator
Sample Name	tZnBP2Th	Instrument	micrOTOF 72
	tZnBP2Th		

Acquisition Parameter

Source Type	ESI	Ion Polarity	Positive	Set Corrector Fill	50 V
Scan Range	n/a	Capillary Exit	250.0 V	Set Pulsar Pull	337 V
Scan Begin	50 m/z	Hexapole RF	400.0 V	Set Pulsar Push	337 V
Scan End	3000 m/z	Skimmer 1	70.0 V	Set Reflector	1300 V
		Hexapole 1	25.0 V	Set Flight Tube	9000 V
				Set Detector TOF	2295 V

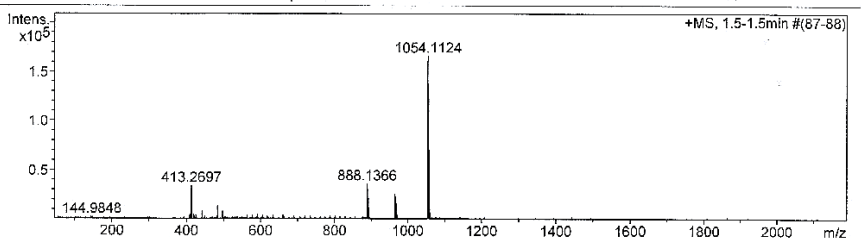

#	m/z	I	I %	S/N	FWHM	Res.
1	409.1691	5228	3.1	22.1	0.0762	5373
2	413.2697	34531	20.8	151.6	0.0725	5701
3	414.2741	9661	5.8	41.5	0.0740	5599
4	420.2195	5266	3.2	21.9	0.0817	5146
5	441.2994	8599	5.2	35.7	0.0811	5440
6	483.3816	14053	8.4	56.5	0.0871	5547
7	497.3660	8760	5.3	34.2	0.0971	5122
8	591.4966	5449	3.3	19.9	0.1118	5290
9	888.1366	36566	22.0	148.6	0.1440	6169
10	889.1403	23274	14.0	94.1	0.1474	6031
11	890.1355	30788	18.5	124.9	0.1462	6086
12	891.1377	19288	11.6	77.7	0.1481	6016
13	892.1331	21698	13.0	87.6	0.1472	6060
14	893.1332	12206	7.3	48.7	0.1422	6280
15	894.1324	5909	3.6	22.8	0.1653	5411
16	964.1699	25699	15.4	106.1	0.1600	6026
17	965.1721	18148	10.9	74.5	0.1625	5938
18	966.1694	23159	13.9	95.5	0.1612	5993
19	967.1685	16532	9.9	67.6	0.1614	5993
20	968.1660	16921	10.2	69.4	0.1581	6125
21	969.1670	9389	5.6	37.9	0.1661	5834
22	1052.1126	161258	96.9	696.1	0.1704	6173
23	1053.1176	118549	71.3	511.6	0.1775	5933
24	1054.1124	166360	100.0	718.8	0.1698	6207
25	1055.1141	111331	66.9	480.7	0.1757	6005
26	1056.1106	121835	73.2	526.4	0.1715	6159
27	1057.1116	70436	42.3	303.8	0.1669	6332
28	1058.1109	37534	22.6	161.3	0.1786	5926
29	1059.1124	16235	9.8	69.0	0.1855	5709
30	1060.1094	6747	4.1	27.8	0.1800	5890

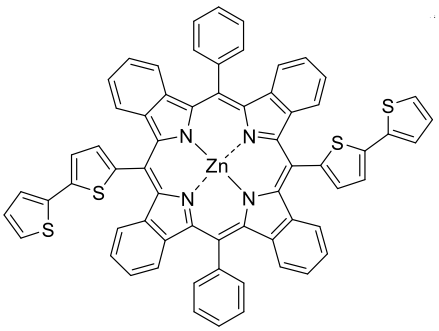

***t*-ZnBP-2Th**

Chemical Formula: $C_{64}H_{36}N_4S_4Zn$

Exact Mass: 1054.1100

Molecular Weight: 1054.6400

$[M+H]^+$: 1055.1160

Bruker Daltonics DataAnalysis 3.3 printed: 11/22/2016 1:26:56 PM Page 1 of 1

Figure A–49: HR-ESI mass spectrum of ***t*-ZnBP-2Th**.

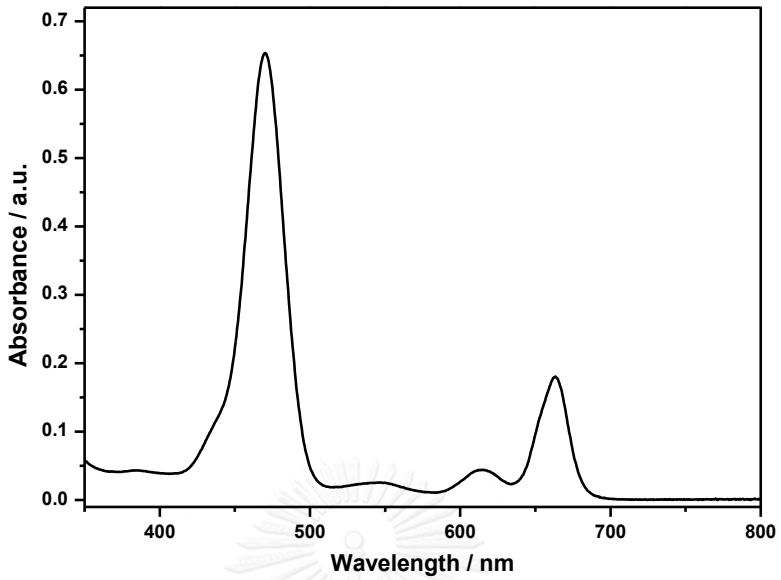

Figure A–50: Absorption spectrum of ***t*-ZnBP-2Th** in toluene.

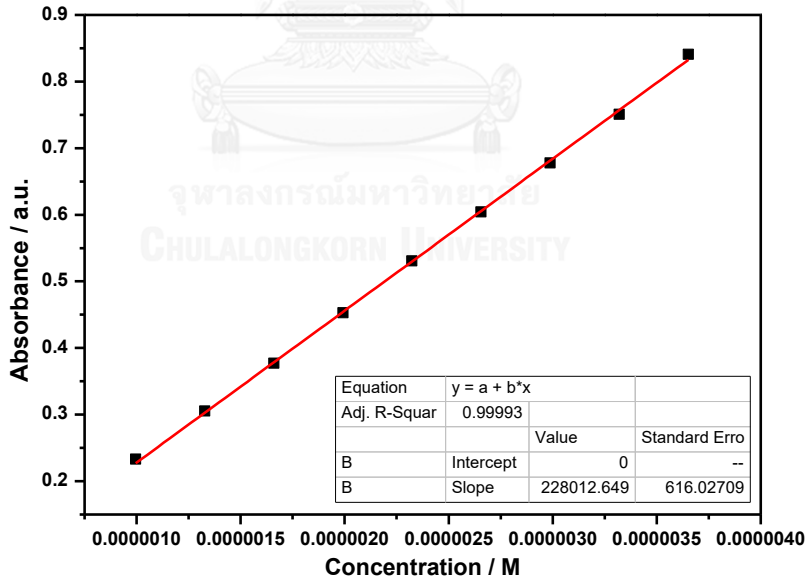

Figure A–51: Calibration curve for quantitative determination of ***t*-ZnBP-2Th** in toluene (λ_{abs} = 470 nm).

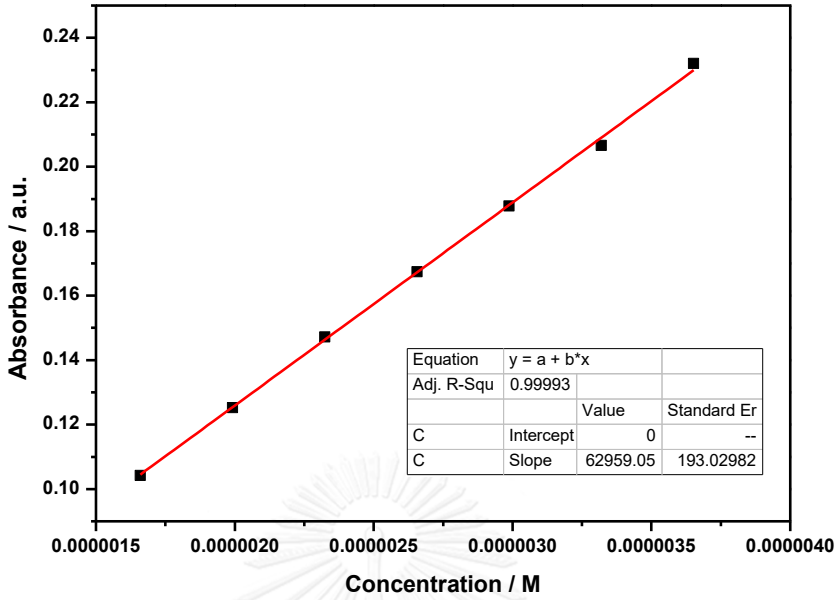

Figure A–52: Calibration curve for quantitative determination of ***t*-ZnBP-2Th** in toluene (λ_{abs} = 663 nm).

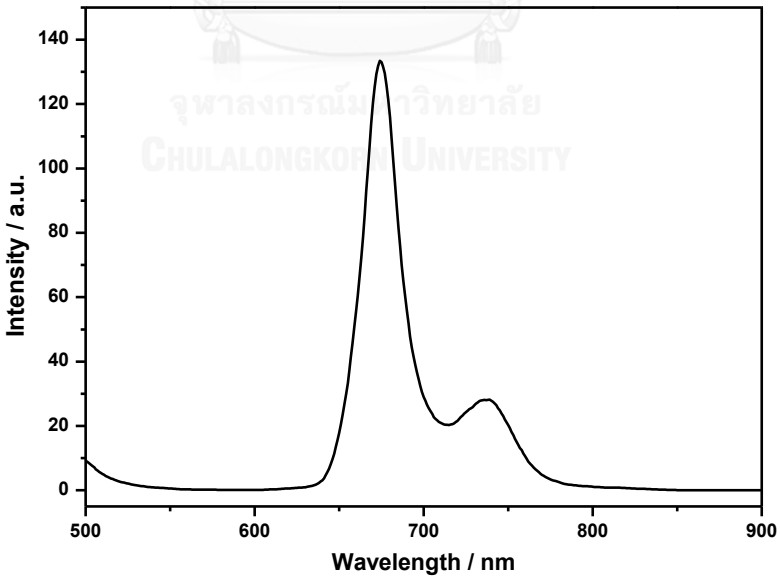

Figure A–53: Emission spectrum of ***t*-ZnBP-2Th** in toluene (λ_{ex} = 470 nm).

VITA

Miss Hathaichanok Seelajaroen was born on March 2, 1992 in Bangkok, Thailand. She got a Bachelor Degree of Chemistry from Faculty of Science at Chulalongkorn University, Bangkok in 2014. Then, she was admitted into a Master Degree in the major of Chemistry, Faculty of Science, Chulalongkorn University, Bangkok in 2014 and completed the program in 2017.